CATÓLICA
ESCOLA SUPERIOR DE BIOTECNOLOGIA
PORTO

NOVEL POLYMERIC NANOPARTICLES AS NANOFERTILISERS FOR ALKALINE IRON-DEFICIENT CONDITIONS

By:

Simão Pedro Fagundes de Pinho

January 2024

CATÓLICA
ESCOLA SUPERIOR DE BIOTECNOLOGIA
PORTO

NOVEL POLYMERIC NANOPARTICLES AS NANOFERTILISERS FOR ALKALINE IRON-DEFICIENT CONDITIONS

Thesis presented to *Escola Superior de Biotecnologia* of the *Universidade Católica Portuguesa* to fulfil the requirements of Master of Science degree in Biomedical Engineering

By:

Simão Pedro Fagundes de Pinho

Under the supervision of Marta W. Vasconcelos, Ph.D.

Under the co-supervision of Tânia Moniz, Ph.D.

January 2024

If you don’t know how,

observe the phenomena of nature,

they will give you clear answers and inspiration.

-Nikola Tesla

Abstract

Iron deficiency chlorosis (IDC) is a nutritional disorder adversely affecting plant health and crop yields, particularly in the approximately 30% of the world's arable land, which is composed of calcareous alkaline soils. The condition compromises effective iron uptake in crops such as soybeans (*Glycine max*), leading to chlorosis and stunted growth. This study introduces a novel nanotechnology-based intervention utilising 3-hydroxy-4-pyridinones (3,4HPO) iron(III) chelates-loaded nanoparticles (NPs) to address IDC, offering a controlled and sustainable release of iron and demonstrating effectiveness in enhancing plant health and chlorophyll content.

Counteracting the limitations of traditional iron chelates like EDTA, which suffer from poor biodegradability and potential environmental risks, the 3,4-HPO chelates, such as $Fe(mpp)_3$ and $Fe(dmpp)_3$, emerge as a sustainable alternative, showing increased iron bioavailability with minimal toxicity. Comparative analysis highlights the superior efficiency of these chelates over conventional treatments in preventing IDC symptoms, fostering greener, more robust plant growth, and higher iron accumulation.

Innovative nanocarriers were developed for fertiliser delivery, capitalising on the nano-porous structure of plant roots and leaves, with the aim of enhancing nutrient uptake and correcting IDC. The research progressed through the production, optimisation, and characterisation of rhodamine B-labelled polymer-based NPs. Their uptake by soybean plants was assessed, identifying the most favourable characteristics for plant absorption.

Building on this, the methodology was adapted to encapsulate the iron chelates $Fe(dmpp)_3$ and $Fe(mpp)_3$ within the NPs. Subsequent *in vivo* studies utilised $Fe(dmpp)_3$ NPs for seed priming in soil, evidencing significant improvements in chlorophyll content, growth rates, and biomass in iron-deficient conditions.

Furthermore, the study's foray into genetic expression analysis revealed upregulated iron-related genes, pointing to a profound molecular impact of NP treatment and an improved mechanism for iron transport and storage.

The findings indicate that $Fe(dmpp)_3$-loaded NPs not only alleviate IDC but also present a potential paradigm shift in the fertiliser industry, promoting more sustainable and efficient agricultural practices. The implications extend beyond increased crop yields, suggesting that engineered NP treatments could be instrumental in the future of agriculture, integrating environmental responsibility with enhanced productivity.

Keywords: 3-hydroxy-4-pyridinones, Iron deficiency chlorosis, iron (III) chelates, nanoparticles, nanofertilisers, nanotechnology, rhodamine B

Resumo

A clorose por deficiência de ferro (IDC, do inglês *"Iron deficiency chlorosis"*) é uma condição nutricional que afeta negativamente a saúde das plantas e os rendimentos das culturas, particularmente nos solos alcalinos calcários, que correspondem a cerca de 30% de terras aráveis do mundo. Esta condição impede a absorção eficaz de ferro em culturas como a soja (*Glycine max*), levando à clorose e a uma diminuição no crescimento das plantas. Este estudo introduz uma nova intervenção com recurso à nanotecnologia, nomeadamente no uso de nanopartículas (NPs) carregadas com quelatos de ferro(III) de 3-hidroxi-4-piridinonas (3,4-HPO) para tratar a IDC, o que permitirá uma libertação controlada e sustentável de ferro, demonstrando eficácia na melhoria da saúde das plantas e no aumento do conteúdo em clorofila.

Ao contrário dos quelatos de ferro tradicionais como o EDTA, que apresentam baixa biodegradabilidade e potenciais riscos ambientais, os quelatos de 3,4-HPO, como o $Fe(mpp)_3$ e o $Fe(dmpp)_3$, surgem como uma alternativa sustentável, mostrando uma maior biodisponibilidade de ferro com toxicidade mínima. A análise comparativa destaca a eficiência superior destes quelatos em relação aos tratamentos convencionais na prevenção dos sintomas da IDC, promovendo um crescimento de plantas mais verde e robusto, e uma maior acumulação de ferro.

Foram desenvolvidas NPs inovadoras para a administração de fertilizantes, aproveitando a estrutura porosa das raízes e folhas das plantas à nanoescala, aumentando assim a absorção de nutrientes e a consequente correção da IDC. A investigação prosseguiu no sentido da produção, otimização e caracterização de NPs poliméricas marcadas com rodamina B. A sua absorção por plantas de soja foi avaliada, identificando as características mais favoráveis para o efeito esperado.

Com base neste estudos preliminares, a metodologia foi adaptada para encapsular os quelatos de ferro $Fe(dmpp)_3$ e $Fe(mpp)_3$ nas NPs. Estudos *in vivo* subsequentes utilizaram NPs de $Fe(dmpp)_3$ para o tratamento de sementes, antes da sua inoculação no solo, evidenciando melhorias significativas no conteúdo em clorofila, nas taxas de crescimento e na biomassa em condições de deficiência de ferro.

Além disso, foi realizada uma análise da expressão genética, que revelou que genes relacionados ao ferro foram regulados positivamente, apontando para um impacto molecular positivo do

tratamento com NPs e melhorias no mecanismo da planta para o transporte e armazenamento de ferro.

Os resultados indicam que as NPs carregadas com $Fe(dmpp)_3$ não só aliviam a IDC, mas também apresentam uma potencial mudança de paradigma na indústria de fertilizantes, promovendo práticas agrícolas mais sustentáveis e eficientes. As implicações vão além do aumento dos rendimentos das culturas, sugerindo que tratamentos com NPs poderiam ser instrumentais no futuro da agricultura, integrando responsabilidade ambiental com uma maior produtividade.

Palavras-chave: 3-hidroxi-4-piridinonas, clorose por deficiência de ferro, quelatos de ferro (III), nanopartículas, nanofertilizantes, nanotecnologia, rodamina B

Acknowledgements

To begin with, I would like to thank my supervisor, Dr. Marta Vasconcelos, for the opportunity to work in this amazing project, for all the guidance over the last 15 months, and for helping me learn so much, as well as for allowing me to be work with and be a part of a tremendous work group.

I would also like to thank my co-supervisor, Dr. Tânia Moniz, for always being available to provide help, for all the care, support, and patience. You helped me learn a lot not only about chemistry and nanotechnology but also all the practical knowledge that does not come from books.

I am also extremely thankful to Dr. Carla Santos, for all your assistance and motivation, for always being available to lend me a hand in whatever challenge I'm facing in my research and for all the insight into the subtleties involved in research.

I would like to thank Dr. Salette Reis for all the support and for welcoming me to an incredible research group, from which I learned a lot.

I would further like to express my gratitude to Dr. Maria Rangel for all the scientific aid and for including me in your group's research.

I also wish to acknowledge Dr. Mafalda Sarraguça for all your help in my FTIR and NIR analysis.

I also want to thank Dr. Andreia Granja for your assistance in the lab and for teaching me how to operate the confocal microscope.

I am also extremely thankful to all the members of the PlanTech research group for all your help, as well as for all the great environment and constant positive attitude.

My sincere thanks also go to all the members of the MB2 research group for your warm welcome and for always being available to help.

I would also like to express my gratitude to all my friends who accompanied me during this journey, who always showed interest in my work and rooted for me to succeed, even with all my rambling about nanoparticles.

Last but not least I would also like to thank my parents and my brother, for all the unending support and for providing me with the conditions to push for this degree, as well as for always showing enthusiasm and care about my research.

Table of contents

Index of Figures

Index of Tables

List of abbreviations

3,4-HPO- 3-hydroxy-4-pyridinone

DLS- Dynamic light scattering

DPPH- 2,2-diphenyl-1-picrylhydrazyl

EDDHA- Chelating agent ethylenediamine-N,N′-bis(2-hydroxyphenylacetic acid).

EE- Encapsulation efficiency

FeDM- Iron (III) complex [$Fe(dmpp)_3$]

FeMP- Iron (III) complex [$Fe(mpp)_3$]

FRO- Ferric reduction oxidase

FTIR- Fourier-transform infrared spectroscopy

ICP-OES, or ICP- Inductively coupled plasma optical emission spectrometry

IDC- Iron deficiency chlorosis

LC- Loading Capacity

NA- Nicotianamine

IRT- Iron regulated transporter

MES- (2-(N-morpholino)ethanesulfonic acid)

NP- Nanoparticle

PDI- Polydispersity index

PLGA- Poly(D,L-lactide-co-glycolide)

PVA- Poly(vinyl alcohol)

RB- Rhodamine B

SPAD- Soil plant analysis development

1. Introduction

1.1. Plants as a source of iron in human diets

Iron is an essential element for human health, some of its main functions including: oxygen transport, carried out through haemoglobin and myoglobin, where it binds to dioxygen; DNA synthesis, where it is part of an essential enzyme; electron transport, where it is present in iron-sulphur enzymes, as well as bound to other forms of haemoproteins (Abbaspour, 2014; Beard, 2001). It has also been shown to be essential for proper brain function and immune response (Beard, 2001). Around 65% of all iron present in the body is found in haemoglobin contained within erythrocytes in the bloodstream, while another 25% is present in ferritin iron storages found primarily in liver tissue, and the remaining 15% are bound to myoglobin in muscle tissue, as well as in a variety of enzymes involved in oxidative metabolism and other functions (Abbaspour, 2014; Beard, 2001).

Iron deficiency refers to decreased iron reserves in the body, primarily those located in macrophages and hepatocytes iron pools (Camaschella, 2019). Since haemoglobin synthesis consumes a large part of the body's supply of iron producing around 200 billion erythrocytes daily, iron deficiency anaemia is one of the most common signs of iron deficiency (Camaschella, 2019). The three stages of iron deficiency are: iron depletion, in which all the storages of iron are expended, but the level of functional compounds remains stable; iron-deficient erythropoiesis, in which the necessity for iron of the erythroid marrow can no longer be satisfied, causing an increase in erythrocyte protoporphyrin and serum transferrin receptor levels, and finally, iron deficiency anaemia, the most extreme degree, in which the restriction to the production of haemoglobin leads to the distortion of the erythrocytes, resulting in serious effects on the individual's health (Hercberg *et al.*, 2001). These effects vary drastically according to the type and acuteness of anaemia, and they can include complications in the gastrointestinal tract, compromised thermoregulatory and neurocognitive functions, as well as being a serious risk factor for many other illnesses such as tuberculosis and heart conditions (Safiri *et al.*, 2021).

A worldwide study conducted in 2019 concluded that around 1.8 billion individuals suffer from iron deficiency anaemia, with this number having large differences between countries with high and low incomes, and although the number of individuals in the world with the broader condition of iron deficiency is not determined, it's expected to be around two times that number (Kassebaum *et al.*, 2014; Safiri *et al.*, 2021). Approximately 29.9% of reproductive-age women, 36.5% of pregnant women, and 39.8% of children aged 6-59 months worldwide are impacted by iron deficiency anaemia, with pregnant women and young children being the most affected, according to the World Health Organization. (WHO, 2008, 2021). In 2019, among individuals below the age of 10, both males and females exhibited a high global point prevalence of anaemia, subsequently, there was a decline in the point prevalence up to the 25–29 age group in males, followed by a resurgence with increasing age. As for females, the point prevalence reached its lowest level in the 10–14 age group, then peaked in the 15–19 age group, and generally decreased with advancing age (Safiri *et al.*, 2021). Overall, females had a higher global point prevalence compared to males in the 10–69 age groups. The global number of prevalent cases reached its peak in the 5–9 years age group and was higher in females across all age groups except those aged 1–9 years (Safiri *et al.*, 2021). Anaemia also has a considerable economic impact, and can vary substantially, mostly based on the acuteness of other underlying conditions, but it is estimated that it can range from 27.448€ on cases where there is congestive heart failure to about 6.596€ in instances of milder conditions, such as comorbid rheumatoid arthritis (Safiri *et al.*, 2021).

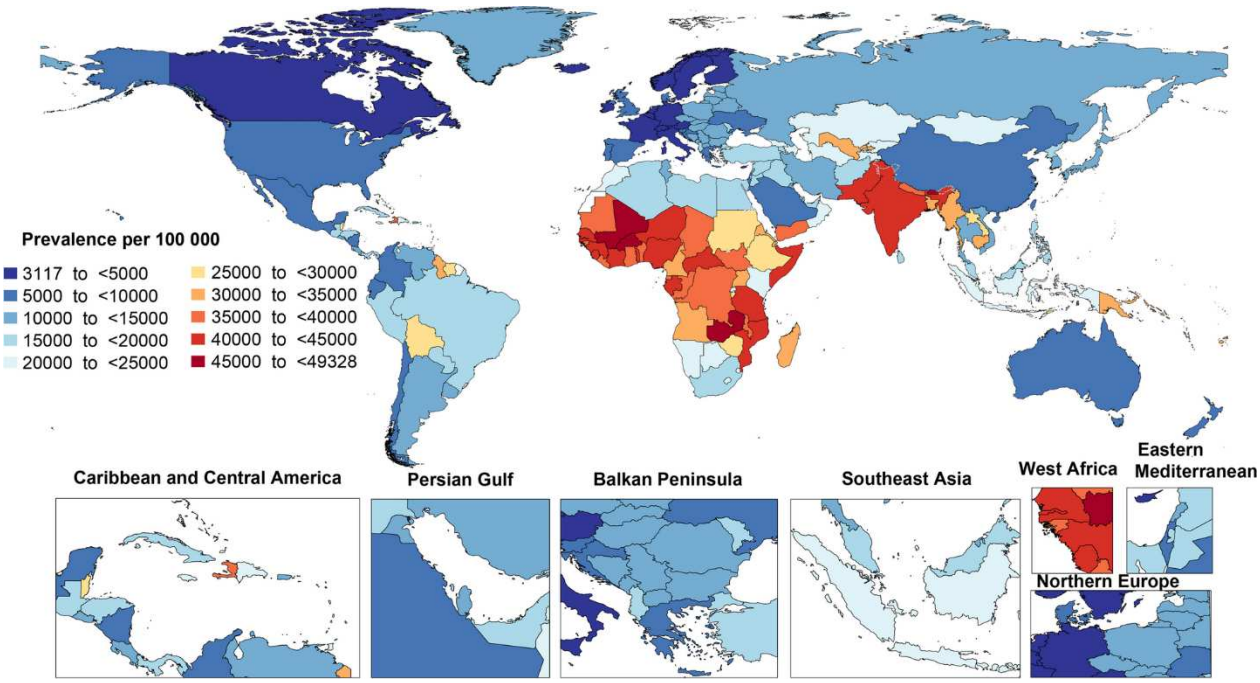

Figure 1.1- Prevalence of iron deficiency anaemia per country per 100.000 people, in 2019 (adapted from Safiri *et al*., 2021).

World population is growing at an exponential rate, and it is expected to reach nine billion by the end of 2050, and agricultural yield is not being able to keep up with the increasing food demand, mostly due to water shortages, exhaustion of soil fertility, as well as the impact of global climate change, which is expected to intensify the occurrence of droughts and floods, leading to further depletion of soil nutrients and reduction of freshwater availability (Basuchaudhuri, 2020).

Since crops provide a direct and indirect source of iron to humans and other animals through their diet, increasing the amount of iron in key foods would be an effective method to mitigate the problem of iron deficiency (Ma & Ling, 2009). This can be achieved through different methods, such as conventional plant breeding, genetic engineering and agronomic biofortification (Carvalho & Vasconcelos, 2013). Several success cases have been reported with these methods, such as: In India, combined efforts by the International Crops Research Institute for the Semi-Arid Tropics and HarvestPlus were able to successfully use conventional breeding to enhance the levels of iron in pearl millet ((CIMMYT), 2023); For transgenic approaches, some studies have shown that by expressing the soybean *FERRITIN* gene in rice endosperm, the total rice accumulation can increase up to three times when compared to regular rice (Senguttuvel *et al.*, 2023); Studies on agronomic

biofortification have found that when using ferrous sulphate or EDDHA iron chelates on plants, by either foliar or soil application, the seed yield is increased (Márquez-Quiroz *et al.*, 2015).

Research has shown that plant-based diets are more cost-effective and may provide several benefits such as a decrease in body mass index, blood pressure and cholesterol level (Tuso *et al.*, 2013). People who follow these diets have also been shown to consume more iron, magnesium, potassium, thiamin, riboflavin, folate, and vitamins and less total fat (Tuso *et al.*, 2013).

As primary producers, plants are the gateway for iron to enter the food chain (Connorton *et al.*, 2017). The iron provided to humans in a plant-based diet exclusively comes from the rhizosphere, and the efficiency with which plants absorb, transport, and store iron directly influences its concentration in the plant's edible parts (Morrissey & Guerinot, 2009).

Considering this information, alongside the fact that Europe's plant-based food industry has grown 49% from 2018 to 2020, it is imperative to thoroughly explore new strategies for a more efficient and environmentally friendly delivery of iron to plants (Cordis, 2022).

Besides plants being important sources of iron for human health, the mechanisms underlying plant and human iron nutrition have several interesting parallelisms (Brown & Jolley, 2008). By understanding mechanisms of iron delivery, uptake, and accumulation in plants, it is possible to develop and extrapolate new hypothesis for iron nutrition in humans.

1.2. Iron nutrition in plants

Because most of the iron in the Earth's crust is in an oxidized form that's not easily absorbed by plants, they have evolved mechanisms to acquire, process, and store iron. Additionally, they've developed safeguards to prevent an excessive accumulation of this metal, as high iron levels can be harmful to their cells. These mechanisms are known as Strategy I and Strategy II, the former being responsible for the uptake of ferrous iron (Fe^{2+}) and the latter for the uptake of ferric iron (Fe^{3+}) (Connorton *et al.*, 2017).

Strategy I is usually carried out by higher plants, such as *Arabidopsis thaliana*, potato, and soybean, and it consists of three steps (Hell & Stephan, 2003). First, plant roots excrete protons via a plasmalemma P-type ATPase to lower the pH of the surrounding solution and increase the solubility of Fe^{3+}. Then, a ferric reductase reduces Fe^{3+} to the more water soluble Fe^{2+} and, finally,

the iron is transported through the cellular membrane with the aid of iron transporters (Hell & Stephan, 2003). Other strategies include changes in the morphology of the roots, root hair growth and increments in the concentration of citrates in the phloem (Hell & Stephan, 2003). The *FRO2* gene plays a central role in producing ferric reductase, along with other genes in the *FRO* family, which have been linked to iron uptake in various plant tissues (Kim & Guerinot, 2007). The *IRT1* gene codes for a membrane-bound root iron transporter. Both the expression of *IRT1* and the activity of the reductase are believed to be regulated by the availability of iron within a common regulatory system (Eide *et al.*, 1996; Kim & Guerinot, 2007).

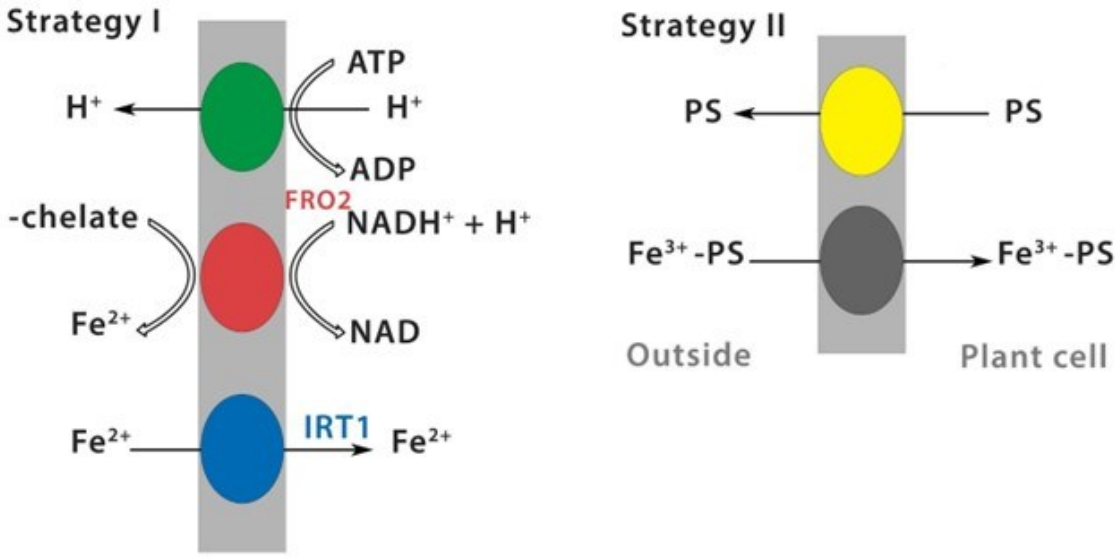

Figure 1.2- Schematic representation of both iron uptake strategies used by plants (adapted from Rehman *et al*., 2020).

Strategy II plants include grasses, or gramineous crops, such as corn and wheat (Kim & Guerinot, 2007). Upon iron deficiency, these plants release phytosiderophores (PS), a type of compound which serves as a chelating agent by binding to Fe^{3+}, forming a complex which is then taken up by the roots by a specific transport system (Mori, 1999).

Certain grass species, like rice, employ elements of the reduction strategy. They produce lower levels of PS but make up for this by generating metal transporters such as *OsIRT1* and *OsIRT2* in the root epidermis when facing iron deficiency (Morrissey & Guerinot, 2009).

Additionally, there are also microbial mechanisms of plant iron uptake. These processes are conducted in low iron conditions, with microorganisms in the soil producing either high-redox iron carriers that reduce Fe^{3+} to Fe^{2+} which can then be directly absorbed by roots, or siderophores, a different type of iron carrier, which is released into the rhizosphere, being able to bind to Fe^{3+} and forming a complex that can then be partially absorbed by plant roots (Ning *et al.*, 2023).

After being absorbed by the roots, iron is transported throughout the plant with the help of various complexing agents that have a strong affinity for iron. This is necessary due to iron's toxicity and limited solubility (Connorton *et al.*, 2017). The toxicity of iron is related to its ability to donate and accept electrons, which, in high concentrations, causes free iron to catalyse, for example, the conversion of hydrogen peroxide to free radicals, harming many cell structures, being able to kill cells in the long run (Rout & Sahoo, 2015). Nicotianamine (NA), a non-proteogenic amino acid, is responsible for the chelation of iron in the phloem, while in the xylem, this function is mainly performed by citrate (Briat *et al.*, 2007). A class of Fe-NA-specific transporters of the YSL family is responsible for the translocation of iron from the xylem to the phloem (Briat *et al.*, 2007). The storage and buffering of iron at the plants' cellular level allow for them to cope with its toxicity and scarcity, and this function is performed by organelles such as plastids and vacuoles, in which ferritins store a large fraction of cellular iron and allow for homeostasis (Briat *et al.*, 2007). Mainly located within the chloroplasts, ferritins are a class of iron-storage proteins responsible for maintaining iron homeostasis, comprising hollow spheres composed by 24 subunits, being able to contain 4500 iron atoms per molecule (Briat *et al.*, 1999). These proteins are encoded by the *FERRITIN* gene family, which is regulated by iron (Briat *et al.*, 2010). The influx of iron molecules into these organelles, in both strategy I and strategy II plants, is thought to require a reduction-based strategy, made possible by a member of the *FRO* family, *FRO7*, responsible for converting iron from the ferric to ferrous form in order to enter the chloroplast (Morrissey & Guerinot, 2009). The synthesis of these proteins is also heavily regulated by the amount of iron inside the cells, being produced in high amounts when there is an excess of iron, as a way to contain the molecules and stop them from reacting with oxygen (Briat *et al.*, 1999).

Due to its importance as a building block of various proteins and enzymes, iron plays a crucial role in basic biological processes such as photosynthesis, chlorophyll synthesis, respiration, nitrogen fixation, uptake mechanisms and DNA synthesis, as well as being an active cofactor of many

enzymes responsible for plant hormone synthesis (Rout & Sahoo, 2015). In the photosynthetic framework, there are twelve iron atoms found in the photosystem I, two or three in the photosystem II and five in the cytochrome complex, resulting in a sharp decrease of photosynthetic activity in situations of iron deprivation (Varotto *et al.*, 2002). Due to their ability to delocalize electron density over both iron and sulphur atoms, iron-sulphur [Fe-S] clusters are essential constituents in the respiratory and photosynthetic electron transport chains; define the electron transport pathways in many membrane-bound and soluble enzymes and are essential elements in the active centres of ferredoxins, a class of proteins responsible for carrying electrons (Johnson *et al.*, 2005). These proteins are responsible for carrying electrons from photosystem I to various enzymes, utilized for nitrogen and sulphur assimilation, nitrogen fixation and to produce NADPH (Fukuyama, 2004).

When iron is limited, such as in the case of alkaline soils, crops may develop iron deficiency chlorosis (IDC), which hampers crop productivity and influences the iron nutritional value of both vegetative states and edible plant parts.

1.3. Iron deficiency chlorosis

IDC is a significant nutritional disorder affecting plants growing on calcareous soils, usually with a pH of between 7.4 and 8.5, which decreases the availability of iron in the rhizosphere, impairing the plants' ability to uptake, transport and utilize this element (Lucena & Hernandez-Apaolaza, 2017). This condition causes yellowing on the upper leaves, interveinal chlorosis and stunted growth, leading to a decline in yield and quality of a large number of crops, causing extensive monetary expenses, especially since around 30% of the world's total arable land is composed of calcareous soils (Lucena & Hernandez-Apaolaza, 2017) (C. S. Santos *et al.*, 2016).

In high pH conditions, iron in the soil tends to be oxidized to the ferric state (Fe^{3+}), after which it is likely bound to anions, covalent metals, and other soil particles, making it unavailable for uptake and transport in strategy I plants (Marschner & Römheld, 1994; Merry *et al.*, 2022). Calcareous soils are also known to possess high amounts of calcium carbonate, which, in conditions of high moisture, is dissolved, forming a solution containing calcium (Ca^{2+}) and carbonate (CO_3^{2-}) ions, the second being able to further increasing the pH of soils, oxidizing Fe^{2+} to Fe^{3+} and acting as a buffer, preventing the strategy I plants from lowering the soils' pH (Merry *et al.*, 2022). Nitrates

are also known to cause iron deficiency in high pH soils, by being taken up by plants, which in turn release carbonate into the soil, causing the changes mentioned above (Merry *et al.*, 2022).

Commonly, IDC's visual symptoms are measured in a scale of 1 to 5, in which 1 represents no symptoms, 2 indicates some chlorosis on the canopy, 3 indicates a higher degree of chlorosis, 4 implies the existence of some necrosis and 5 represents severe chlorosis and major necrosis, or even plant death, however, this visual rating system is quite subjective (Merry *et al.*, 2022).

Figure 1.3- Iron chlorosis visual rating scale representation in soybean plants (adapted from NDSU, 2020).

The Soil Plant Analysis Development (SPAD) is often used to monitor IDC symptoms, by measuring the levels of chlorophyll in the leaves of the plant. Other methods include measuring the activity of iron reductase at the root level, determining the contents of iron inside the plants and analysing the expression of certain key genes (C. S. Santos *et al.*, 2020).

Dicotyledonous plants show changes in the expression of genes coding for proteins IRT1, FRO2 and Ferritin in conditions of iron deficiency, although these changes can vary from plant to plant, with further research being required to understand this relation (Carla S. Santos *et al.*, 2016). The analysis of the expression of these genes may offer valuable insight to the degree of which the plant has been affected by IDC (C. S. Santos *et al.*, 2020).

1.3.1. Soybean as a model organism to study IDC

Soybean *(Glycine max L.*) is a dicotyledonous, non-gramineous plant (Roriz *et al.*, 2021). Legumes such as soybean have been shown to be a rich source of protein, dietary fibre and minerals such as iron, with studies showing that soybean has an iron concentration of 137 μg/g, which is extremely high compared to cereals such as rice (*Oryza sativa*) which has a concentration of 34.9 μg/g (Hermila Valdes-Miramontes *et al.*, 2019; Meng *et al.*, 2005). In the past 50 years, the global production of soybean has risen rapidly, having increased from 20 to 30 million tonnes per year to

about 350 million tonnes in 2021 (FAO, 2021). The two main soybean producing countries are the United States of America and Brazil, which together produce about 69% of the world's total yield (Roser, 2021). This crop has become one of the most produced agricultural products in the world, due to its high protein and oil content, along with other components, such as phospholipids, vitamins, minerals and some other minor substances such as trypsin inhibitors, phytates and oligosaccharides and isoflavones (K. Liu, 1997). Soybean oil is one of the most produced vegetable oils in the world, and most of it is used in industrial food manufacturing and as a biofuel. A significant part of the total world production of soybean is also used for animal feed, due to its high nutritional value, and only about 6% of all output is converted into products such as soybean milk and tofu, destined for human consumption (Fraanje, 2020). The gross production value of soybeans has increased rapidly in the last 30 years, having reached around 150 billion US$ in 2021 (FAO, 2021). In the European Union, the European Commission has formulated a strategy to reduce the dependency on plant proteins imported from the Americas, with the intent of increasing self-reliance, encouraging more balanced diets within the EU countries and reducing deforestation in South America (Debaeke *et al.*, 2022). The Green Deal issued in 2019 has reinforced this direction by endorsing soybean and other legumes as crucial elements of the diversification strategy for the agroecological transition and lowering greenhouse gas emissions in agriculture. On 17 July 2017, 14 Member States endorsed the "European Soya Declaration," pledging their support for the promotion of sustainable and certified production and marketing of soybean (and other legumes) within Europe. Following this growing demand and encouragement, particularly for locally sourced and non-genetically modified soybeans, the dedicated cultivation areas in Europe have seen a rapid expansion in recent years. Within the EU-27, these areas have seen a twofold increase, reaching nearly one million hectares since 2013, with the production rising to 2.9 million tons in 2018. In 2021, for the first time since 1987–1989, the area devoted to soybean production in the EU-27 surpassed 1 million hectares.

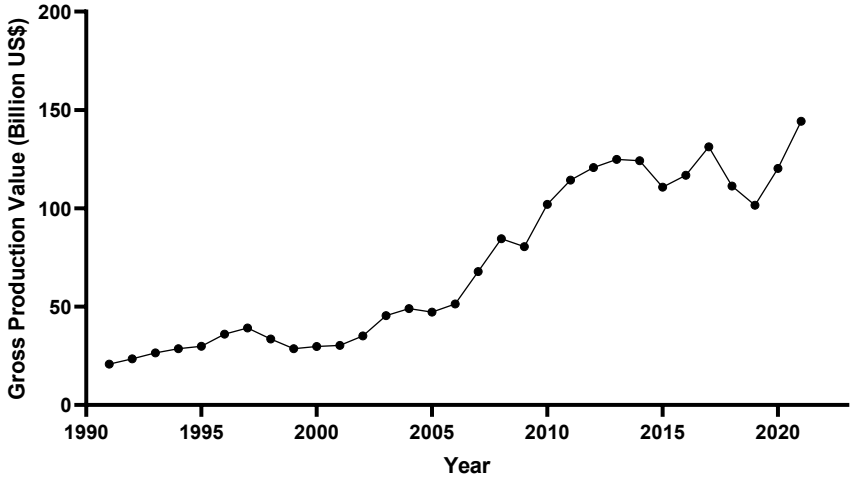

Figure 1.4- Change in worldwide gross production value of soybean in billion US$ since 1991 to 2021 (adapted from FAO, 2021).

The first few vegetative stages of soybean plants can be described as follows: At the Vegetative Emergence stage, water absorption by the soybean seed is approximately equal to 50% of its weight, initiating the process of germination. During the Cotyledon stage, the unifoliate leaves fully expand, with the cotyledons primarily providing the necessary nutrients. The First Trifoliate (V1) stage is marked by the emergence of the first set of trifoliate leaves. This is followed by the Second Node (V2) stage, where the second set of trifoliate leaves appears, and active nitrogen fixation by bacteria begins. By the Third Node (V3) stage, the soybean plants have developed their third set of trifoliate leaves and typically reach a height of around 20 cm. The symptoms relating to IDC have been shown to start appearing in these early stages (C. S. Santos *et al.*, 2015).

1.3.2. Management of IDC

Conventional plant breeding is one of the techniques usually put into practice to reduce the prevalence of IDC. It consists of breeding exceptionally tolerant cultivars to mitigate the effects of this condition. Genetic engineering is another approach for biofortification that can be used to prevent or reduce the symptoms or IDC, by creating transgene crops resistant to the condition (Carvalho & Vasconcelos, 2013).

The application of different types of iron-based fertilisers is one of the most commonly used methods, consisting of ligands with an appropriate affinity for iron, high solubility in water and

bioavailability (Carvalho & Vasconcelos, 2013; C. S. Santos *et al.*, 2016). The main three types of iron fertilisers are: inorganic iron compounds, which are relatively inefficient in the soils, since they turn into insoluble compounds, being usually applied as foliar fertilisers; natural iron complexes, which are also quite unstable in the soil and usually applied in the same manner; and synthetic iron chelates, which possess certain artificial ligands that give them the desired properties for either foliar or soil application (Carla S. Santos *et al.*, 2016).

Several different iron (III) chelates such as ethylenediamine tetraacetic acid (EDTA) and ethylenediamine-*N,N*'-bis(o-hydroxyphenylacetic) acid (EDDHA) have been used in the soil as a way to provide the necessary supply of bioavailable iron, however, like many other commercial fertilisers, these compounds have been shown to be extremely resistant to biodegradation, and can cause severe damage to the environment by binding to other heavy metals and potentially leaking to groundwater (Carla S. Santos *et al.*, 2023; Ylivainio, 2010). Some more recently studied options include IDHA (*N*-(1,2-dicarboxyethyl)-D,L-aspartic acid) and [*S,S′*]EDDS (ethylenediaminedisuccinic acid, *S,S* isomer), however, due to their relatively low stability in soil, these options are primarily recommended for soilless cultures and foliar applications (Lucena & Hernandez-Apaolaza, 2017).

More recently, chelates of the 3,4-HPO family have shown great potential in their ability to increase iron bioavailability in soybean plants (C. S. Santos *et al.*, 2016; C. S. Santos *et al.*, 2020; C. S. Santos *et al.*, 2021). These compounds were first used in **biomedical** applications for combating iron-induced carcinogenesis and heavy metal poisoning, important conditions where patients over accumulate iron in their tissues, as well as in Parkinson's Disease therapy (X. Liu *et al.*, 2020; M. A. Santos *et al.*, 2022; Tosato & Di Marco, 2019).

These ligands are useful due to their affinity towards M(II) and M(III) metal ions and their synthetical versatility, as certain physicochemical properties can be altered to benefit each specific situation, without changing the affinity of these chelates towards specific metal ions and the redox potential of the metal ion complexes (C. S. Santos *et al.*, 2020). These molecules are amphiphilic, as they contain both hydrophilic and hydrophobic parts, granting them the property of hydrophilic-lipophilic balance (Burgess. & Rangel, 2008; C. S. Santos *et al.*, 2020).

In the first study using these compounds as potential plant fertilisers, $Fe(mpp)_3$, or FeMP, (Figure 1.5) was shown to be more efficient than FeEDDHA, the most commonly used iron complex in

agriculture, in preventing symptoms of IDC in soybean plants grown hydroponically, and showed minimal toxicity (Carla S. Santos *et al.*, 2016). Results revealed that plants treated with $Fe(mpp)_3$ complex were significantly greener, had increased biomass. and accumulated about 50% more iron than those treated with the commercial chelate. Plants treated with the 3,4-HPO complex were able to translocate iron from the roots to the shoots and did not elicit the expression of the iron stress related genes *FRO2* and *IRT1.* The data pointed out for the first time, the potential of 3,4-HPO chelates as a new class of plant fertilising agents.

In the following studies, also considering soybean plants grown hydroponically, the efficiency of the three other structurally-related iron(III) chelates from the 3,4-HPO family (Figure 1.5) was compared at different concentrations and at different pH conditions. It was concluded, through morphological, physiological and genetic expression analysis, that $Fe(mpp)_3$ is the most efficient complex at preventing IDC symptoms, followed by $Fe(dmpp)_3$ and $Fe(etpp)_3$ as the least effective one (C. S. Santos *et al.*, 2020). Since all [$Fe(3,4\text{-}HPO)_3$] chelates were able to provide iron to plants and prevent IDC but with at different efficiency levels depending on the ligand, it was hypothesized that the activity may be related with the different physicochemical properties of ligands and complexes, namely, the diverse hydrophilic–lipophilic balance. A biophysical study using labelled liposomes prepared from a soybean lipid extract proved that the most effective chelate, Fe(mpp)3, has a preferential location close to the surface while the others prefer the hydrophobic region inside the bilayer (C. S. Santos *et al.*, 2020).

This class of chelators have numerous potential advantages when compared to most fertilisers in the market, and $Fe(mpp)_3$, $Fe(dmpp)_3$ and $Fe(etpp)_3$ (Figure 1.5) have shown to be able to deliver Fe^{3+} to hydroponically grown soybean plants successfully, and even prevent or mitigate some effects of IDC, with no observable negative side effects to the environment (L. S. Mesquita *et al.*, 2020; R. B. R. Mesquita *et al.*, 2022; M. A. Santos *et al.*, 2022).

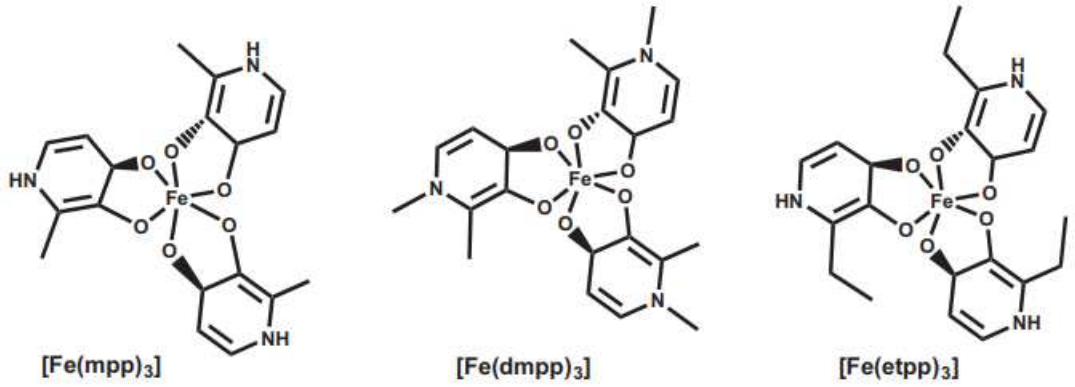

Figure 1.5- Chemical structure of three different of 3-hidroxy-4-pyridinones iron chelates (adapted from C. S. Santos *et al*., 2020).

In further studies, the efficacy of $Fe(mpp)_3$ was inspected under soil conditions in soybean grown from seed to full maturity. Chlorophyll levels, plant growth, root and shoot mineral accumulation (K, Mg, Ca, Na, P, Mn, Zn, Ni, and Co) and *FERRITIN* gene expression were accessed at V5 phenological stage. Results demonstrated that foliar application of $Fe(mpp)_3$ appeared to be more effective at preventing or reducing symptoms of IDC than the same type of application of FeEDDHA (C. S. Santos *et al.*, 2016; C. S. Santos *et al.*, 2021). In a similar study, where seed coating with $Fe(mpp)_3$ and FeEDDHA was attempted, and the amount of time it took for plants of each group to reach each vegetative stage up to V5, as well as the relative chlorophyll levels and the productivity of the plants were analysed, however, no significant differences were found, except in the first test, where plants whose seeds were treated with FeEDDHA seemed to reach stages V4 and V5 faster than $Fe(mpp)_3$ and control group (Rodrigues, 2018). These experiments inspected for the first time on the use of Fe(mpp)3 under alkaline soil conditions for IDC correction and have shown that its foliar application has a longer-lasting effect than FeEDDHA, inducing efficient root responses and promoting the uptake of other nutrients.

Although these chelates are more efficient and environmentally friendly than the commercially available ones, new strategies need to be put in place in order to reduce the amount of product that remains in the soil. This may be achieved by employing different methods of application that provide a controlled uptake by the plants' roots.

1.4. Nanoparticles in plant fertilisation

Nanoparticles (**NPs**) are usually defined as small particles in the range from 1 nanometre to 1 micrometre (Naito *et al.*, 2018). The small size of these particles, as well as their large surface area, high particle number per mass unit and the fact that the atoms in the surface have fewer direct neighbours, grants NPs special properties relating to their ability to successfully interact with their surrounding environment compared to particles inside the bulk solid of the same material, since they tend to be more affected by the behaviour of the atoms or molecules that comprise them (Joudeh & Linke, 2022; Naito *et al.*, 2018). Some of these properties include lower energy per atom and high reactivity (Joudeh & Linke, 2022). Additionally, due to their small size, NPs may be impacted by quantum confinement, leading to changes in magnetic properties and electron affinity (Joudeh & Linke, 2022). These particles can possess different shapes, sizes and structures, as well as be uniform or composed by different layers, which are usually divided in surface layer, shell layer and core layer (Joudeh & Linke, 2022).

These particles are considered extremely useful in several fields such as agriculture, cosmetics and medicine, due to their suitability to be absorbed through biological membranes, and are usually classified based on their composition, namely, organic, carbon-based and inorganic NPs (Figure 1.6) (Joudeh & Linke, 2022; Naito *et al.*, 2018; Vega-Vasquez *et al.*, 2020).

Organic NPs, which include lipidic and polymeric NPs, such as dendrimers, liposomes, micelles and protein complexes, are normally biocompatible and biodegradable, as well as often being formed by non-covalent intermolecular interactions, which allows an easier clearance from the body, making them the most suitable for the biomedical field, where they can be used as nanocarriers (Joudeh & Linke, 2022). Nanocarriers, which are often composed by NPs, are delivery systems of bioactive compounds, such as pharmaceutical drugs or agrochemical agents, designed to provide a targeted delivery of a required dose, in a more time-controlled and eco-friendly manner, as well as protect the therapeutic loads and make them overcome biological barriers (El-Hammadi & Arias, 2022; Vega-Vasquez *et al.*, 2020).

Carbon-based NPs, consisting of NPs built exclusively from carbon atoms, such as fullerenes, carbon black NPs, carbon nanotubes and carbon quantum dots, which, due to their electrical conductivity, high strength, electron affinity, optical, thermal and sorption properties, make these

particles appropriate for applications such as drug delivery, energy storage, bioimaging and photovoltaic devices (Joudeh & Linke, 2022).

Inorganic NPs, including metal NPs, possess unique optical, electrical, thermal magnetic and biological properties, making them relevant materials for the development of nanodevices, mostly for chemical, biomedical and pharmaceutical applications; ceramic NPs, which are made of carbonates, carbides, phosphates, oxides of metals and metalloids, are mainly used for biomedical applications; semiconductor NPs, which possess properties between metals and non-metals, represent important materials in photocatalytic, optic and electronic devices (Joudeh & Linke, 2022; Naito *et al.*, 2018; Vega-Vasquez *et al.*, 2020).

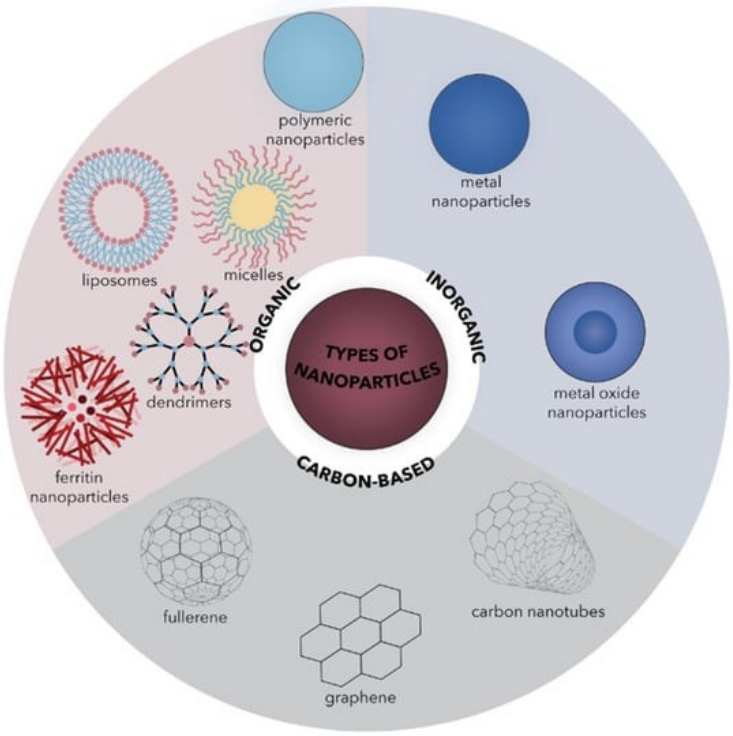

Figure 1.6- Simplified representation of the predominant types of nanoparticles (adapted from Spirescu *et al*., 2021).

As NPs degrade inside the target body or environment, the drugs are released in a controlled manner, providing a longer circulation time inside the vascular system and improved drug efficacy and delivery (El-Hammadi & Arias, 2022). Factors such as polymer composition, degree of crystallinity, glass transition temperature, molecular weight, size, shape and environment pH, all

influence the rate of degradation of NPs, therefore influencing the drug release rate (El-Hammadi & Arias, 2022).

Nanoparticles have demonstrated effectiveness in various biomedical applications, including their use as vectors in intravenous iron infusions for treating iron deficiency anaemia, and in the targeted delivery of trastuzumab for breast cancer treatment (Schaefer *et al.*, 2020; Yetisgin *et al.*, 2020).

Poly(D,L-lactide-co-glycolide) (PLGA) is one of the most commonly used biocompatible polymers to produce NPs due to their interesting advantages, such as improved drug efficacy and delivery, augmented drug solubility, modified pharmacokinetic profile, low toxicity and a longer blood circulation time, among others (El-Hammadi & Arias, 2022). PLGA-based NPs have been widely tested as nanocarriers in the last decade, and show a great deal of promise for several types of therapy, for example, in colon cancer therapy, where it has been shown to be able to deliver 5-Fluorouracil, a chemotherapeutic agent, more effectively to the target area, inducing a higher cancer cell death rate (Alsaab *et al.*, 2022).

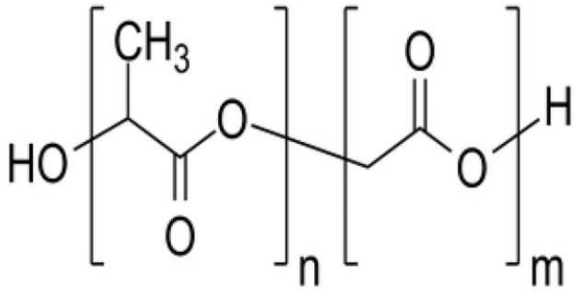

Figure 1.7- Chemical structure of Poly(D,L-lactide-co-glycolide). n is the number of units of lactic acid; m is the number of units of glycolic acid (adapted from Rapier *et al.*, 2021).

1.4.1. Nanoparticles as nanofertilisers

As mentioned before, the systematic use of commercial fertilisers has a tendency to create significant environmental and economic impacts, which can have long lasting effects (Vega-Vasquez *et al.*, 2020). One of the main issues with the current method of application of chemical fertilisers is that a considerable portion of these materials is not absorbed by crops, remaining instead on the soil, where they may eventually be washed away by water, either horizontally or vertically to the groundwaters, or go into the atmosphere by volatilization (Vega-Vasquez *et al.*,

2020). By utilizing nanocarriers for the delivery of fertilisers, the uptake and interaction of nutrients can be augmented, improving release profiles, enhancing uptake efficiency and increasing yields, therefore offering relevant economic and environmental advantages (Mastronardi, 2015; Mittal *et al.*, 2020). This efficiency is exacerbated by the fact that plant roots, as well as leaves, are extremely porous on the nano level, allowing for NPs to enter the plant more easily, either via root or foliar application (Mastronardi, 2015).

Several nanofertilisers have shown very promising results, such as: Zinc Oxide (ZnO) NPs, which, through seed priming, were shown to increase the total amount of zinc in peanut seeds, providing improvements such as enhanced germination rates, robust root and shoot growth, increased dry weight, and a bountiful pod yield among the treated seeds (Prasad *et al.*, 2012); Titanium Dioxide (TiO_2) NPs, where a study on interactions of wheat plants with different dosages and sizes of TiO_2 NPs reveals the potential benefits of these nanofertilisers in enhancing the germination and growth of wheat seeds, when compared to bulk TiO_2 (Feizi *et al.*, 2012); Iron oxide (Fe_2O_3) NPs, which, through soil application and in hydroponic conditions, have been shown to have positive effects on spinach growth and development, namely by enhancing stem and root lengths, biomass production, and magnetization properties of spinach plants (Jeyasubramanian *et al.*, 2016).

Although these studies show promise, the mechanisms with which NPs are taken up by plants through root or foliar application, as well as seed priming, must be more extensively researched.

1.4.2. Are nanoparticles taken up by plants?

The uptake of NPs inside plants is highly dependent on various factors, such as plant physiology, and NP size, surface charge (zeta potential) and shape (Mittal *et al.*, 2020).

For root uptake, NPs are initially adsorbed to the root surface, either on the primary or secondary root epidermis, where they can cross it via small pores in the root cell wall, or pass through the intercellular space without crossing the cell membrane (Lv *et al.*, 2019; Wang *et al.*, 2023). Some studies have shown that while positively charged NPs have a greater affinity for the negatively charged outside layer of root epidermis, they are more likely to remain adsorbed to the roots, while negatively charged particles are more likely to be translocated into the apoplast (Avellan *et al.*, 2017; Lv *et al.*, 2019). In order for uptake and translocation to occur, NPs have to transverse the root surface cuticle, epidermis, cortex, endodermis and Casparian strip until finally reaching the

xylem, in order to be transported upwards into the shoots (Lv *et al.*, 2019). Since the cuticle is underdeveloped on the surface of root hairs, NPs may be directly exposed to the epidermis in those regions, where they are hypothesized to take the apoplastic pathway, in which NPs penetrate the space between the cell wall and the plasma membrane or pass through the intercellular space, or the symplastic pathway, which consists in cell-to-cell transport (Lv *et al.*, 2019). In the apoplastic pathway, the particles are then allowed to pass through the cortex and reach the endodermis, but the Casparian strip has to be bypassed by the entry through zones where it has not properly developed (Lv *et al.*, 2019). In the symplastic pathway, it is hypothesized that NPs may cross cells through ion channels, endocytosis or broken membrane intubation (Lv *et al.*, 2019). After reaching the xylem, NPs can then be transported through it upwards to the shoots (Wang *et al.*, 2023).

For foliar uptake, once NPs are sprayed onto the leaves, they deposit in the leaf surface, where they are afterwards absorbed through the cuticle, which only allows for NPs in the scale of 5 nm to pass, or through the stomata, which can allow for the entry of hydrophilic NPs up to 100 nm (Wang *et al.*, 2023). It has also been shown that rod shaped NPs have an advantage in being taken up by the leaves, compared to other shapes, and that positively charged NPs might enter the mesophilic tissue more easily (Wang *et al.*, 2023). The ability of NPs to enter through the openings is also dependent on the characteristics of the species of plant itself, with some studies showing that dicotyledonous plants, such as soybean, may be more efficient in taking up NPs (Lv *et al.*, 2019). After entering the leaf apoplast by the stomatal pathway, NPs are able to undergo long-distance transport through the vascular system, namely, through the phloem, which allows NPs to go from leaf to root (Lv *et al.*, 2019).

Another method of application of nanofertilisers to plants is seed priming, where seeds may be previously treated with nanosuspensions, usually in an aqueous medium, containing key chemicals or drugs, which, due to the small size of NPs, may penetrate the seed coats, reducing certain targeted adverse effects such as salinity, drought, and heavy metal stresses (Shelar *et al.*, 2023). This has been shown, in recent studies, to be related to the ability of these particles to slowly release their carriers and activate key genes during germination, promoting certain stress resistances (do Espirito Santo Pereira *et al.*, 2021). Although seed priming shows promise, there is still a limited number of studies on that topic.

1.5. Knowledge Gaps

There is an extensive knowledge gap regarding the uptake of NPs by plant roots, with very few information regarding the ideal size for uptake of these particles, and there seems to only be a consensus regarding the fact that negatively charged NPs seem to be more easily absorbed by root tissue.

One of the most critical areas yet to be fully explored is the usage of iron(III) chelates from the 3,4-HPO family as nanofertilisers, and the effectiveness of these particles in providing iron to plants in iron-deficient conditions, as well as comparing their performance to solutions of the same compounds.

Additionally, no studies have been found regarding the application of seed priming techniques to reduce the symptoms of IDC, and this field requires further investigation to the fact that this method of application is extremely useful in reducing the environmental impact of fertilisers.

Finally, although some studies have shown that iron scarcity induces the expression of *IRT1* and *FRO2*, further experimentation is necessary in order to validate this hypothesis (C. S. Santos *et al.*, 2020).

1.6. Research Objectives

The main goal of this study was to develop polymeric NPs, able to supply iron chelates ($Fe(dmpp)_3$ and $Fe(mpp)_3$) to soybean plants grown in alkaline, iron-deficient conditions and to alleviate plant's symptoms of IDC.

The specific objectives were to:

- Evaluate the potential of NPs to enter plant roots. To do this, we aimed to produce and label different-sized polymeric NPs with **rhodamine B** (RB) and test these for root uptake using confocal fluorescence microscopy.
- Based on the compound's transport to plant leaves, **determine the most suitable NP size** for future iron nanofertiliser development.
- **Produce iron nanofertilisers** by replacing the RB with the iron chelates Fe(mpp)3 or Fe(dmpp)3 and evaluate the chelate encapsulation rates and physicochemical properties.

- **Evaluate the effectiveness of such nanofertilisers on plants** grown under iron deficient conditions via morphological and genetic analysis (*FRO2*, *IRT1*, and *FERRITIN*).

2. Materials and Methods

2.1. Preparation and optimization of rhodamine B loaded nanoparticles

Firstly, a Poly(vinyl alcohol) (PVA) 2.0% stock solution was prepared, by weighing 2 grams of PVA (Sigma-Aldrich®, St. Louis, MO, USA) and dissolving it in 100 mL of water in a RT 15 heating plate (IKA Werke®, Staufen, Germany). This solution was later separated and diluted into the required concentrations for NPs production.

Secondly, the RB (Sigma-Aldrich®, St. Louis, MO, USA) stock solution (1mg/mL) was prepared, by dissolving 2 mg of rhodamine B (RB) in 2 mL of acetone (VWR Chemicals, Radnor, PA, USA) and using an ultrasonic bath to homogenize the mixture.

In order to obtain several different-sized nanoformulations, several strategies for their production were devised, with the objective of selecting three different groups, which would later be labelled as “small”, “medium” and “large” nanoformulations, according to their size.

Strategy 1

In the first optimization attempt, and with the intent of obtaining NPs with a size ranging between 110 and 250 nm, nine 10 mL suspensions were prepared (Table 2.1), three of which contained 5 mg of PLGA (Corbion® PDLG 5004A, Amsterdam, Netherlands) and concentrations of PVA of 0.1%, 0.5% and 1.0%. For the six other nanoformulations, 10 mg of the polymer was used, with concentrations of PVA equal to the ones mentioned above. Using a VCX-130 Vibra-Cell™ Ultrasonic Liquid Processor sonicator (Sonics & Materials®, Newtown, CT, USA), different sonication times were selected for each sample. After all the main reagents were assembled, 100 µL of RB stock solution and 900 µL of acetone were added to each microtube containing PLGA, forming the organic phase. Then, one at a time, the nanosuspensions were prepared in a sonication tube by adding 5 mL of the PVA solution with the desired concentration and then 1 mL of the organic phase with the required PLGA amount was slowly added. The tubes were then slightly stirred by hand and sonicated at 70% for the specified time (Table 2.1). After each sonication, the contents of the tube were transferred to a flask and 5 mL of 0.1% PVA solution was added to all

types of nanoformulations obtained from this strategy. The flasks were then placed, one at a time, in a heating plate at 20 ºC with magnetic stirring at intensity 4 and left overnight. The following day, the flasks were removed from the plate and put in the freezer at 4ºC and left for 24 hours (Chaves *et al.*, 2018).

Strategy 2

In the second optimization attempt, fifteen suspensions were prepared using the same protocol as before but testing more combinations comprising different sonication times, as well as PLGA and PVA concentrations. This time, six of the formulations contained 2 mg of PLGA, three of which were sonicated for 1 minute and the others for 5 minutes, at 70 of amplitude. Three others contained 5 mg of PLGA and were sonicated for 1 minute and the remaining six containing 10 mg of the polymer and were also divided into two groups with the same sonication times as the 2 mg PLGA suspensions (Chaves *et al.*, 2018). The experimental conditions are summarized in Table 2.1.

Table 2.1- Experimental conditions for the suspensions of strategies 1 and 2, aiming to produce nanoparticles of around 200 nm.

Strategy	[PLGA] (mg/mL organic phase)	[PVA] (%)	Sonication time (m)
2	2	0.1; 0.5; 1.0	1; 5
1; 2	5	0.1; 0.5; 1.0	1
1; 2	10	0.1; 0.5; 1.0	1; 5

Strategy 3

In addition, a third optimization was performed, with the objective of obtaining particles of smaller size. For this, an aqueous phase of 100 mL of H_20 with 0.1% PVA was prepared. Then, an organic phase was formulated by combining 200 µL of the same RB stock solution previously prepared in 1.8 mL of acetone and dissolving 10 mg of PLGA in this solution. After this, this phase was added to the aqueous one in a slow and controlled manner, and, after a one-minute sonication at 70% intensity, the suspensions were left in a heating plate at 25º and moderate stirring. Additionally, an attempt at nanoprecipitation was made, where the organic phase was added to the aqueous one

with a syringe at the rate of around 2 mL/min and the sonication step was skipped. The suspensions were then maintained in the refrigerator at approximately 4ºC (Huang & Zhang, 2018). The experimental conditions are summarized in Table 2.2.

Besides the alterations made to the production protocol, some modifications were also taken into account for the analysis method. One alternative to the direct measurement in the dynamic light scattering (DLS) device ZetaPALS (Brookhaven Instrument Corps, Holtsville, NY, USA) equipment was the centrifugation of the samples at 11000 rpm for 30 minutes using an FC5816R centrifuge (OHAUS, Parsippany, NJ, USA). Then, the supernatant was discarded, and the pellets were resuspended in H_20. The suspensions were subsequently analysed using DLS as standard. Another alternative was the use of lyophilized samples from the prepared nanosuspensions. After keeping them at about -80ºC for about 24h, they were lyophilized at around that same temperature and 1 MPa of pressure. The resulting solid compound was then resolubilized in water, first by adding 1 mg to 2 mL of H_20 and then 3 mg to that same volume followed by rigorous stirring.

Strategy 4

In the fourth optimization attempt, the surfactant used was Pluronic F-68 (Sigma-Aldrich®, St. Louis, MO, USA) instead of PVA. In the beginning, a solution of 10 mL and 1% of this compound was prepared to be used as the aqueous phase. After this, the organic phase was prepared by mixing 10 mL of ethyl acetate (Sigma-Aldrich®, St. Louis, MO, USA) with 300 µL of RB/acetone stock solution. After 100 mg of PLGA was dissolved in this phase, the resulting solution was added dropwise to the aqueous phase under continuous stirring, after which the final mixture was vortexed for one minute and sonicated at 30%, for 25 seconds on an ice bath (Haque *et al.*, 2018). Subsequently, 20 mL of H_20 were added to the suspension on a heating plate at 25 ºC and 800 rpm after which it was left in those conditions for 24 hours. In the following day, the suspension was centrifuged at 11000 rpm for 30 minutes. The supernatant was removed by evaporation at room temperature and pressure and the precipitate was diluted in 2 mL of water, and then diluted by 9 times and 27 times for DLS analysis. The experimental conditions are summarized in Table 2.2.

Strategy 5

The next method attempted aimed at the production of NPs with 60 nm, and employed the use of a different polymer, sodium alginate. Firstly, 1g of honey was dissolved in 100 mL of deionized water to function as a surfactant and stabilizer. After this, 1g of the polymer and 200 µL of the RB/acetone stock solution previously described were added to the solution. Lastly, 10 mL of a 1% $CaCl_2$ was added dropwise by using a syringe. The suspension was then sonicated at 70% intensity for 1 minute and left in the heating plate for 4 hours (Thomas *et al.*, 2020). The resulting formulation was subsequently centrifuged at 11000 rpm for 30 minutes before DLS analysis. The experimental conditions are summarized in Table 2.2.

Strategy 6

To continue attempting to obtain NPs with an average size in the range of 100 nm, the following procedure was attempted: 10 mg of PLGA was weighed and dissolved in 650 µL of acetone with 150 µL of 99% Ethanol (Labchem®, Zelienople, PA, USA) and 200 µL of RB/acetone stock solution. This organic phase was then homogenized and quickly added with a syringe to the aqueous phase of either 10 mL deionized water or 10 mL 0.5% Tween 20 solution (Sigma-Aldrich®, St. Louis, MO, USA). The nanoformulations were then kept under stirring for 3 hours at 20ºC (maximum stirring mode). Lastly, the suspensions were filtered by using a 200 nm filter and placed at 4 ºC for 24h (Chang *et al.*, 2009). The experimental conditions are summarized in Table 2.2.

Table 2.2- Experimental conditions for the suspensions of strategies 3 to 6, aiming to produce nanoparticles of 100 nm or less.

Strategy	Polymer used	Polymer mass (mg)	Surfactant used	Surfactant concentration (%)	Sonication intensity (%)	Sonication time (s)
3	PLGA	10	PVA	0.1	70	60
4	PLGA	10	Pluronic F-68	1.0	30	25
5	Sodium Alginate	1000	Honey	1	70	1
6	PLGA	10	Tween 20; No surfactant	0.5; 0	-	-

Strategy 7

With the intent of creating PLGA NPs with an average size of about 300 nm, 8mg of PLGA was dissolved in 1 mL of dichloromethane (Honeywell®, Charlotte, NC, USA) and 30 µL of RB/acetone stock solution. This organic phase was then added to 2 mL of a 2% PVA solution. The suspension was then sonicated at 70% intensity for 30 seconds and put in the heating plaque at 20ºC in the maximum stirring setting for 3 hours (Fonseca *et al.*, 2021). These conditions are summarized in Table 2.3.

Strategy 8

To formulate NPs with an average size in the range of 500 nm, a 1% medium molecular weight Chitosan (Sigma-Aldrich®, St. Louis, MO, USA) in a 1% acetic acid (VWR Chemicals, Radnor, PA, USA) solution was prepared, and 0.5 mL of a 1% Fucoidan (Sigma-Aldrich®, St. Louis, MO, USA) solution was mixed with 1.5 mL of deionized water. 1.5 mL of the Chitosan solution was added to 1.5 mL of the Fucoidan solution. 30 µL of the RB/acetone solution was also added. The resulting suspension was then pulse-sonicated at 100% intensity (3 seconds of pulse-on and 7 seconds of pulse-off for 30 seconds) and subsequently filtered by using an 800 nm filter (Barbosa *et al.*, 2019). These conditions are summarized in Table 2.3.

Table 2.3- Experimental conditions for the suspensions of strategies 7 and 8, aiming to produce nanoparticles of 300 nm or more.

Strategy	Polymer used	Polymer mass (mg)	Surfactant used	Surfactant concentration (%)	Sonication intensity (%)	Sonication time (s)
7	PLGA	8	PVA	2	70	30
8	Chitosan + Fucoidan	1.5 + 0.5	-	-	100	Pulse (3 seconds on 7 seconds off) for 30 seconds

2.2. Preparation of unloaded nanoparticles

After choosing the most effective strategies to obtain the desired particles, suspensions of unloaded NPs were prepared, by using the same strategies employed in the formulation of RB loaded NPs but replacing the volume of RB stock solution by the same amount of the organic solvent used in each strategy. These nanosuspensions were posteriorly analysed by DLS, considering the same parameters and settings described for RB loaded NPs (section 2.3.1).

2.3. Physicochemical characterization of rhodamine B loaded nanoparticles

2.3.1. Nanoparticle size, polydispersity index and zeta potential

To analyse the NPs' size, polydispersity index (PDI) and zeta potential, DLS was used. Both mean particle size and PDI were obtained by using a light incidence angle of 90º at 25 ºC, and the obtained results were the mean of a total of four runs of 2 minutes. The zeta potential was analysed at 20 ºC, with a total of eight runs of ten cycles each. The same studies were performed for unloaded NPs.

2.3.2. Entrapment efficiency and loading capacity

To analyse the encapsulation efficiency (EE) and loading capacity (LC), a calibration curve of RB fluorescence in water was performed and analysed by fluorescence spectroscopy. Three different stock solutions were prepared: the first and second consisted of dissolving 2 mg of RB in 4 mL of deionized water with 10% ethanol (EtOH) and the third was created by combining 20 µL of each of the previous solutions. After this, an aliquot of 7.5 µL of each solution was diluted multiple times first by adding it to a microtube and adding water to a final volume of 500 µL. Then, four more dilutions were performed by adding 250 µL of the previous one to 250 µL of water to create a concentration gradient, as depicted in Figure 2.1.

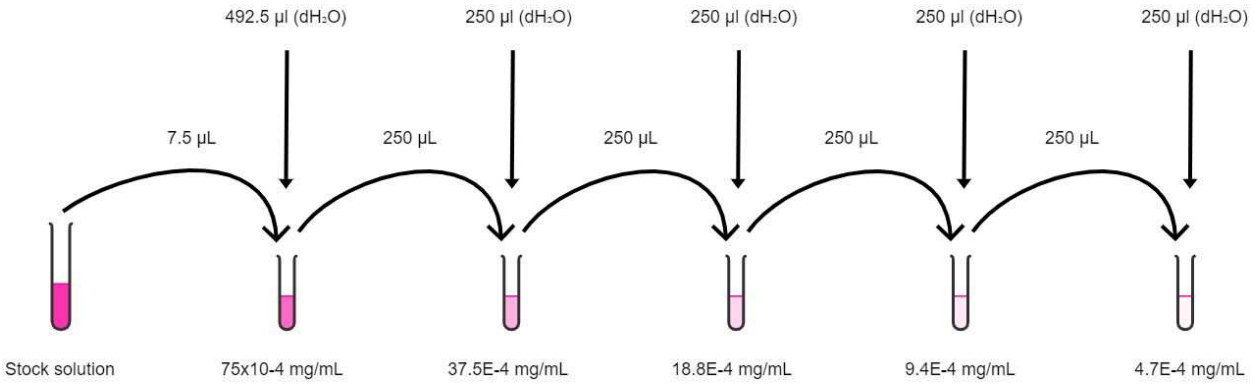

Figure 2.1- Representative scheme of the preparation of the rhodamine B calibration curve.

The samples were then centrifuged at 11000 rpm and 20ºC for 30 minutes. Then, 200 µL of supernatant was transferred to a microplate and its absorbance was analysed considering the following conditions: excitation wavelength 485 nm and emission wavelength 590 nm, with a gain of 50% (Duarte, July 2022).

The EE represents the percentage of compound incorporated into the polymeric matrix of the NPs compared to the total amount of the same compound used for the encapsulation process (Giridhar Reddy & Thakur, 2019). It is calculated using the following formula:

$$\%EE = \frac{total\ compound\ mass - free\ compound\ mass}{total\ compound\ mass}$$

The LC is defined as the total mass of the compound incorporated into the polymeric matrix divided by the mass of the total polymeric system (Massella *et al.*, 2018). It is calculated using the following formula:

$$\%LC = \frac{total\ compound\ mass - free\ compound\ mass}{total\ compound\ mass + total\ polymer\ mass}$$

2.3.3. Release profile

With the aim of changing the entrapment capability of each type of NP over time, a stability study was performed on selected NP formulations (Duarte, July 2022).

To perform the study, 500 µL of each nanoformulation was mixed with 1.5 mL of deionized water in microtubes and incubated at 25ºC and 50 rpm. This process was repeated several times for each

one, since the incubation periods tested were 3 days, 2 days, 1 day, 6 hours, 5 hours, 4 hours, 2 hours, 1 hour, 45 minutes, 30 minutes, 15 minutes and 0 minutes, in triplicates. These tubes were then centrifuged at 11000 rpm for 30 minutes and at 20 ºC. After this, 200 µL of the supernatant of each tube was transferred to a microplate, analysed in a Synergy™ HT plate reader (Biotek®, Winooski, VT, USA) and analysed in the same conditions as mentioned before, in order to determine the amount of RB released by each NP over time.

2.4. Preparation and optimization of PLGA-based nanoparticles loaded with iron chelates

With the intent of creating stock solutions containing both iron chelates for the production of NPs, an organic solvent was selected. Initially, to produce a FeDM stock solution, acetone was chosen, since it was the solvent used in the previously mentioned RB stock solution. However, it proved to be unable to dissolve the iron chelate properly. After this, methanol was attempted, and a final solution of 10 mg/mL was achieved. For the creation of a FeMP stock solution, acetone was also unable to dissolve the compound, so a methanol solution with the same concentration as the FeDM one was selected.

The production of FeDM-loaded NPs was based on the formulations previously used in the preparation of RB loaded NPs but using the FeDM stock solution instead of the RB stock solution. Nanoparticles with “small” size were created by using the same method as in strategy 6, with no surfactant. A nanoformulation with “medium” sized NPs was then produced, based on strategy 1 with 10 mg of PLGA and a 0.1% PVA solution. Lastly, a formulation of “large” NPs was prepared, based on strategy 7. These nanosuspensions were characterized as described in subsections 2.5.1 and 2.5.2.

For FeMP-loaded NPs, dichloromethane was selected as the optimal organic solvent to mix with the methanol-based stock solution. After this, two nanoformulations were created: “small” NPs were obtained, without surfactant, by adding an organic solvent composed of 200 µL of FeMP stock solution, 650 µL of dichloromethane and 150 µL of pure ethanol to 10 mL of deionized water, sonicating it for 1 minute at 70% intensity, kept under stirring for 3 hours and then filtered using a 200 nm filter and kept at 4ºC overnight; the other nanoformulation called “medium” was based on strategy 1 with 10 mg of PLGA and 0.1% PVA, containing FeMP stock solution instead

of RB stock solution and replacing acetone by dichloromethane. These suspensions were characterized as described in subsections 2.5.1 and 2.5.2.

2.5. Physicochemical characterization of iron chelate-loaded nanoparticles

2.5.1. Nanoparticle size, polydispersity index and zeta potential

To analyse the NPs' size, PDI and zeta potential, the same steps as explained in subsection 2.3.1 were taken.

2.5.2. Entrapment efficiency and loading capacity analysis

To determine the EE and LC of the iron chelate loaded nanosuspensions, a calibration curve of both FeDM and FeMP absorbance in water was created. With the intent of achieving this, the same process was performed for both compounds. This consisted of creating two 0.07 mg/mL stock solutions of each chelate in deionized water, and a third one composed by a combination of the two previous ones. After this, nine other solutions were created per stock, by adding, successively, 900 µL, 800 µL, 700 µL, 600 µL, 500 µL, 400 µL, 300 µL, 200 µL and 100 µL, for a total volume of 1 mL per solution, completed with water, as depicted in Figure 2.2. These solutions were then homogenized, 200 µL of each were added to a transparent microplate, which was then placed in a plate reader to determine the absorbance of each solution in a range of wavelengths from 400 to 600 nm. After the first results, the specific wavelength of both chelates was determined to be 455 nm.

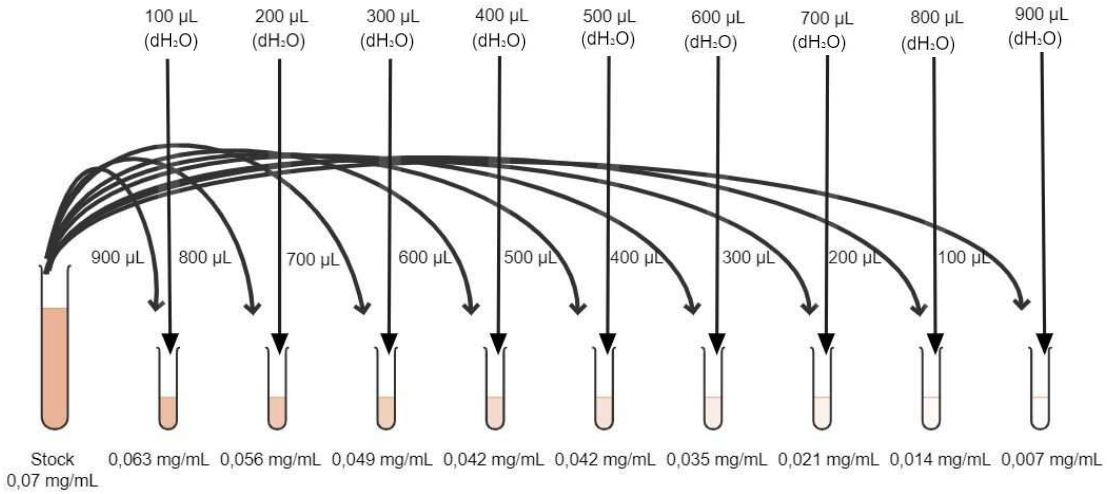

Figure 2.2- Representative scheme of the preparation of both FeDM and FeMP calibration curves.

After centrifuging the nanosuspensions at 11000 rpm and 20ºC for 30 minutes, 200 µL of supernatant was added to a transparent microplate, then analysed in a plate reader for absorbance at 455 nm with the intent of determining the EE and LC of their NPs.

2.5.3. Storage stability studies

With the objective of determining the storage life of both iron-loaded NPs both at room temperature (≈21ºC) and at 4ºC, stability studies were performed. Four replicates of "small" and "medium" nanosuspensions of each chelate were prepared and their volumes divided in half and distributed in two groups, one for each temperature of the study. For FeDM, eight nanosuspensions of "large" particles were produced and four were allocated to each group.

After preparing all the nanosuspensions, one group was kept at room temperature while the other was stored at 4ºC, and the study lasted for six weeks. In this duration, various analysis was performed on the particles' size, PDI, zeta potential, EE and LC on the week the study began and the first, second, fourth and sixth weeks after the beginning of the study.

2.6. Fourier-transform infrared spectroscopy analysis

The next part of the study consisted of performing a Fourier-transform infrared spectroscopy (FTIR) analysis, using Frontier FT-IR spectrophotometer (PerkinElmer, Beaconsfield, UK) equipped with an attenuated total reflectance (ATR) accessory. The three types of RB-loaded NPs,

their unloaded counterparts, as well as all reagents used for their creation were analysed, in order to assess the interaction between them, as well as identifying notable chemical bonds on the products. This process was then repeated for all the FeDM and FeMP NPs described in sections 2.4., as well as all the reagents used in their protocol, including the iron chelates themselves. Spectra were collected from 4000 to 600 cm-1, considering 32 scans and a resolution of 4 cm-1.

2.7. Evaluation of nanoparticle uptake by soybean plants

2.7.1. Soybean germination

A total of twenty-five soybean seeds (variety V26) were germinated in wet filter paper on Petri dishes and left in the dark at room temperature for a week (Figure 2.3).

Figure 2.3- Germinating seeds in a petri dish.

2.7.2. Soybean hydroponic culture

After germination, seeds were transferred to a hydroponic system. A maintenance solution was prepared to provide the necessary nutrients and medium for the germination and growth of *G. max* plants. The solution was composed by 1.2 mM KNO_3; 0.8 mM $Ca(NO_3)_2$; 0.3 mM $MgSO_4.7H_2O$;

0.2 mM $NH_4H_2PO_4$; 25 µM $CaCl_2$; 25 µM H_3BO_3; 0.5 µM $MnSO_4$; 2 µM $ZnSO_4.H_2O$; 0.5 µM $CuSO_4.H_2O$; 0.5 µM MoO_3; 0.1 µM $NiSO_4$; 0.1 g L^{-1} CaO; 0.06 g $NaHCO_3$. A 20 mM ferric sodium solution (FeNaEDDHA) was prepared added to each hydroponic growth pot independently. The pH of the solutions was monitored using a IKA RH basic 2 pH meter (IKA Werke®, Staufen, Germany) and buffered with a 200 mM (2-(N-morpholino)ethanesulfonic acid) (MES) medium solution (Sigma-Aldrich®, St. Louis, MO, USA) adjusted to 5.5.

Plants were grown in black pots filled with 5 L of hydroponic solution and 2.5 mL of FeNaEDDHA (Figure 2.4) and placed in a climate chamber (Aralab Fitoclima 10000EHF) with 16 h day photoperiod providing 325 µmol s^{-1} m^{-2} of photosynthetic photon flux density at plant level supplied by a mixture of incandescent bulbs and fluorescent lights. Temperature was set to 25°C during the light period and to 20°C during the dark period, whereas relative humidity was maintained at 75% throughout day and night.

Figure 2.4- Hydroponic culture arrangement.

Plants grew for two weeks, in which the hydroponic solution, along with FeNaEDDHA, was renewed at the 7^{th} and 10^{th} days.

2.7.3. Rhodamine B uptake study

After the 14th day, ten plants were randomly selected and carefully removed from their pots, and their respective roots were placed, in duplicate, in contact with 40 mL of different solutions/nanoformulations for 24 hours. These groups included the 'small', 'medium', and 'large'

nanosuspensions, as well as a 20 μM aqueous RB solution, while ensuring the plants remained intact throughout this process. A control group was also assembled, which consisted of allocating the plants' roots to be in contact with deionized water. This experiment was performed in duplicate, and the arrangement is represented in Figure 2.5.

Figure 2.5- Rhodamine B uptake study arrangement.

2.7.4. Confocal fluorescence microscopy of rhodamine B in plant tissues

After performing the RB uptake study in soybean plants, two representative samples of the roots, stems and leaves of each plant were cut, separated, and kept in formaldehyde (Merck, Darmstadt, Germany) and sent to the histology service at "Instituto de Ciências Biomédicas Abel Salazar (ICBAS)" for sectioning and preparation for analysis. Each sample was paraffin-embedded and sectioned at a thickness of 5 μm without any additional staining. Then, histological analysis was performed by fluorescence microscopy. Images were acquired with a resolution of 1024x1024 using a 10x objective.

Each microscope slide was analysed by a Leica Stellaris 8 confocal microscope (LeicaMicrosystems, Wetzlar, Germany) equipped with the Leica Application Suite X package (LAS X), in order to get qualitative information on the uptake of the different RB labelled NPs,

along the different tissues of the plant. The wavelength chosen was 560 nm for excitation and 575 nm for emission. The obtained images were then processed using ImageJ software.

2.8. Seed priming and soil cultivation studies

2.8.1. Preparation of artificial soil

To obtain a soil with an easily controlled pH, a standard artificial soil was created, containing, in relative mass, 70% quartz sand (Intex®, Portugal), 20% expanded clay (Argex®, Portugal) and 10% peat (Siro®, Portugal) (OECD, 1984; C. S. Santos *et al.*, 2021). In total, 20 kg of soil were produced, containing 14 kg of quartz sand, 4 kg of expanded clay and 2 kg of peat. In order to increase the pH of the soil to simulate alkaline soils, 1 g of calcium oxide (CaO) (Tintinhas®, Portugal) was added for each kg of soil, with a total of 20 g being added, in order to reach the pH of 8, which was measured using a pH meter (C. S. Santos *et al.*, 2021). The different components were then homogenized thoroughly.

2.8.2. Preparation of FeDM-loaded nanosuspensions and solutions

Thirty mL solutions of the chelate FeDM at concentrations of 20 μM and 10 μM were prepared by diluting the 100 μL of FeDM stock solution in water.

The "medium" FeDM-loaded nanosuspensions were selected and prepared using the method described in subsection 2.4. Thirty mL of FeDM nanosuspensions at 20 μM and 10 μM were prepared by diluting 10 mL of the original preparation in water.

2.8.3. Seed priming

Plants were divided into five groups in individual falcon tubes: four groups were subjected to the different solutions and nanosuspensions described in subsection 2.8.2, and one control group contained water. Twelve seeds were submerged for 24 hours in each one of the priming solutions, nanosuspensions or in water, in the absence of light, at room temperature and without stirring. After the priming process, each group of seeds was transferred to a petri dish, with moistened filter paper with the corresponding solution or suspension. The setup was then kept in the dark, at room temperature, for a duration of 48 hours. These steps are represented in Figure 2.6.

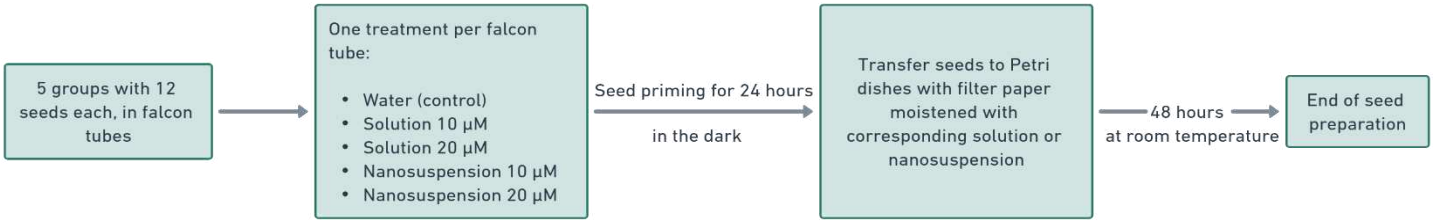

Figure 2.6- Workflow of seed priming and incubation.

2.8.4. Growth conditions

Prior to sowing the seeds, 275 g of the artificial soil were distributed into pots. Thirty litres of nutritive solution was formulated as described in section 2.7.2.

Two primed seeds were sown in each pot, and plants were watered every two days with 80 mL of nutritive solution. The pots were placed in a climate chamber with 16 h day photoperiod providing 325 µmol s^{-1} m^{-2} of photosynthetic photon flux density at plant level, supplied by a mixture of incandescent bulbs and fluorescent lights. Temperatures were set to 25ºC during the light period and to 20ºC during the dark period, whereas relative humidity was maintained at 75% throughout day and night. Following germination, each pot containing two viable plants had one of them transplanted to a suitably labelled pot, to which the same watering regime was applied. Ten independent replicates were maintained for a duration of three weeks starting from sowing date until the V3 phenological stage was reached. At this stage, plant tissues were divided into: **i.** roots; **ii.** 3rd trifoliate; **iii.** 1st and 2nd trifoliates; **iv.** cotyledons, unifoliates and stem. Tissues were placed in liquid nitrogen in order to carry out the determinations for subsection 2.8.5 and stored at -80 ºC, to preserve the biological material for further studies.

Figure 2.7- Pot setup after seed sowing.

2.8.5. Morphological and productivity parameters

Plant size was measured daily, and the dates of formation and maturation of each trifoliate were recorded. Leaf chlorosis was assessed from V1 to V3 with SPAD readings, measured with a portable chlorophyll meter (Konica Minolta SPAD-502Plus) using the youngest trifoliate leaf of each individual replicate.

At harvest, each plant was separated between the root and the aerial part, to measure the root and shoot fresh weight, followed by a separation of the V3 trifoliate from the other leaves and freezing at -80 ºC.

2.8.6. Genetic analysis

Plants' roots and V3 trifoliates were pulverized in liquid nitrogen, and the total RNA was extracted using RNeasy® Plant Mini Kit (#74904) (Qiagen, Hilde, Germany), according to the manufacturer's instructions. The obtained RNA's quality and quantity was then verified by UV-spectrophotometry, using a nanophotometer (Implen, Isaza, Portugal). Posteriorly, single-strand cDNA was synthesized using the protocol and reagents provided by iScript™ cDNA Synthesis Kit (Bio-Rad, Laboratories, Inc, Hercules, CA, USA). *FERRITIN*, *FRO2* and *IRT1* primer sequences, as well as the ones for the reference genes *18S* and *ACTIN* were taken from (C. S. Santos *et al.*, 2020) and are shown in Table 1A (in appendix).

qPCR reactions were performed on a CFX96 TouchTM Deep Well Real-Time PCR Detection System (Bio-Rad, Laboratories, Inc, Hercules, CA, USA), using SYBR Green Supermix (Bio-Rad, Laboratories, Inc, Hercules, CA, USA), and in the following reaction conditions: 95 ºC denaturation for 10 minutes, followed by 40 cycles with 15 s at 95 ºC, 30 s at 56-58 ºC (depending on the annealing temperature of the specific primer being used, shown in Table 1A), followed by melt curve stages to check that only single products were amplified. In order to perform the relative quantification of iron-related genes' expression values, the comparative ΔΔCt method (Livak & Schmittgen, 2001) was used, in which the geometric mean of the expression of the two stable reference genes (*18S* and *ACTIN*) is used as controls transcripts and the samples from plants not treated with iron as reference samples. Two technical replicates were analysed, and the data was transferred to Excel files and plotted as graphs of normalized fold expression of target genes.

2.8.7. Mineral analysis

Inductively coupled plasma optical emission spectrometry (ICP-OES, or ICP) was used to quantify metal concentrations in third trifoliate samples and were performed at Unidade de Análise Instrumental (Universidade de Santiago de Compostela, USC, Galicia, Spain). ICP-OES analysis were registered with with a spectrometer Agilent 5900 with One-Neb nebulizer and cyclonic spray chamber.

2.9. Statistical analysis

Statistical analysis was performed using GraphPad Prism Software (Version 9.0 for Windows; GraphPad Software Inc, San Diego, CA, USA). T-student test, one-way and two-way ANOVA analysis of variance was used to assess the differences in the results. The test used in specified in each figure.

3. Results and Discussion

3.1. Production and characterization of rhodamine B-loaded nanoparticles

One of the main aims of the present work is to get insight on the eventual relevance of NPs' size for their uptake by plants. For this, several polymeric nanosuspensions were produced with the objective of obtaining NPs with a range of sizes from 100 nm to around 300 nm. This may be a key step in ascertaining the efficiency with which plant tissues could absorb these particles and then manage IDC. Polydispersity index (PDI), which is associated with the degree of homogeneity of the NPs, is usually considered acceptable in the range of 0.3 and below, since the particles are intended for biomedical applications (Zhang & Wang, 2023). Additionally, and as explained previously, having negative zeta-potentials is one of the objectives, as these are more likely to be translocated into the apoplast. Moreover, having substantial EE and LC is also crucial, since it means that the compounds are successfully incorporated into the polymeric matrix, ensuring that the NPs are able to carry them to the desired location.

3.1.1. Physicochemical properties

Strategies 1 and *2* consisted of the same method with different conditions of surfactant (PVA) concentration and sonication time. Particles had sizes varying from around 135 to 290 nm and PDI of 0.04 to 0.136. Considering the two smaller amounts of PLGA, it was not possible to obtain measurable NPs. The conditions of 0.1% PVA, 1 minute of sonication and 10 mg of PLGA were later chosen as the protocol for "medium" NPs, with a size of 246±5.5 nm and a PDI of 0.10±0.03, and their zeta potential, EE and LC were determined later to be -6.6±0.18 mV, 72.3±5.58% and 1.40±1.0%, respectively. This variant was chosen due to their favourable size, significant zeta-potential and relatively high EE percentage.

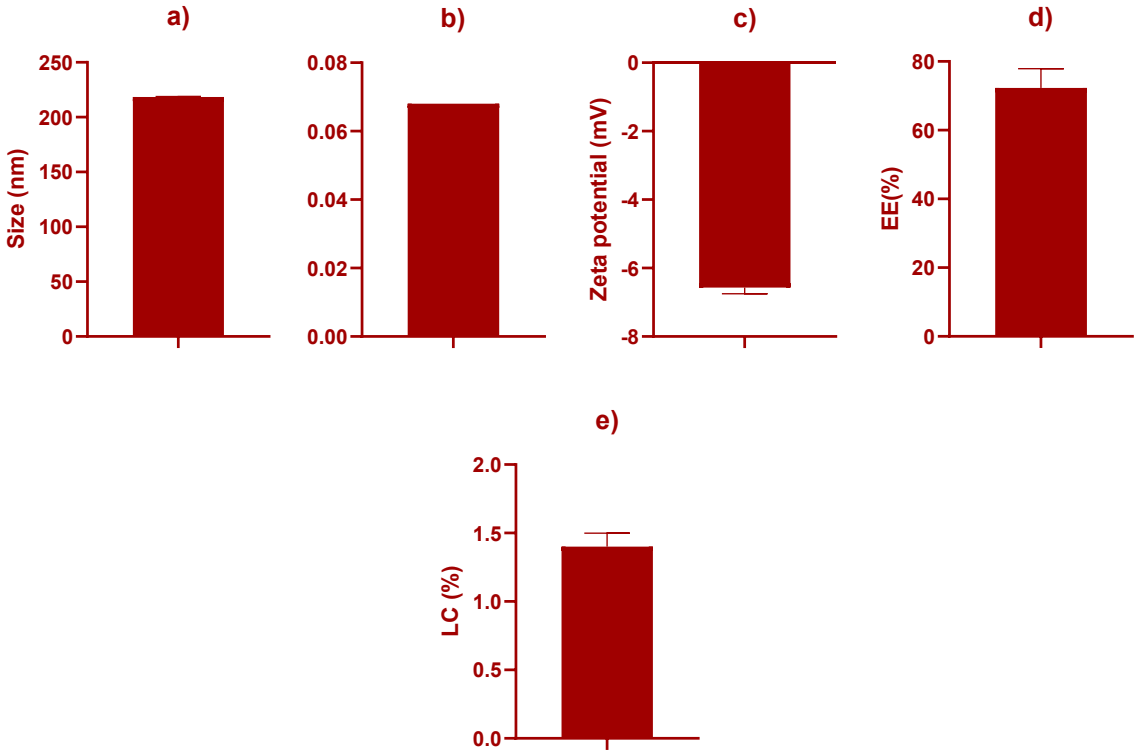

Figure 3.1- Size (a), polydispersity index (PDI) (b), zeta potential (c), encapsulation efficiency (EE) (d) and loading capacity (LC) (e) of "medium" nanoparticles produced by *strategies 1* and *2*.

Aiming to obtain NPs of lower size, *strategy 3* was considered, and sizes varied between 175 and 245 nm, while PDI varied between 0.06 and 0.38. However, since the protocols were more laborious than the one for *strategies 1* and *2*, and the results were similar, this method was discarded, and no further analysis was conducted.

Strategy 4 produced NPs in the range of 600 nm for both the attempted dilutions, which was much higher that desired, since it was expected to obtain NPs with approximately 50 nm (Haque *et al.*, 2018).

Regarding *strategy 5*, the particles created had a size in the range of 6 µm for the supernatant and 25 µm for the pellet, in contrast with the 60 nm that were expected (Thomas *et al.*, 2020), and were also considered too high to be a feasible option, and no further analysis was conducted.

Strategy 6 allowed the obtention of NPs with a size of around 121±2.8 nm, a PDI of 0.09±0.04, a zeta potential of around -15.2±4.5 mV, an EE of around 31.3±4.0% and a LC of 0.63±0.06% for the nanosuspensions without a surfactant. In addition, NPs showing a size of 140 nm, a PDI of

0.06, -5 mV of zeta potential, an EE of 31% and a LC of around 0.6 were obtained by considering the use of tween 20 as a surfactant. The protocol that does not include a surfactant was later chosen to produce "small" NPs, due to their small size and the high negative value of its zeta potential, probably indicating a more stable nanosuspension. Moreover, this approach was considered more sustainable since it does not use additional reagents. Overall, this approach yielded results very similar to the expected ones (Chang *et al.*, 2009).

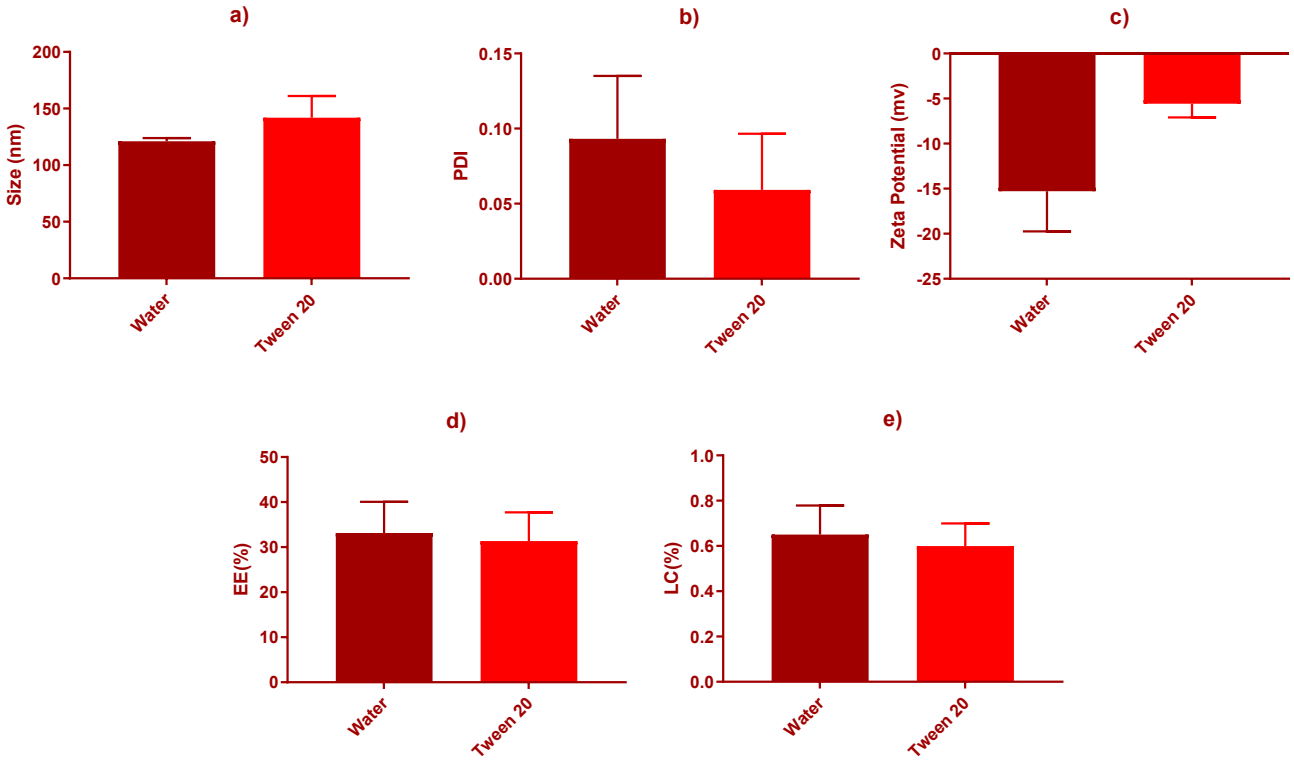

Figure 3.2- Size (a), polydispersity index (PDI) (b), zeta potential (c), encapsulation efficiency (EE) (d) and loading capacity (LC) (e) of nanoparticles produced by *strategy 6*, according to the surfactant used.

To obtain larger NPs, the *strategy 7* was tested, and the produced NPs had a size of 322±33 nm, with a PDI of around 0.15±0.01, a zeta potential of -4.0±1.3 mV, EE of around 38.5±11.3% and LC of 0.17±0.06%. This method was later defined to produce "large" NPs, due to their larger size and their relatively favourable encapsulation properties. The results obtained are similar to those expected (Fonseca *et al.*, 2021).

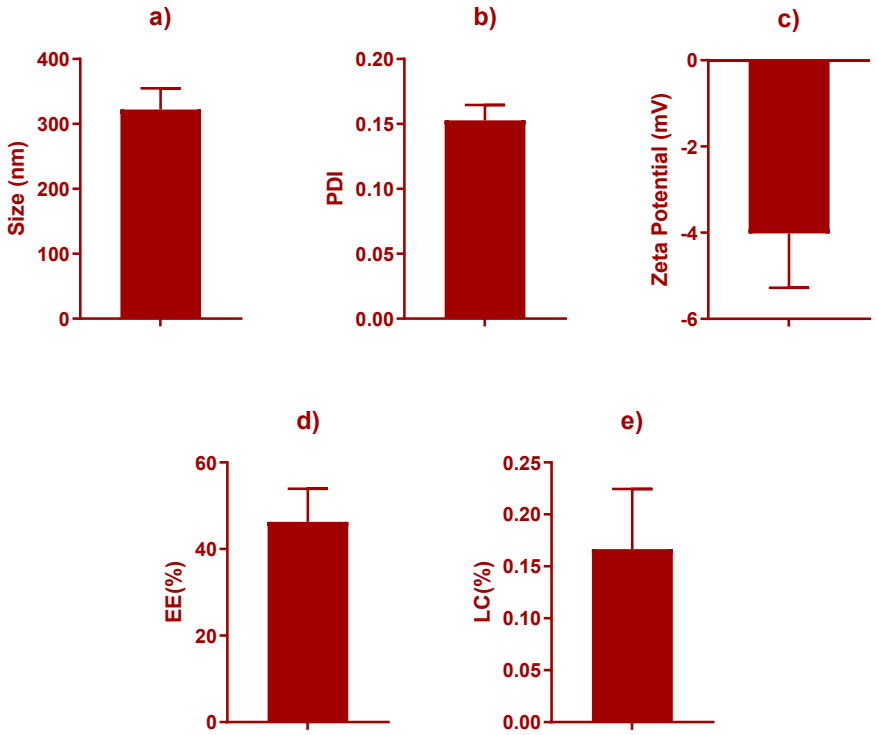

Figure 3.3- Size (a), polydispersity index (PDI) (b), zeta potential (c), encapsulation efficiency (EE) (d) and loading capacity (LC) (e) of nanoparticles produced by *strategy 7*.

The NPs created by *strategy 8* were in the range of 500 nm, also as expected, with a PDI of around 0.25, zeta potential of 44 mV, EE of 59% and LC of around 0.57%. Even though the results obtained were similar to the expected ones, no further analysis was conducted with this method, due to the very large size of the particles (Barbosa *et al.*, 2019).

When the three types of particles that would undergo further analysis were chosen, the full physicochemical analysis on their properties was conducted, depicted in Figure 3.4.

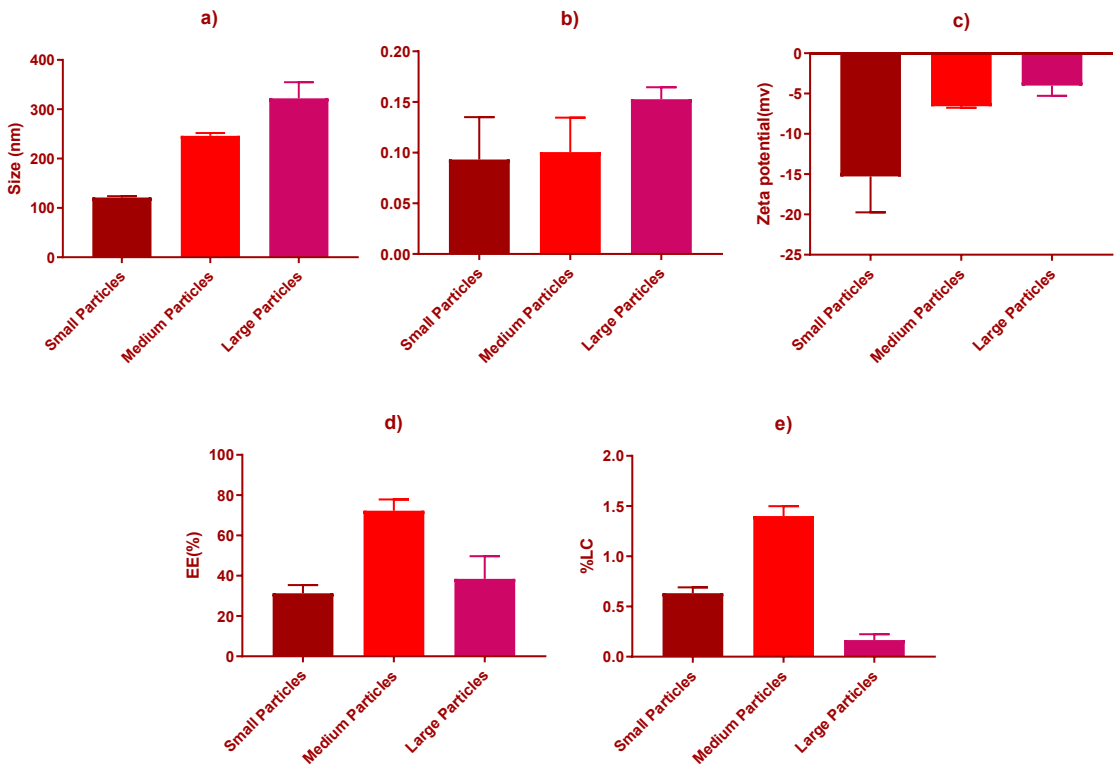

Figure 3.4- Size (a), polydispersity index (PDI) (b), zeta potential (c), encapsulation efficiency (EE) (d) and loading capacity (LC) (e) of "small", "medium" and "large" rhodamine B-loaded nanoparticles.

3.1.2. Release profile

Afterwards, a study on the release profile of the previously described "small", "medium" and "large" NPs was conducted, to determine the ability of the formulations to retain or release RB.

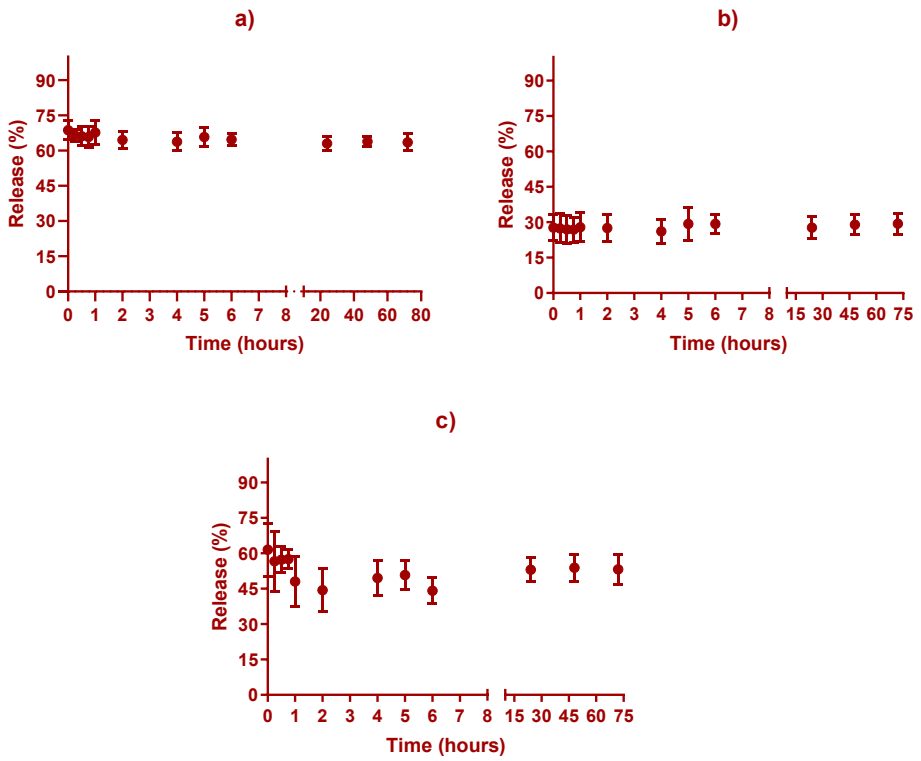

Figure 3.5- Release study for "small" (a), "medium" (b) and "large" (c) nanoparticles.

From Figure 3.5, it can be concluded that for all three types of NPs, the amount of compound released remains stable over three days, at 25 ºC and 50 rpm, in water. These results show that all three nanosuspensions have the potential to keep a significant amount of RB encapsulated for that time, which is a positive characteristic, since it means that the NPs can remain in contact with the target tissues for at least three days without releasing the compound.

3.2. Analysis of the properties of unloaded nanoparticles

The three types of unloaded NPs produced based on the previous methods for the RB-loaded particles were then analysed, and their physicochemical properties were then compared to the ones of the RB loaded NPs of the same type with an unpaired t-test with Welch's correction, with the aim of determining the impact of the compound in the properties of the NPs. The results obtained by the analysis of their physicochemical properties are shown in Figure 3.6. The results comparing unloaded NPs to RB-loaded NPs are represented in Figure 3A of the Appendix.

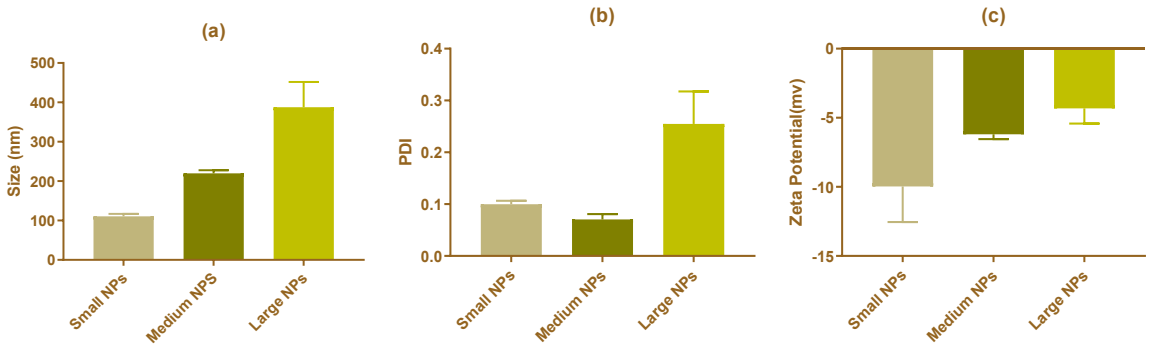

Figure 3.6- Size (a), polydispersity index (PDI) (b) and zeta potential (c) of "small", "medium" and "large" unloaded nanoparticles.

The analysis of data from Figure 3.6 shows that "small" NPs, when unloaded, have a size of 110±6.1 nm, a PDI of 0.1±0.01 and a zeta potential of -10.0±2.6 mV. When compared to the "small" RB-loaded NPs, no statistically relevant differences were encountered (p>0.05), from which we can conclude that the compound has no impact on the physicochemical properties of the NPs.

The unloaded "medium" NPs had a size of 220±7.8 nm, a PDI of 0.07±0.01 and a zeta potential of -6.2±0.3 mV. After statistically comparing these results to those of the RB-loaded "medium" NPs, it was found that these NPs are significantly (p<0.05) smaller. This enlargement may be due to the presence of the compound inside the particle.

Finally, the unloaded "large" NPs had a size, PDI and zeta potential of 368±64 nm, 0.26±0.06 and -4.3±1.1 mV, respectively. No significant differences (p>0.05) were found between this group and the RB-loaded "large" NPs. Therefore, we can assume that the compound does not change the physicochemical properties of the NPs.

3.3. Production and characterization of iron chelate-loaded nanoparticles

3.3.1. FeDM-loaded nanoparticles' physicochemical properties

The next part of the study consisted of developing NPs, similar to the ones developed in the previous sections, but loaded with the 3,4-HPO iron chelate FeDM, in order to later be tested *in*

vivo in soybean plants. The three types of NPs are based on the protocols used for the RB-loaded suspensions with the same designation. The results obtained from analysing their sizes, PDI, zeta potentials, EEs and LCs are depicted in Figure 3.7. These properties were then compared to the ones of the RB loaded NPs of the same type with an unpaired t-test with Welch's correction in order to understand the similarities between the two, so that after studying the uptake of each type of RB-loaded NP by plants, a decision could be made on which class of iron-chelate NP would be used in the final study. The results comparing these two groups are represented in Figure 4A of the Appendix.

The values for LC on FeDM-loaded NPs are all significantly higher (p<0.05) than their counterparts for RB-loaded NPs, showing that the particles' mass is composed of a larger amount of the encapsulated compound (Chaves *et al.*, 2018).

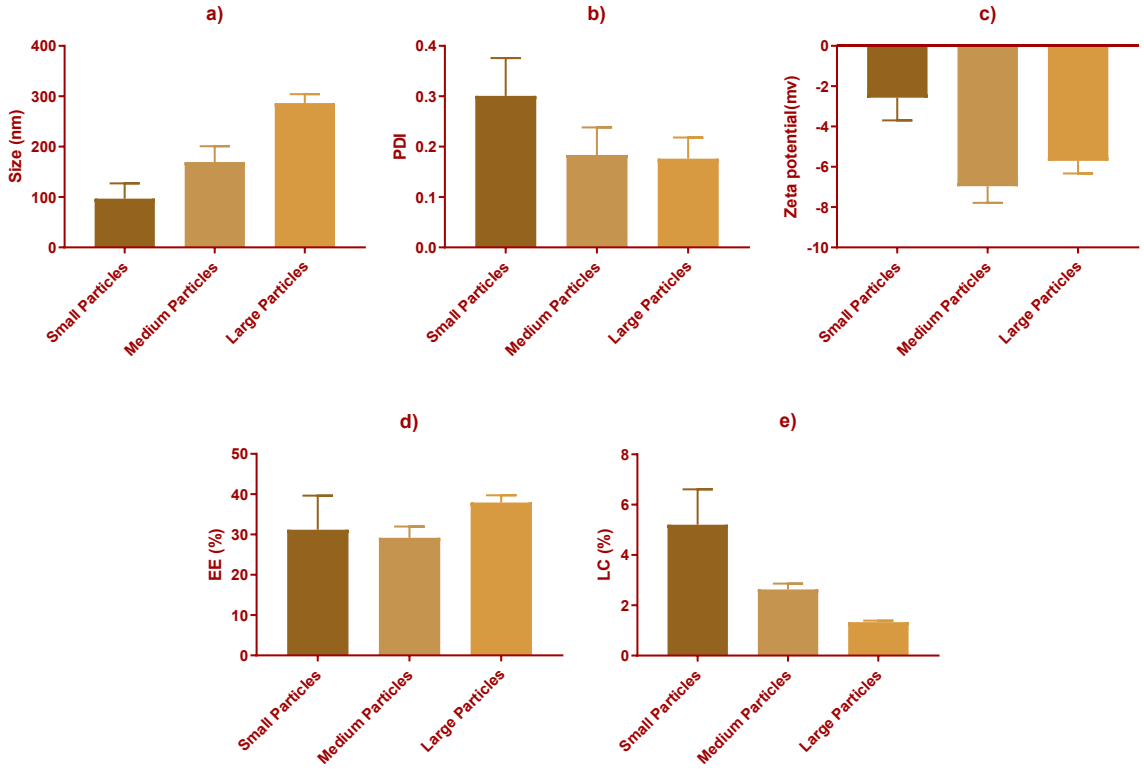

Figure 3.7- Size (a), polydispersity index (PDI) (b), zeta potential (c), encapsulation efficiency (EE) (d) and loading capacity (LC) (e) of "small", "medium" and "large" FeDM-loaded nanoparticles.

As represented by Figure 3.7, the analysis of the physicochemical properties of FeDM-loaded NPs revealed that the "small" ones have a size of 97±17.5 nm, a PDI of 0.30±0.04, a zeta potential of -

2.6±0.7 mV, EE of 31.2±4.9% and LC of 5.2±0.8%. No significant differences (p>0.05) were found in size or EE relatively to "small" RB-loaded NPs, while the FeDM loaded ones had a significantly (p<0.05) higher PDI, most likely due to the higher concentration of the encapsulated chelate and the differences in solubility. Additionally, the zeta potential of the FeDM-loaded NPs is significantly (p<0.05) higher.

The "medium" NPs loaded with FeDM have a size 170±18.0 nm, a PDI of 0.18±0.03, zeta potential of -7.9±0.5 mV, EE of 29.2±1.6% and LC 2.6±0.1%. These NPs were found to be significantly (p<0.05) smaller than the RB-loaded ones, as well as having a lower (p<0.05) EE value. The differences can be related to the different physicochemical properties of the compounds. Nevertheless, the values obtained for the size and EE are in the same magnitude and aligned with the requirements for subsequent tests in plants.

The "large" FeDM-loaded NPs have a size of 287±10,1 nm, a PDI of 0.18±0.02, zeta potential of -5.7±0.4 mV, an EE of 37.9±1.0% and LC of 1.3±0.3%. Except for the latter, none of the physicochemical properties had statistically significant (p>0.05) differences when compared to RB-loaded "large" NPs. The LC value is higher for the FeDM-loaded NPs which represents a positive aspect for the obtained nanoformulations.

3.3.2. FeMP-loaded nanoparticles' physicochemical properties

Afterwards, the same process as the one in section 3.3.1 was attempted for the FeMP iron chelate of the 3,4-HPO class. After several attempts with different organic solvents, particles based on the "small" and "medium" protocols were conceived. The protocol used for "large" RB-loaded NPs was considered but, after various attempts and some modification in the experimental conditions, no NPs were produced with the desired size.

The results obtained from analysing their sizes, PDI, zeta potentials, EE and LC are depicted in Figure 3.8, and these properties were then compared to the ones of the RB loaded NPs of the same type with an unpaired t-test with Welch's correction. The results comparing these two groups are represented in Figure 5A of the Appendix. After analysis, it was concluded that "medium" FeMP-loaded NPs were not able to encapsulate any of the compound, since no chelate was detected upon characterization of the obtained formulation.

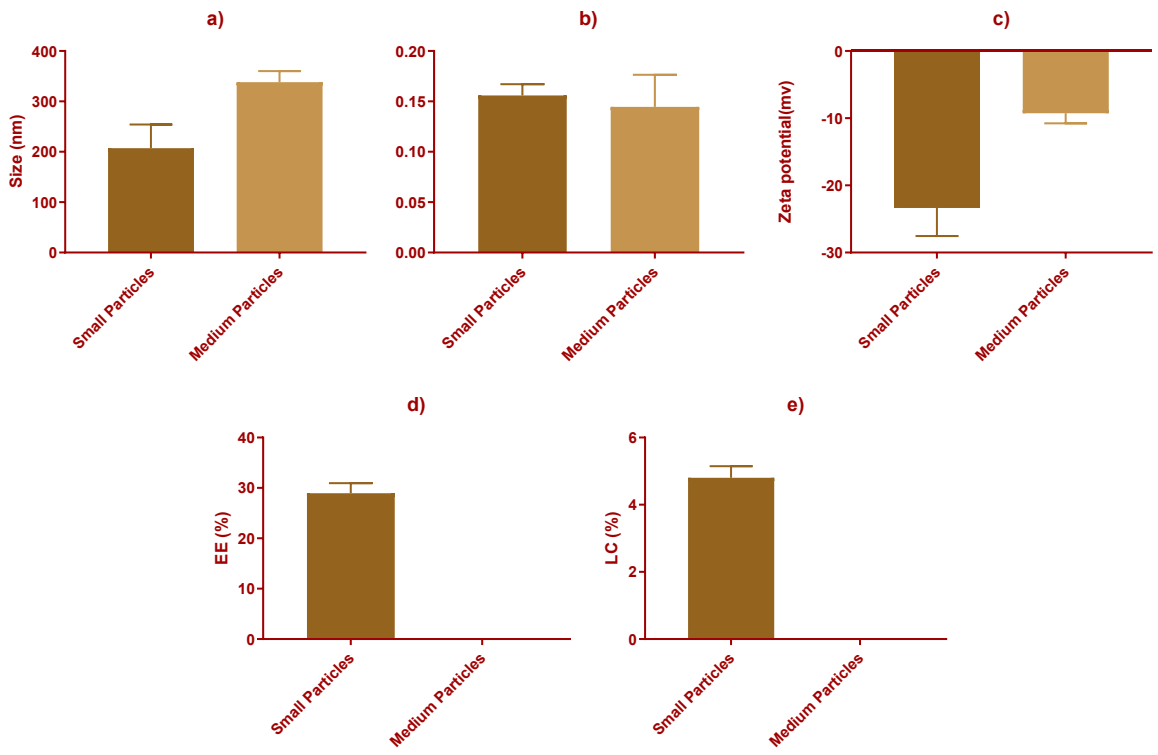

Figure 3.8- Size (a), polydispersity index (PDI) (b), zeta potential (c), encapsulation efficiency (EE) (d) and loading capacity (LC) (e) of "small" and "medium" FeMP-loaded nanoparticles.

The results in Figure 3.8 indicate that the "small" FeMP-loaded NPs have a size of 207±21 nm, a PDI of 0.16±0.01, a zeta potential of -23.4±4.2 mV, an EE of 28.9±1.2% and a LC of 4.8±0.2%. The size and LC of these NPs was found to be significantly (p<0.05) higher than that of the RB-loaded NPs, indicating that a higher percentage of mass of the particles is composed by the encapsulated compound. The PDI, zeta potential and EE don't have any significant (p>0.05) differences between the two groups.

The "medium" FeMP-loaded NPs have a size of 338±9 nm, a PDI of 0.15±0.01, a zeta potential of -9.3±1.5 mV and an EE and LC under the limit of detection with the spectrophotometric method used, suggesting that the particles did not have the ability to encapsulate any of the compound. After comparing these results to the ones for the "medium" RB-loaded NPs, it was concluded that the FeMP ones are significantly (p<0.05) larger, with a significantly (p<0.05) more negative zeta potential. No significant (p>0.05) differences were found regarding PDI.

3.3.3. FeDM and FeMP-loaded nanoparticles' storage stability

The next stage of the study consisted of analysing the storage stability of the iron chelate-loaded NPs, in order to determine how stable the physicochemical properties remain over time, to make conclusions about the storage life of the formulations. With this intent, the different types of NPs described in sections 3.3.1 and 3.3.2 were produced and kept at room temperature and 4ºC, and their properties were monitored for 6 weeks. The results are demonstrated in Figures 6A-10A of the Appendix section.

The "small" FeDM-loaded NPs (Figure 6A) kept at 4ºC had all their physicochemical properties remain stable over the full duration of the study, while the ones kept at room temperature had their PDI significantly (p<0.01) increased in week 6 compared to week 0. Based on this, and even though no significant (p>0.05) difference was observed between groups at any point in the study, it is reasonable to assume that the product is better suited to be stored at 4ºC, since it retains its original properties more efficiently.

Regarding the "medium" FeDM-loaded NPs (Figure 7A), all properties remained stable for both temperature groups up to week 2. At week 4 and up to week 6, the zeta potential for both groups increased significantly (p<0.0001) compared to the value recorded in week 0 for each respective group. Throughout the study period, no significant differences (p>0.05) were observed between the two temperature groups. For these nanoformulations, there is no difference between storage conditions, and even though the zeta potential decreases over time, it remains negative, indicating that the nanosuspensions can still be applied effectively to plant tissue.

In relation to "large" FeDM-loaded NPs (Figure 8A), their size, PDI and zeta potential remained (p>0.05) stable through the six weeks of the study, as well as between the two temperatures. Regarding EE and LC, both groups had a significant (p<0.01) increase in week 1, and these values remained relatively stable until week 6, being higher than week 0 at all points with different degrees of confidence. In the final week, the two properties were still significantly (p<0.001) higher for the particles kept at room temperature compared to week 0, and even higher (p<0.0001) for the ones kept at 4ºC. The values remained equal between conditions over the weeks except in the last week, where the EE and LC of the nanosuspensions kept at 4ºC were significantly (p<0.01) higher than those of the ones kept at room temperature. This increase in the encapsulation and

loading properties may be due to a stabilization of the polymeric matrix over time, allowing for a higher encapsulation along the study. Particles kept at 4ºC ended up with a higher EE and LC, so we can conclude that this is the most recommended way to store this product.

The "small" FeMP-loaded NPs (Figure 9A) had all their physicochemical properties remain stable (p>0.05) in both conditions and over the duration of the study, from which we can conclude that the product can be stored equally at room temperature and at 4ºC, for a total of six weeks, without major differences.

Finally, the "medium" FeMP-loaded NPs (Figure 10A) also maintained their size, PDI and zeta potential over the six weeks and between temperatures. As determined in section 3.3.2, the encapsulation properties were null. From this we can infer that, for at least six weeks, the temperature at which the NPs are stored does not influence their properties.

Overall, the most stable and more favourable types of NPs for the posterior studies are the "small" and "medium" FeDM-loaded NPs, as well as the "small" FeMP-loaded NPs. This is due to their small and unvarying size, low PDI, low zeta potential and relatively high and stable encapsulation properties. We can conclude that the temperature of 4ºC is more advantageous for the storage of the produced NPs.

3.3.4. Fourier-transform infrared spectroscopy assessment

To assess the chemical composition of RB-loaded NPs, a FTIR assessment was performed. This included analysis on the particles themselves, the unloaded NPs and on the reagents that compose them. The results are represented on Figure 3.9.

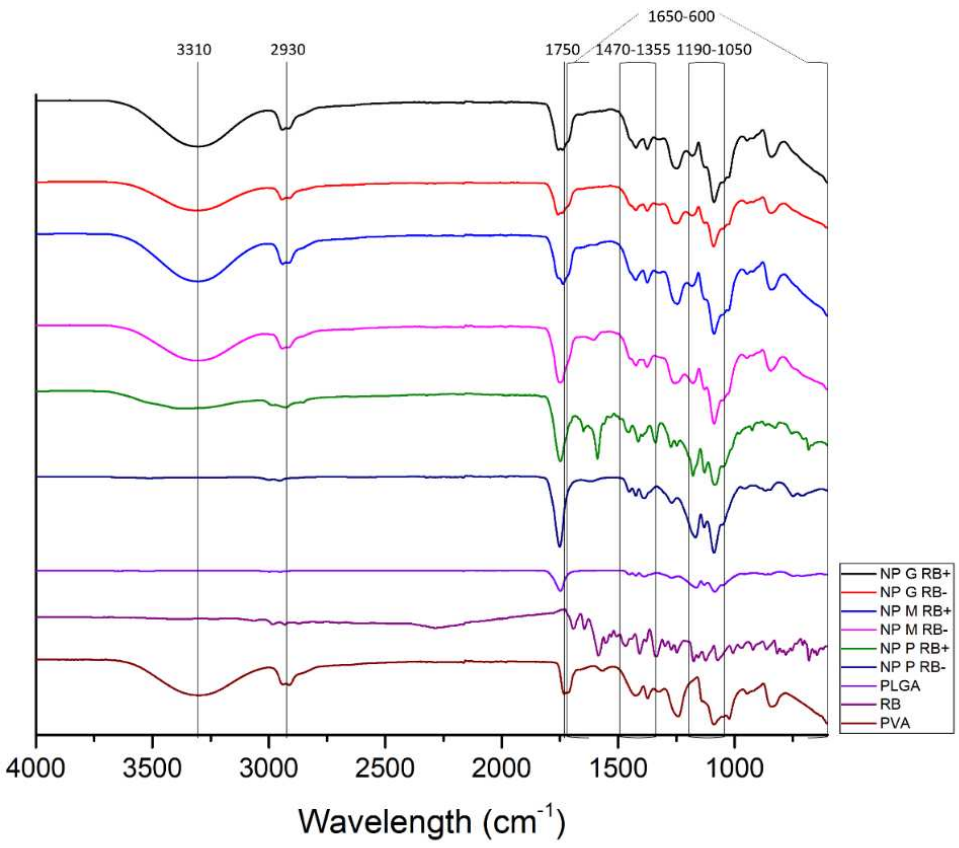

Figure 3.9- Fourier-transform infrared spectroscopy spectra of the three types (P– small; M- medium; G- large) of rhodamine B-loaded nanoparticles (RB+), their unloaded counterparts (RB-), Poly(D,L-lactide-co-glycolide) (PLGA), rhodamine B (RB) and Poly(vinyl alcohol) (PVA), from 600 to 4000 cm^{-1}.

By analysing the spectrum of PVA in Figure 3.9, we can identify two characteristic peaks in the wavelengths of 3310 and 2930 cm^{-1}, which represent OH stretching and CH_2 asymmetric stretching, respectively (Kharazmi *et al.*, 2015). These peaks are all clearly seen in both pairs of "medium" and "large" NPs, since this surfactant was used in their production, in opposition to the "small" NPs which do not have PVA in their composition. Additionally, there is a peak around the wavelength of 1750 cm^{-1} on both PVA and PLGA spectra, which represents a carbonyl stretching (Ahmad *et al.*, 2020). This signal is seen in all NPs, because they are all composed of PLGA, and the "medium" and "large" NPs also contain PVA. The PLGA spectrum also has two bands with distinct signals at 1355-1470 and 1050-1190 cm^{-1}, which should represent an OH group of a carboxylic acid and a C-O group stretching of an aliphatic polyester, respectively (Bukhari *et al.*, 2023). These bands are seen in all NPs, due to the presence of the polymer. Between 600-1650

cm^{-1}, there are a high number of weak bands in both RB and PVA spectra. These peaks for PVA are well seen in all NPs, except for the "small" ones. The RB peaks are more evident in the "small" RB-loaded NPs, although in the "medium" and "large" NPs there may be some small peaks that correspond to the RB chemical structure. However, RB is present in a very small amount in the formulation and the visualization of their characteristic peaks may be compromised by this reason.

Through these spectra we concluded that "medium" and "large" NPs appear to have the same key chemical bonds as PVA, showing that this surfactant is a part of the structure of the particles. We can observe the peaks present in PLGA in all the particles, due to it being the main component in the polymeric matrix. The peaks seen in RB are more evident in the "small" RB-loaded NPs, due since these have a concentration of 2% (v/v) of this compound, while the "medium" ones have 1% (v/v) and the "large" ones have 1.5% (v/v). Overall, the results confirmed the successful incorporation of the different components in the obtained formulations.

Subsequently, the same process was applied to the three FeDM-loaded and the two FeMP loaded NPs, as well as to each iron chelate, to the polymer and the surfactant, in order to ascertain information about the molecular structure of the particles. The spectra are shown in Figure 3.10.

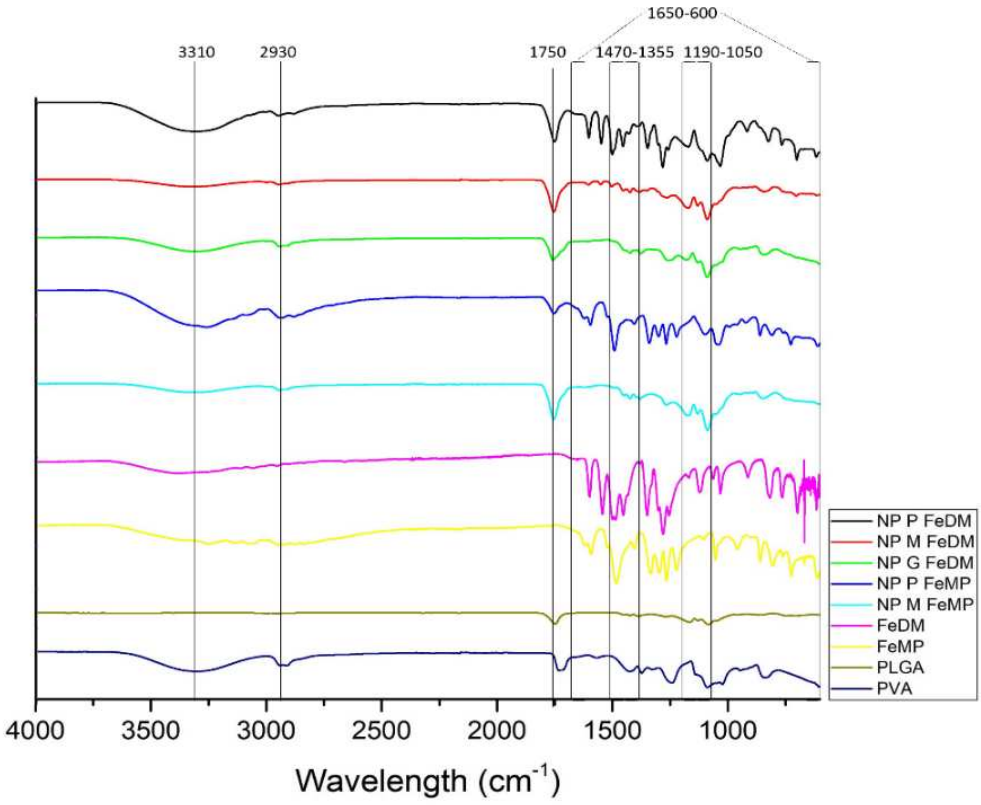

Figure 3.10- Fourier-transform infrared spectroscopy spectra of the three types (P– small; M- medium; G- large) of FeDM-loaded nanoparticles, two types (P– small; M- medium) of FeMP-loaded nanoparticles, FeDM, FeMP, Poly(D,L-lactide-co-glycolide) (PLGA) and Poly(vinyl alcohol) (PVA), from 600 to 4000 cm^{-1}.

From the spectra in Figure 3.10, we can once again observe the presence of the PVA characteristic peak at 3310 cm^{-1} representing an OH stretching. This peak is also seen in both iron chelates, although with a broader and weaker signal which may be assigned to the OH vibration group of the water contained in the chelates. Due to this fact, this peak is seen in all NPs, due to the presence of either FeDM or FeMP. As mentioned before, PVA has another peak at 2930 cm^{-1} representing a CH_2 asymmetric stretching. However, this peak is seen in all types of NPs, including "small" FeDM and "small" FeMP-loaded NPs, which do not include the usage of a surfactant in their production. An explanation for these bands is that there may be an interaction between the complexes and the polymer, however, there are also discrete signals in this wavelength on both chelates which may correspond to the CH3 groups of the chelates (Darwish *et al.*, 2022; Jin *et al.*,

2016). Additionally, the carbonyl stretching is present in both PVA and PLGA by a peak around the wavelength of 1750 cm^{-1}, which is then manifested, due to the presence of the polymer, in all types of NPs. The spectrum for PLGA also contains the bands described before, at the wavelengths of 1355-1470 and 1050-1190 cm^{-1}, which are also visible in the spectra of the NPs. There are several characteristic peaks in the spectra for both FeDM and FeMP-loaded NPs, as well as for PVA in the wavelength range of 600-1650 cm^{-1}. In this interval, "medium" and "large" FeDM-loaded NPs have the characteristic peaks from PVA, with some small peaks present in FeDM, while for "medium" FeMP-loaded NPs, the same combination is found with the FeMP iron chelate. Both "small" FeMP-loaded and FeDM-loaded NPs have peaks similar to the spectra of their respective iron chelate on this interval.

Based on this data, it is possible to conclude that chemical bonds found in PLGA are present in all NPs, showing that a polymeric matrix is found in all of them. Additionally, signals found in PVA are found in the spectra of NPs that use that surfactant. Finally, characteristic peaks seen in the FeDM spectrum are seen in FeDM-loaded NPs, similarly, FeMP-loaded NPs exhibit the unique spectral signals found in the FeMP spectrum. It can therefore be concluded that the NPs were successful in encapsulating the iron chelates.

3.4. Evaluation of rhodamine-B loaded nanoparticles' uptake by soybean plants

The next part of the study consisted in performing an uptake study of RB-loaded NPs by soybean plants grown in hydroponic solution. After 14 days of growth, ten plants were divided in groups of two and placed in contact with "small", "medium" and "large" RB-loaded nanoformulations, a 20 μM RB water-based solution, as well as water (control). After 24 hours, the roots, stems and leaves were separated and later analysed by confocal microscopy to determine which type of NPs are more efficient in being taken up by the plant. Figure 3.11 displays representative images of the detected fluorescence signals for each plant organ under different treatments.

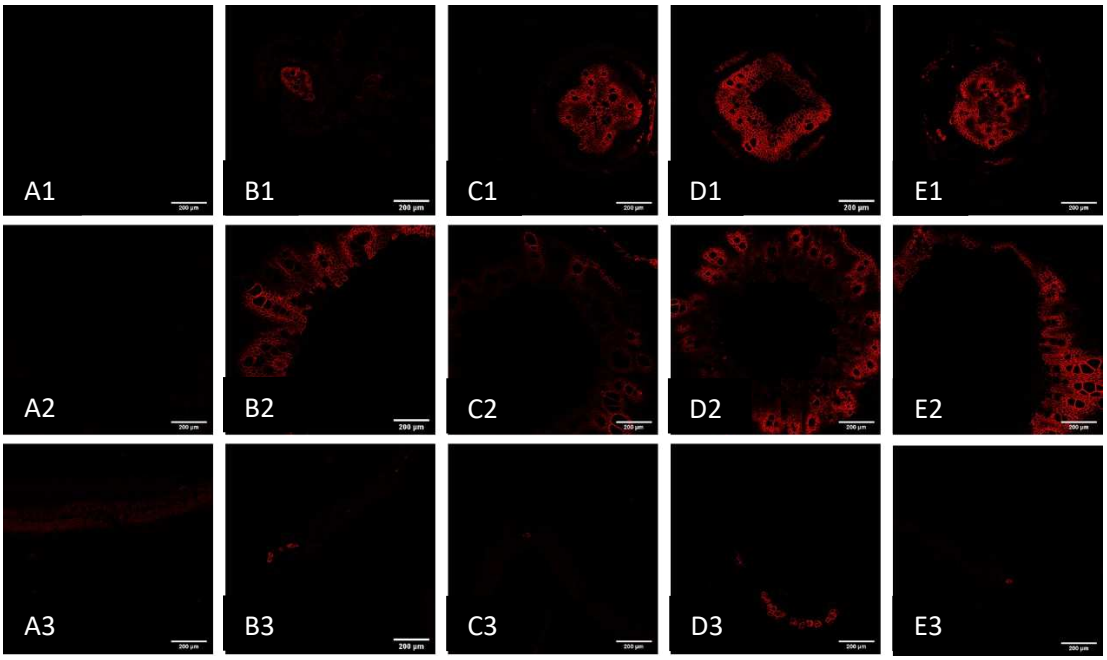

Figure 3.11- Representative image of the detected fluorescence signals at an excitation wavelength of 560 nm and an emission wavelength of 575 nm for each plant organ (1-3) under different treatments (A-E). (A) Control group, (B) Rhodamine B solution, (C) "Small" rhodamine B-loaded nanoparticles, (D) "Medium" rhodamine B-loaded nanoparticles, (E) "Large" rhodamine B-loaded nanoparticles. (1) Roots, (2) Stems, (3) Leaves.

After observing the images of fluorescent signals, it was possible to qualitatively deduce certain aspects about the uptake of the NPs.

Firstly, it is possible to observe that there was no fluorescent signal in the roots treated with water, while there was a clearly visible fluorescence intensity in the ones treated with all types of NPs, as well as the RB solution (although in lower amounts for the latter). It is therefore likely that all the NPs were able to carry RB inside the roots, and therefore being successful in providing the compound to the plants. This information is consistent with previous research conducted, in which *Arabidopsis thaliana* plants were grown hydroponically, and exposed to different sized silica NPs, and particles up to 200 nm were able to accumulate in root cells, although no studies containing NPs in the range of 300 nm in this context were found (Slomberg & Schoenfisch, 2012).

Regarding the stems, there was no visible signal in the control group, while once again there was a considerable amount of fluorescence in the plants treated with three types of NPs and the RB solution. The ones treated with "small" RB-loaded NPs seem to have a lower fluorescence intensity

signal, and thus it can be hypothesised that the “medium” and “large” NPs were able to transport RB up to the stem, through the xylem, while the “small” NPs appear to be less successful in their delivery.

Finally, regarding the leaves, there is a slight observable signal in the control group. Nevertheless, there seems to be low-intensity signal in the plats treated with RB solution and “large” NPs, while the ones treated with “medium” NPs have a more intense signal than all the other ones. By this assessment, we can speculate that “small” RB-loaded NPs are not able to deliver the compound to the leaves, “large” NPs appear to be able to deliver a small amount of RB to the leaves and “medium” NPs seem to be the most effective in transporting RB from the roots up to the leaves. Although no previous studies using NPs with RB have been conducted, it has been previously shown that snap bean roots treated hydroponically with the compound were able to exhibit fluorescence at similar wavelengths in the leaves (Su *et al.*, 2020).

In sum, "medium" NPs seem to be more effective in transporting the encapsulate to leaf tissue, the critical site for iron delivery. This insight, coupled with the fact that medium-sized FeDM NPs possess favourable characteristics in terms of size, PDI, zeta potential, EE and LC, has led to the decision to utilise this type of particle in the study regarding iron chelate-loaded NPs. Although some studies have shown that molybdenum NPs with sizes up to 250 nm were able to successfully provide this nutrient to chickpea, most research indicates that particles of 100 nm or smaller seem to be the most effective in transporting nutrients inside plant tissue, and most nanofertilisers are usually created with particles in that range (An *et al.*, 2022; R. Liu & Lal, 2015; Yadav *et al.*, 2023). Given this context, the fact that the nanoparticles of medium size were the most efficient in transporting rhodamine B to plant leaves is unexpected and necessitates further investigation for a thorough understanding.

3.5. Soil cultivation study analysis

A popular method for delivering fertilisers and biostimulants in plants, is to conduct seed coating, in which seeds are enriched with the chosen nutrients and fertilisers before being sown (Skrzypczak *et al.*, 2021). The following part of the study consisted of an *in vivo* study in soybean plants grown in alkaline soils, whose seeds were treated with different concentrations of nanosuspensions and solutions to test the efficacy of the NPs in reducing the symptoms of IDC.

Several parameters were analysed for each group of plants. These included physiological parameters such as the time it took from sowing to reach each development stage, plant height, and the relative chlorophyll levels at stages V1 to V3, along with root and shoot fresh weights on the final day of the study. Additionally, the study involved the analysis of gene expression for iron metabolism-related genes, including *FERRITIN*, *FRO2*, and *IRT1*, as well as a mineral analysis.

3.5.1. Plant development and physiological assessment

Regarding the number of days necessary to reach each development stage (Figure 3.12), it was observed that all groups achieved the emergence stage and V2 concurrently. However, only the group exposed to 20 µM nanosuspensions attained stage V1 in fewer days compared to the control. Additionally, this group, along with the one treated with a 20 µM solution, progressed to stage V3 more rapidly than the control group. Hence, the group treated with the 20 µM nanosuspension was the only one that reached stage V1 faster than the control group, a fact that pointed out the advantage of the nanoencapsulation for the plants' growth. Since IDC has been shown to mainly affect plants from stage V1 up to V3, getting through these stages faster can be useful to reduce the impact of this condition (Bayer Group, 2019)

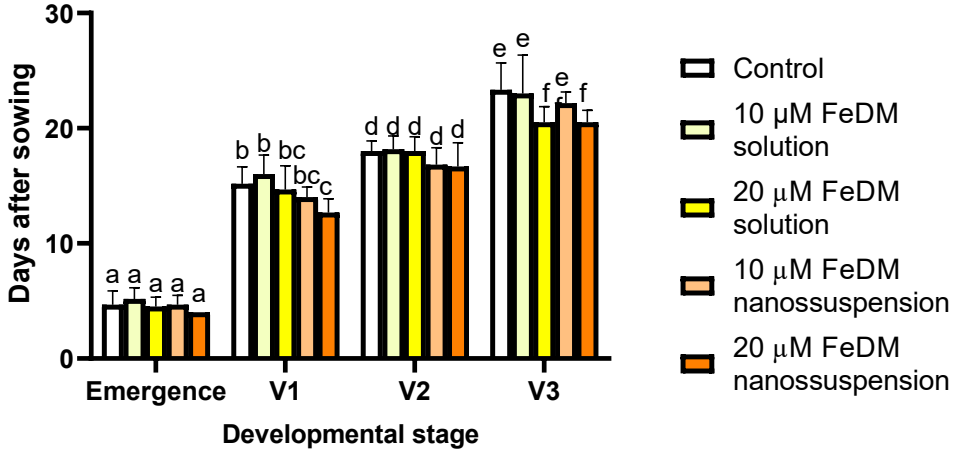

Figure 3.12- Days it took to reach each development stage after sowing the seeds, per treatment. Different letters in each development stage indicate significant differences (p<0.05) by two-way ANOVA with Tukey's test.

In relation to height, no significant differences were found between groups at any development stage, suggesting that the different treatments do not significantly impact the size of the plant at any point during its growth up to V3. In agreement, previous research on soybean plants grown in hydroponic conditions and treated with FeDM solutions did not report any changes in plant height (C. S. Santos *et al.*, 2020).

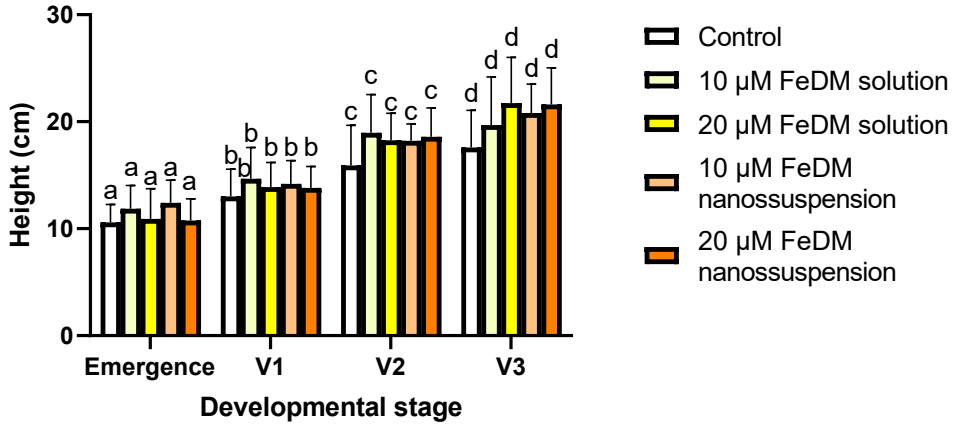

Figure 3.13- Plant height for 21 days, according to the different treatments. Different letters in each development stage indicate significant differences (p<0.05) by two-way ANOVA with Tukey's test.

Relating to chlorophyll content, only the groups exposed to nanosuspensions demonstrated statistically elevated SPAD levels compared to the control at stage V1, although these levels were not significantly different (p>0.05) from those in groups treated with FeDM solutions. This suggests that at this growth stage, the nanosuspensions were not more effective at promoting chlorophyll synthesis than the FeDM solutions. At the V2 stage both nanosuspensions, as well as the 20 µM solution-treated group showed SPAD levels significantly above the control. Relating to the V3 stage, all FeDM solution and nanosuspension-treated groups exhibited higher SPAD values than the control, notably with the 20 µM solution and nanosuspension treatments yielding significantly greater values than the 10 µM solution treatment. Overall, the groups treated with nanosuspensions consistently maintained notably higher chlorophyll levels than the control across all developmental stages. Furthermore, the 10 µM nanosuspension also recorded a higher level than its solution counterpart, suggesting that at this concentration, nanosuspension treatments might be more effective than the respective chelates' solutions.

Previous studies using iron-based nanofertilisers applied to peanut roots have shown that these particles can be efficient in increasing SPAD values of leaves (Rui *et al.*, 2016). This result, together with the one in the current study, seems to imply that the NPs can supply iron to plants in iron-deficient conditions, as it has been observed that chlorophyll levels decrease when there is an iron deficit (Kobraee, 2016).

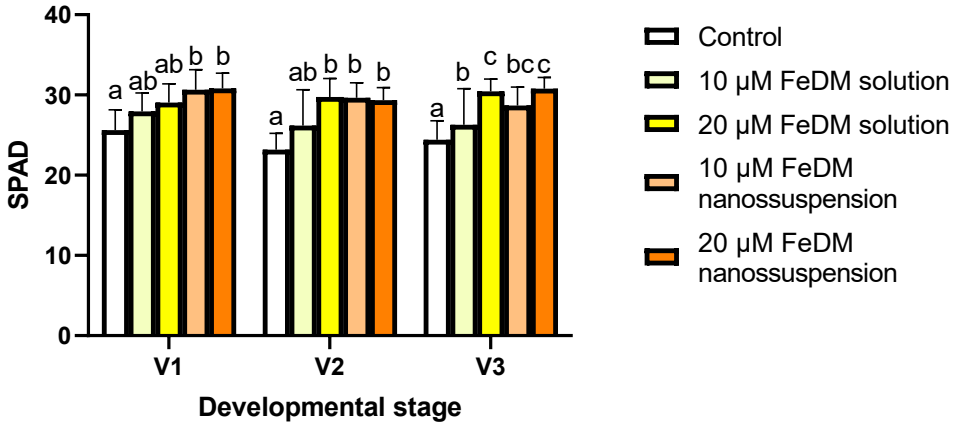

Figure 3.14- Soil Plant Analysis Development values per treatment. Different letters in each development stage indicate significant differences (p<0.05) by two-way ANOVA with Tukey's test.

Regarding the fresh weights of roots and stems, the statistically significant differences were the same in both cases. The plants treated with 20 µM nanosuspensions had significantly more weight than control and plants treated with 10 µM solutions and nanosuspensions. Even though there were no substantial differences between plants treated with 20 µM nanosuspension and the solution of the same concentration, the first group seems to have a higher mass in both roots and shoots. To conclude, these results seem to reveal a similar trend to the other morphological analysis, with the more concentrated FeDM nanosuspension being the only one able to contain a higher biomass than the control group.

Previous research comparing dry weights of hydroponically grown plants treated with FeDM with plants grown in iron-deficient conditions showed that roots of plants treated with the compound were significantly heavier than those in iron deficiency, however, the weight of the shoots was not significantly higher than control (C. S. Santos *et al.*, 2021). The results for 20 µM solution treatment in the shoots compared to the iron-deficient plants are similar to the ones in this study, since the weight of the treated plants' shoots is apparently higher but not statistically significant.

This result reinforces that the 20 µM nanosuspension was more effective in reducing the symptoms of IDC in shoots since it was the only treatment that made the exposed plants' roots heavier than control. The results for the plants' roots in the referred study are different from the ones obtained in this study since the plants treated with solutions had significantly heavier roots than control. This difference is due to the fact that the study of C. S. Santos *et al.* (2020) was conducted in hydroponic culture, utilised a different method of application, continued until the V5 stage, and involved drying the plants' organs before weighing them.

Since IDC has been shown to reduce soybean plants' biomass, our data suggests that these nanofertilisers are able to reduce this symptom (Bai *et al.*, 2018).

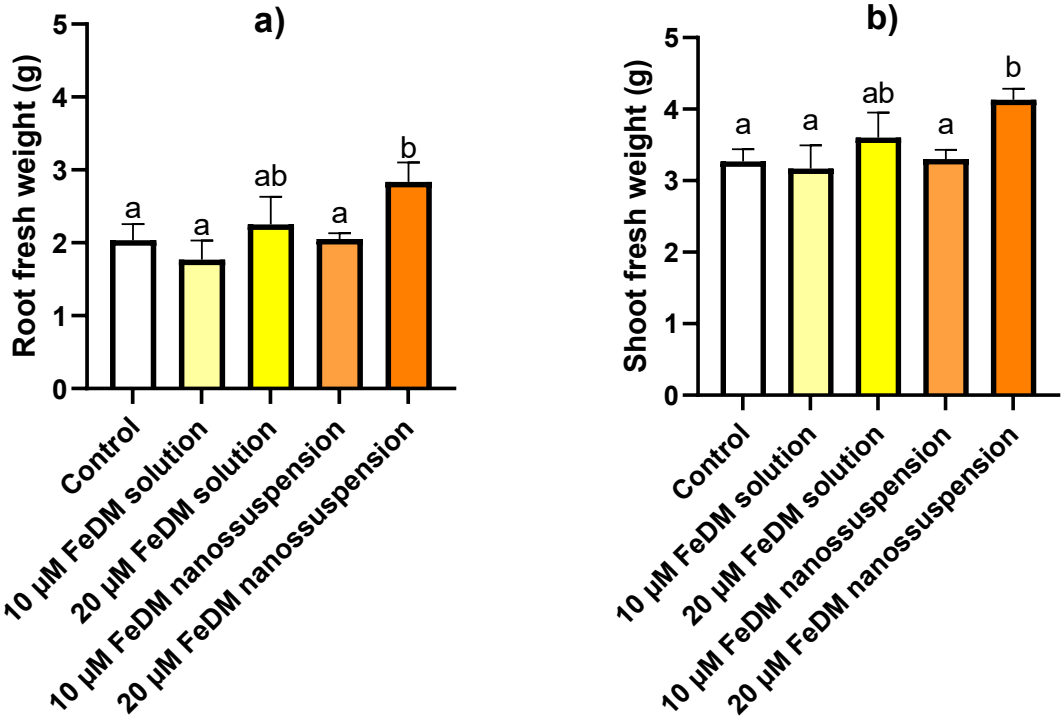

Figure 3.15- Fresh weight of roots (a) and shoots (b), in grams. Different letters in each development stage indicate significant differences (p<0.05) by one-way ANOVA with Fisher's Uncorrected LSD method.

Overall, while these FeDM NPs showed promise, further analysis was required in order to make deeper conclusions on the effectiveness of the NPs in providing iron to plants grown in iron-deficient, calcareous soils.

3.5.2. Genetic expression evaluation

In order to further understand the efficacy of the developed NPs, a genetic expression study was conducted, with the intent of obtaining information on the levels of expression of three key genes associated with iron storage, transport and absorption: *FERRITIN*, a gene responsible the production of a protein that stores iron in the leaves, which is regulated primarily by the presence of this element (Masuda *et al.*, 2001); *FRO2,* which codes for ferric reductase, an enzyme responsible for reducing iron in the soils to a more water-soluble form, and requires the presence of iron for its expression and *IRT1*, which codes for an iron transporter protein, allowing for the mobility of iron inside the roots, and also requires the presence of this element for its accumulation (Roriz *et al.*, 2021; Vert *et al.*, 2003).

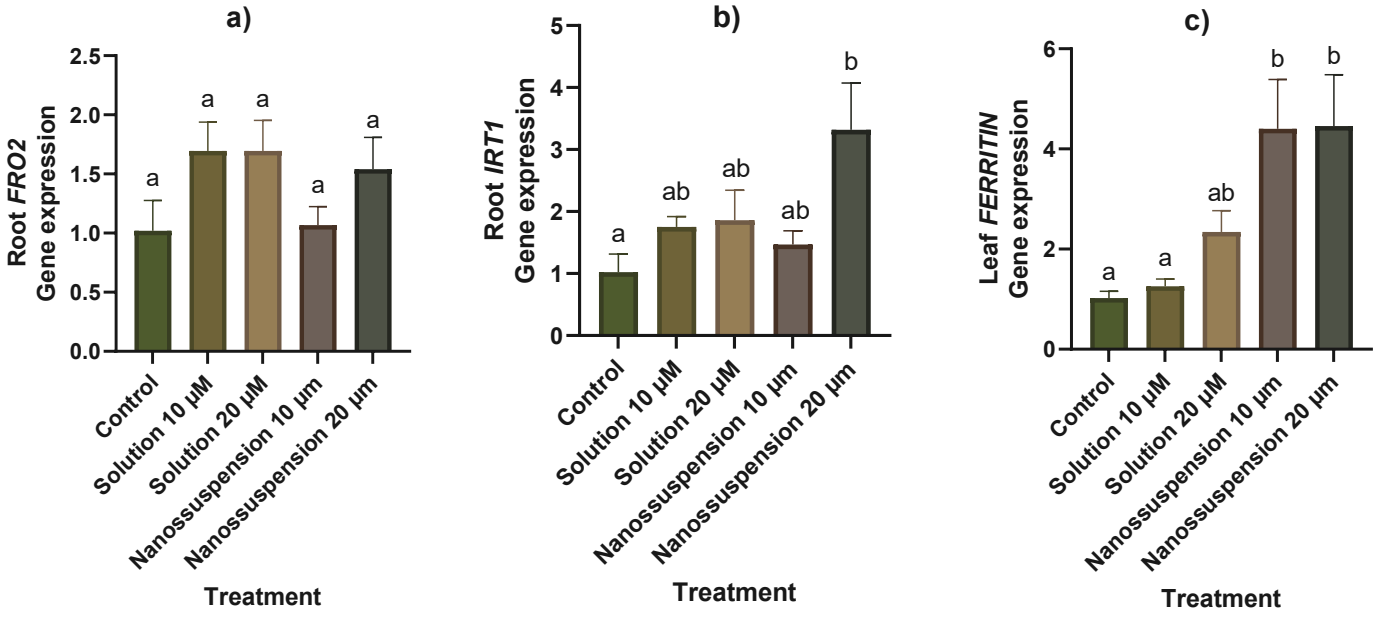

Figure 3.16- Relative gene expression of root *FRO2* (a) and *IRT1* (b), and leaf *FERRITIN* (c), per treatment. Different letters in each development stage indicate significant differences (p<0.05) by two-way ANOVA with Šidák's test.

From Figure 3.16, we can observe that no significant differences were detected in the relative gene expression of *FRO2* in any treatment. Regarding *IRT1* however, the group of plants treated with 20 µM nanosuspensions was the only one having a significantly higher expression compared to control, and seemingly higher than all the other treatments, suggesting that there was enough iron

present in the roots to induce the expression of this gene. The genes coding for *IRT1* and *FRO2* have been shown to be overexpressed in conditions of iron deficiency, since the production of these proteins continues for as long as the plant is exposed to iron stress, in order to try to increase the uptake of this element (C. S. Santos et al., 2020). Conversely, the gene coding for the ferritin protein is under expressed in conditions of iron deficiency, since the production of this protein is correlated with the accumulated amount of iron (C. S. Santos et al., 2020). Relating to the relative expression of *FERRITIN,* both groups treated with nanosuspensions had substantially higher expressions than those of control and treated with 10 μM solution. While apparently having a much higher average gene expression, no significant differences were found between the groups treated with the two nanosuspensions and one treated with the 20 μM solution. This information allows us to deduce that the 10 μM NPs were more efficient in delivering iron to the leaves than the solution with the same concentration, suggesting that this product has a potential to be more effective in mitigating the effects of IDC than the traditional method of deploying fertilizers. The plants treated with the 20 μM nanosuspension were also, on average, very successful in delivering iron up the plant. These results for the nanosuspensions are also consistent with the results obtained for SPAD values, suggesting that the levels of *FERRITIN* are indeed correlated to the amount of chlorophyll present in the leaves.

A previous study conducted in hydroponics showed that treatment with 20 μM solution does not increase *FRO2* expression, which is consistent with this study, and showed that that same treatment significantly increased *IRT1* and *FERRITIN* expression (C. S. Santos *et al.*, 2021). The fact that the solutions were able to increase the expression of these last two genes significantly is likely due to the facts that the study was conducted in hydroponics, had a different method of application and continued until the V5 stage.

In conclusion, the relative gene expression analysis results corroborate the findings from the various morphological parameters previously outlined, indicating the efficacy of FeDM NPs in treating soybeans. This treatment appears effective in alleviating IDC symptoms. While further studies are required to compare the iron delivery efficiency of these nanoparticles with that of FeDM fertiliser solutions, the advantages of nanofertilisers, as discussed earlier, point to their considerable potential in agricultural applications.

3.5.3. Mineral concentration analysis

With the objective of detecting potential changes in mineral concentration in leaf tissue induced by the application of the nanofertilisers, an ICP analysis was performed on several minerals, namely zinc, calcium, potassium, magnesium, manganese, sodium, phosphorous and most importantly, iron.

The results regarding the concentration of iron in leaf tissue are represented in Figure 3.17, and an overall depiction of mineral accumulation is shown in Table 2A of the Appendix.

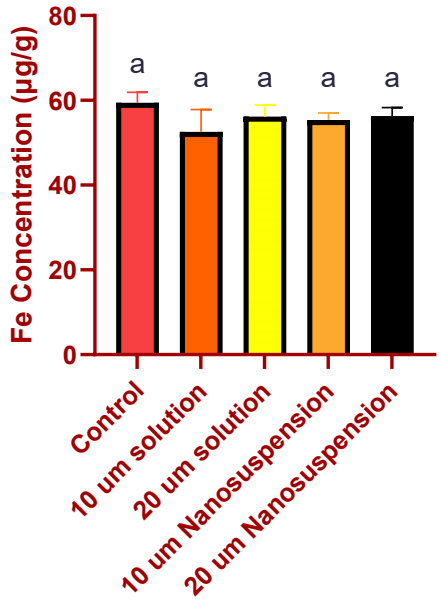

Figure 3.17- Iron (Fe) concentration (µg/g) in 3rd trifoliates. per treatment. Different letters in each development stage indicate significant differences (p<0.05) by one-way ANOVA with Tukey's multiple comparisons test.

From Figure 3.17, we can conclude that no significant differences (p>0.05) were found between treatments, implying that the different fertilisers and nanofertilisers did not significantly increase the amount of iron in the 3rd trifoliate leaves.

A similar analysis was conducted regarding the other previously mentioned minerals, and none of them yielded significant differences between control and the other treatments. This suggests that seed coating with FeDM NPs does not impact the concentration of iron in the 3rd trifoliate leaves,

which may be due to the method of application and the duration of the treatment. Previous studies (C. S. Santos *et al.*, 2020) using FeDM with a foliar application revealed that this compound is able to increase iron, sodium and magnesium levels in trifoliates, which suggests that further analysis with different methods, such as foliar application, are required to determine the efficacy of these NPs in providing iron to leaves.

4. Conclusions and Future Perspectives

This research sought out to explore the potential of 3,4-HPO iron chelate-loaded NPs in enhancing plant health, focusing on addressing IDC in soybean. This study was a significant step towards integrating nanotechnology with agricultural practices, aiming to bridge the gap between these two fields. The comprehensive approach of the study included the synthesis of NPs of varying sizes, detailed analysis of their physicochemical properties, evaluation of their release profiles and stability, assessment of their uptake by plant tissues, and exploration of their impact on plant growth in conditions of IDC, including an in depth morphological, mineral and gene expression analysis, providing a good understanding of the NPs' influence on plant health and development.

The design of PLGA NPs, a crucial aspect of this study, initially involved the production of RB particles ranging in size from 100 nm to 300 nm. This step was not only about producing nanoparticles of a certain size but was intricately focused on engineering nanoparticles with optimal characteristics for plant uptake. This included the consideration of various aspects such as PDI, zeta potential, EE, and LC. This preliminary study's success was extremely important since it provided the necessary data to later help in deciding on the type of NP with the most favourable characteristics for uptake. FTIR analysis confirmed that the NPs were able to successfully incorporate RB to the polymeric matrix.

A key aspect of the study was the examination of the release profiles of these NPs. The stability in the release of encapsulated substances is crucial for their effectiveness in agricultural applications. The research showed that the NPs, irrespective of their size category, maintained a stable release over a period of three days. This feature is particularly beneficial for agricultural applications, ensuring that the NPs consistently interact with plant tissues and effectively release their encapsulated substances over a sustained period.

Afterwards, the process to produce of RB-loaded NPs was replicated for two chelates of the 3,4-HPO class, namely FeDM and FeMP, with only slight alterations in the protocol. After their production, their physicochemical properties were analysed, and the chelate that was encapsulated with the more favourable characteristics for plant uptake was determined to be FeDM. A six-week storage stability study was also conducted with these NPs, to determine how their properties

changed over time and at different storage temperatures, to draw conclusions about their shelf-life. FTIR analysis corroborated that the iron chelates were incorporated into the PLGA NPs.

Investigating the uptake of the RB-loaded NPs by soybean plants was a pivotal part of the research. The findings revealed that the 'medium' sized nanoparticles seemed to be the most effective in transporting RB, the encapsulated compound, to plant's leaf tissues. Given the crucial role of leaves in a plant's iron utilization and photosynthesis, this finding was significant.

The soil cultivation study provided practical insights into the application of this research. The use of FeDM-loaded NPs had a positive effect on soybean plants grown in iron-deficient, calcareous soils, as evidenced by improvements in chlorophyll content, growth rate, and the fresh weight of roots and shoots. These findings suggested a strong potential for these NPs as an alternative to traditional iron fertilizers, offering a new solution to combat IDC in crops.

Beyond physical growth parameters, the study ventured into genetic expression analysis. The increase in expression of iron-related genes such as *FERRITIN* and *IRT1*, aligned with the observed physical improvements in the plants, suggested a more profound, molecular-level effect of the NP treatment. This was indicative of an enhanced capability for iron transport and storage, a critical aspect in addressing IDC.

Overall, the FeDM-loaded NPs were successful in mitigating the effects of IDC, proving themselves to be a potentially valuable asset in agriculture and in the fertiliser industry. The practical implications of this research are vast, suggesting that custom-designed NP treatments could revolutionize the management of IDC in crops, leading to more sustainable agricultural practices and increased crop yields.

Future research based on these findings is required to better understand certain characteristics. First, the biodegradability of the NP-chelate complex has to be studied and documented thoroughly, as well as its potential impact on the soils, and analyse the product’s overall impact for the environment through a biosafety study. Foliar application should also be studied, both in a larger scale and in natural calcareous soils. Additionally, studies in different types of soils, with varying matrixes, moistures and pH have to be conducted, to analyse the behaviour of these nanofertilisers in different conditions, as well as using different dosages, nanofertiliser application time and frequencies of application. Moreover, certain other parameters should be analysed

regarding the final study in soil, to make further conclusions on the effectiveness of the application of the NPs, namely an amino acid analysis, to determine the peptide and protein composition of the samples, a FTIR and Near Infrared Spectroscopy (NIR) analysis on leaf tissue as described for previous studies to obtain information on the molecular composition of the tissue (Carla S. Santos *et al.*, 2023). It is also envisaged an anti-oxidant activity analysis to evaluate the eventual phytotoxicity of the designed nanoformulations, and a more holistic transcriptomic study, to determine the impact of the nanofertilisers on the expression of a larger array of genes. Finally, these fertilisers should also be tested in other crops, to determine their versatility and compatibility with different agricultural systems.

In summary, this thesis represents a significant stride in the field of agricultural nanotechnology, demonstrating the potential of NPs in enhancing plant health and combating IDC. To the best of our knowledge, this is the first study of 3,4-HPO iron chelates-loaded NPs used as nanofertilisers. Its findings open new possibilities for research and application, not only in agriculture but in various other fields where nanotechnology could play a transformative role. The successful integration of nanotechnology in addressing critical issues like IDC and bioavailable iron delivery opens the possibility for its application in other agricultural challenges, potentially transforming conventional farming practices. The study serves as a model for future research, showing the importance of interdisciplinary collaboration, innovative thinking, and a comprehensive approach to problem-solving in the quest to address some of the most pressing challenges of our time.

5. Appendix

Table 1A - Primer sequences, annealing temperatures and correspondent accession numbers.

Primer	Forward (5'-3')	Reverse (5'-3')	Annealing temperature (ºC)	Accession Number
18S	TTAGGCCATGGAGGTTTGAG	GAGTTGATGACACGCGCTTA	56.3	X75080.1
Actin	TGCATACGTTGGTGATGAGG	AGCCTTGGGGTTAAGAGGAG	56.4	NM_001358094.1
IRT1	ACAACAATGGCCACTTCACT	GCCAATTATGCTTGAGGCTA	54.4	KF542819.1
FRO2	AGAACATGGAAGGGTCAACA	AGCAAGAACTCCCACACTTG	54.3	XM_003528793.2
FERRITIN	CAATGCTTCCTATGCGTACC	CTGAGGGGACATTCTTGATG	54.5	NP_001236534

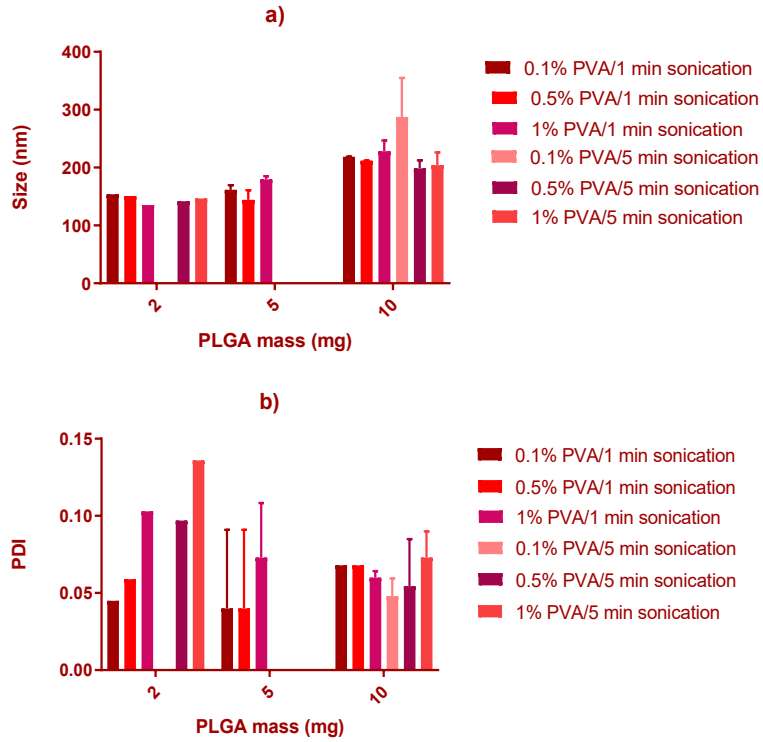

Figure 1A- Graphs representing the size (a) and polydispersity index (PDI) (b) of nanoparticles produced by *strategies 1* and *2*, according to Poly(D,L-lactide-co-glycolide) (PLGA) mass.

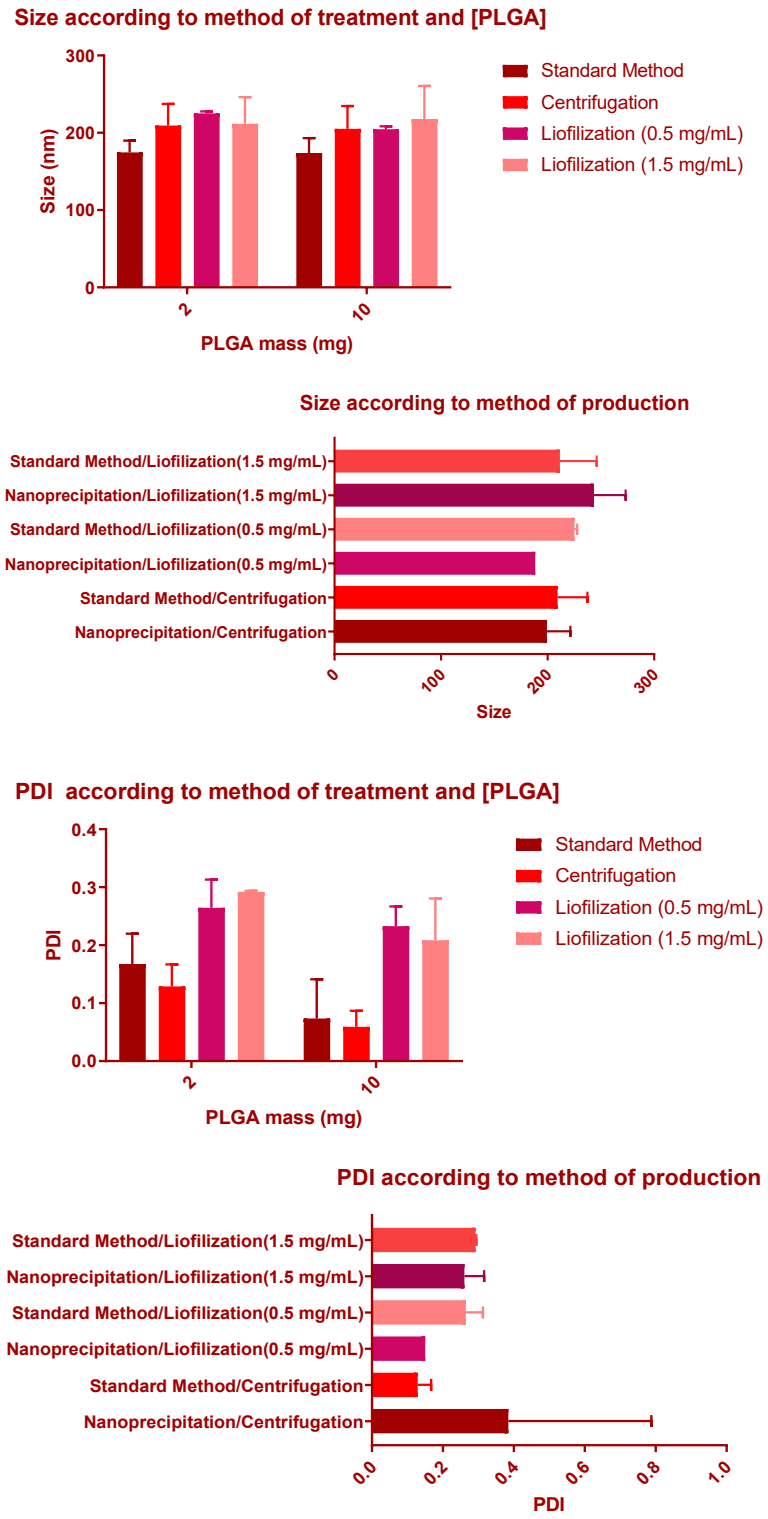

Figure 2A- Size and polydispersity index (PDI) of nanoparticles (NPs) produced by strategy 3, according to method of treatment, production and Poly(D,L-lactide-co-glycolide) (PLGA) mass.

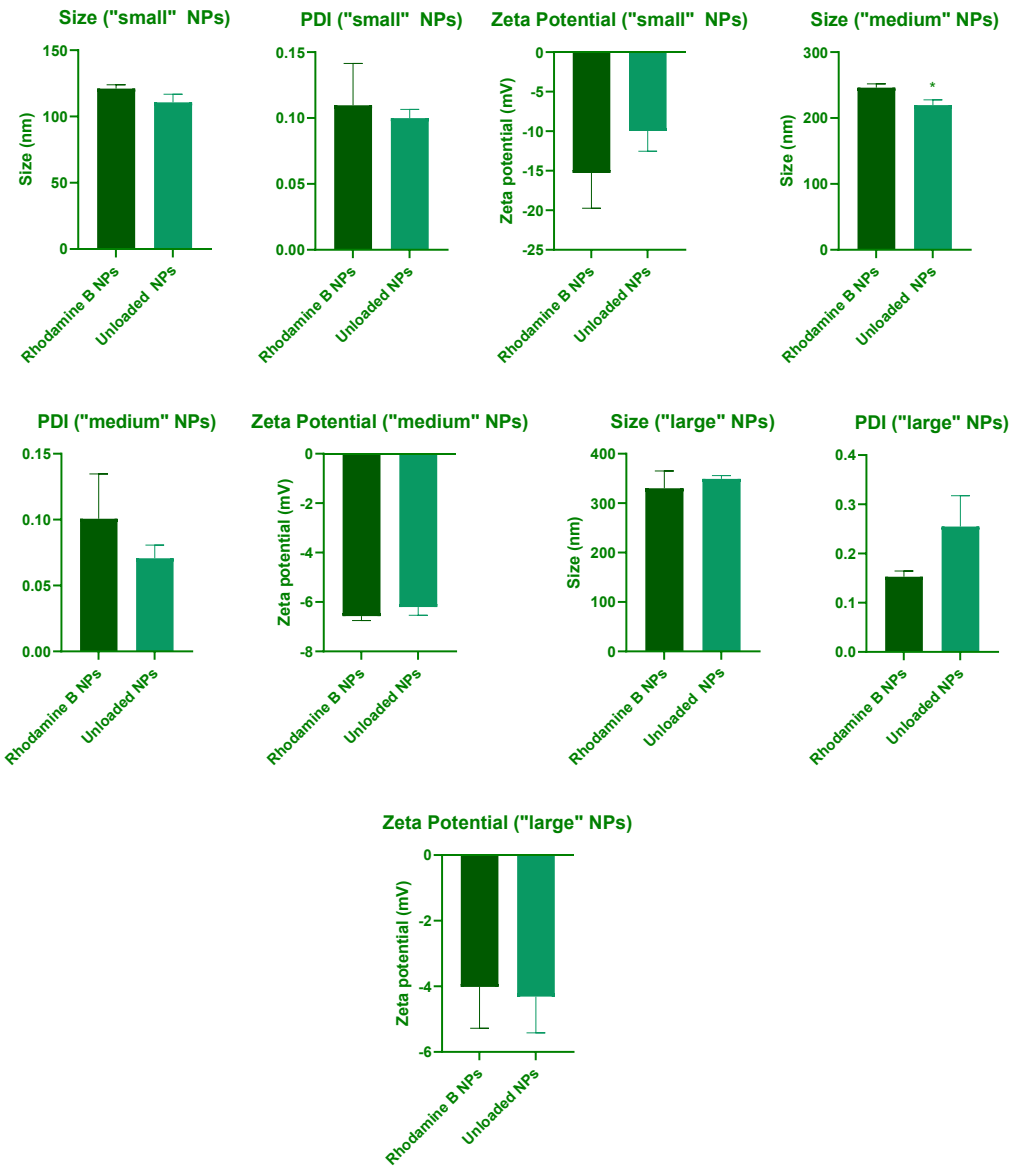

Figure 3A- Comparison of sizes, polydispersity index (PDI) and zeta potentials between rhodamine B-loaded and unloaded nanoparticles (NPs). Statistical significances are indicated: **p*<0.05 by unpaired t-test with Welch's correction.

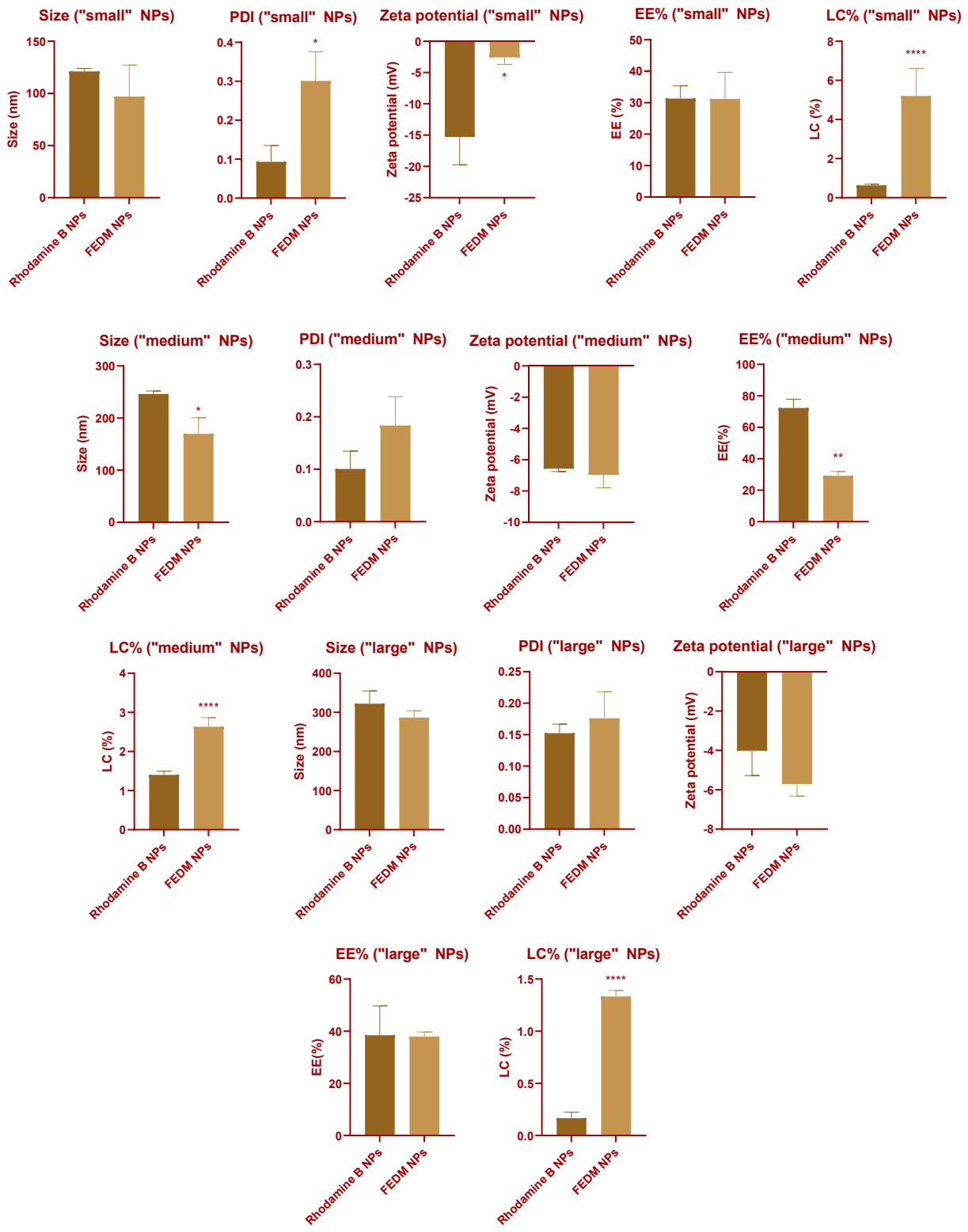

Figure 4A- Comparison of sizes, polydispersity index (PDI), zeta potentials, encapsulation efficiency (EE) and loading capacity (LC) between rhodamine B-loaded and FeDM-loaded nanoparticles (NPs). Statistical

significances are indicated: *p<0.05, **p<0.01, ***p<0.001, ****p<0.0001 by unpaired t-test with Welch's correction.

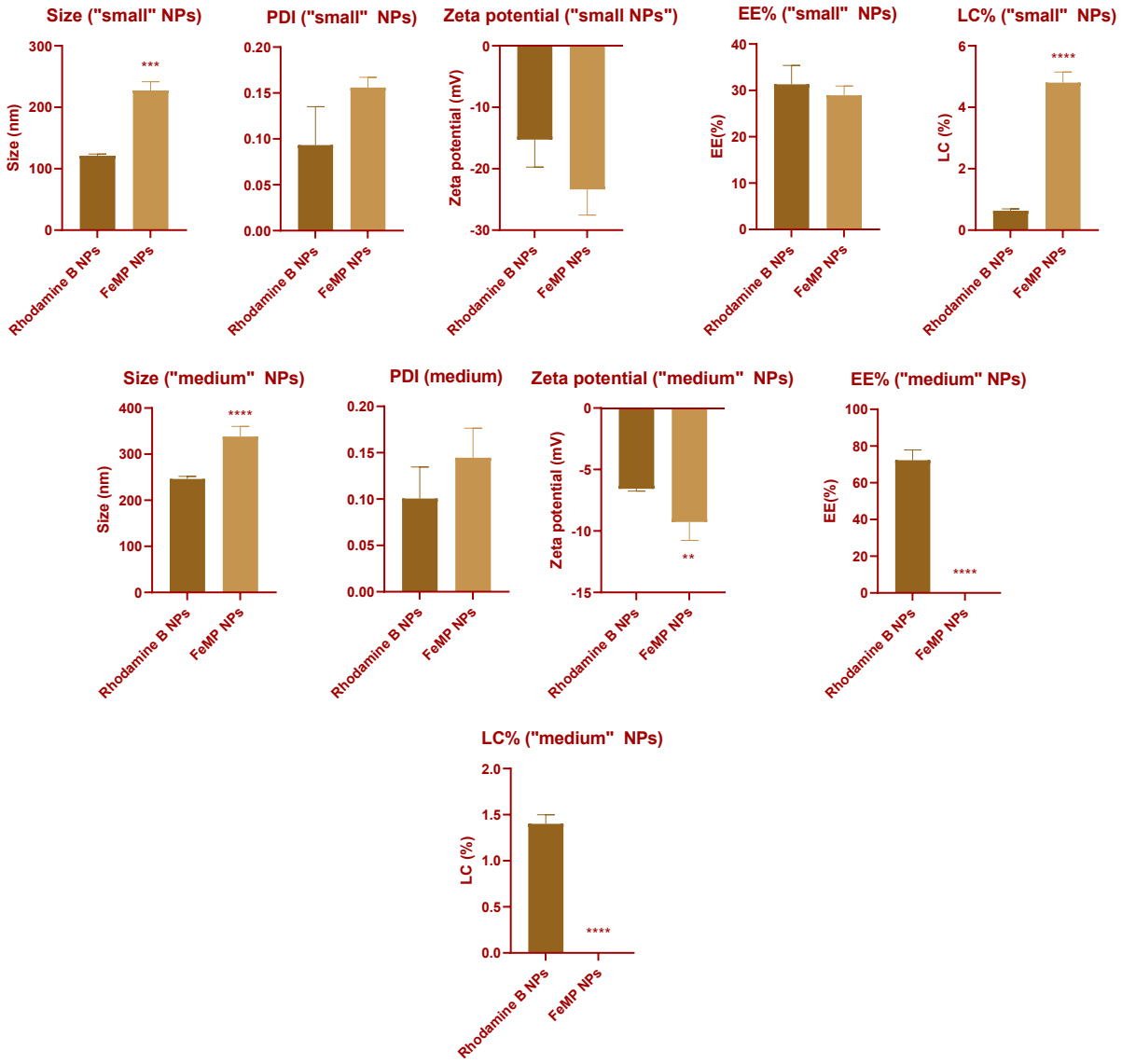

Figure 5A- Comparison of sizes, polydispersity index (PDI), zeta potentials, encapsulation efficiency (EE) and loading capacity (LC) between rhodamine B-loaded and FeMP-loaded nanoparticles (NPs). Statistical significances are indicated: *p<0.05, **p<0.01, ***p<0.001, ****p<0.0001 by unpaired t-test with Welch's correction.

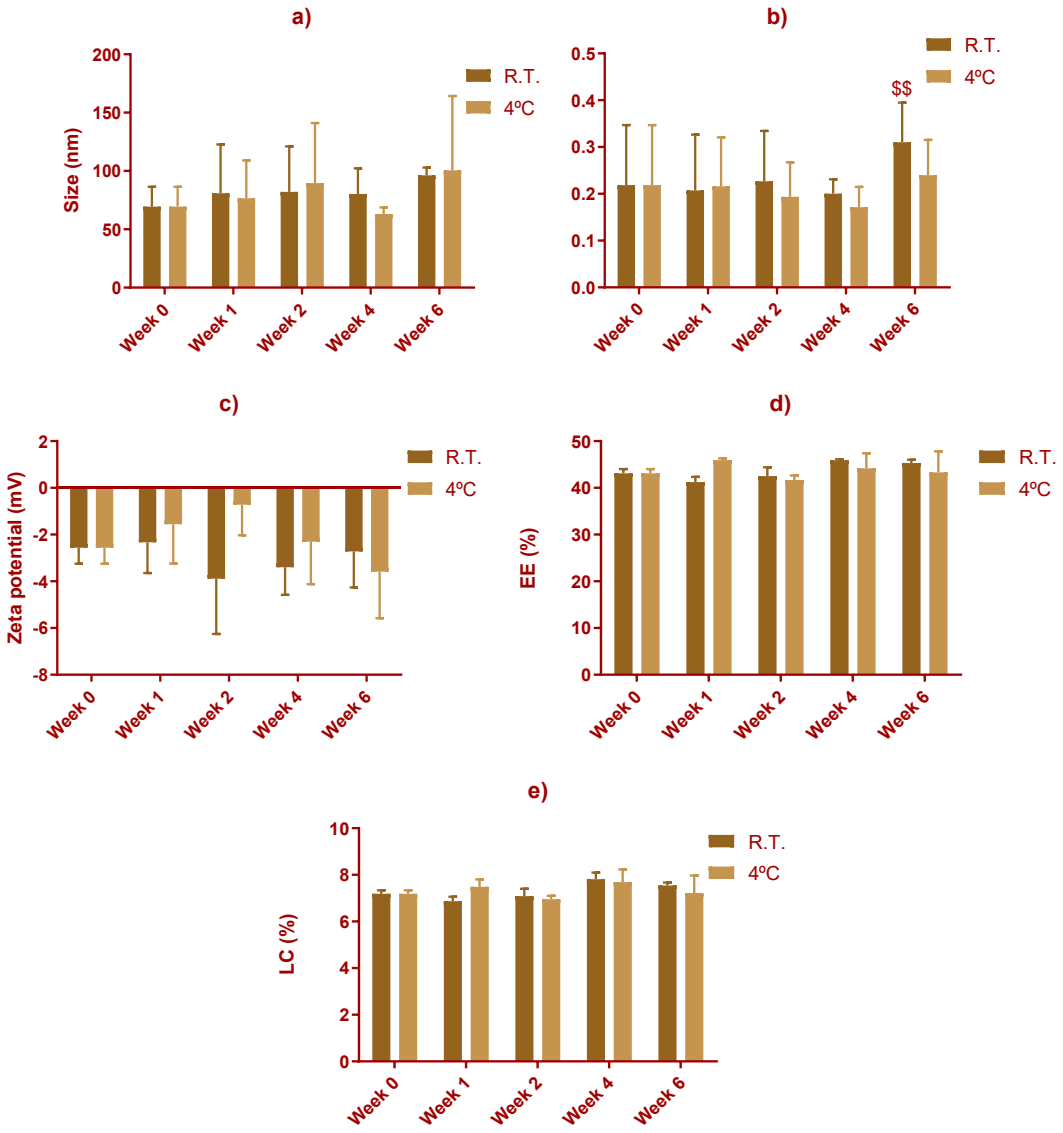

Figure 6A- Size (a), polydispersity index (PDI) (b), zeta potential (c), encapsulation efficiency (EE) (d), and loading capacity (LC) (e) of "small" FeDM-loaded nanoparticles (NPs) observed over 6 weeks, stored at room temperature (R.T) and 4ºC. Statistical significances are indicated: *p<0.05, **p<0.01, ***p<0.001, ****p<0.0001 (differences between particles kept at 4ºC and room temperature); \$$p$<0.05, \$\$$p$<0.01, \$\$\$$p$<0.001, \$\$\$\$$p$<0.0001 (differences from week 0 for the same temperature) by two-way ANOVA with Dunnett's test.

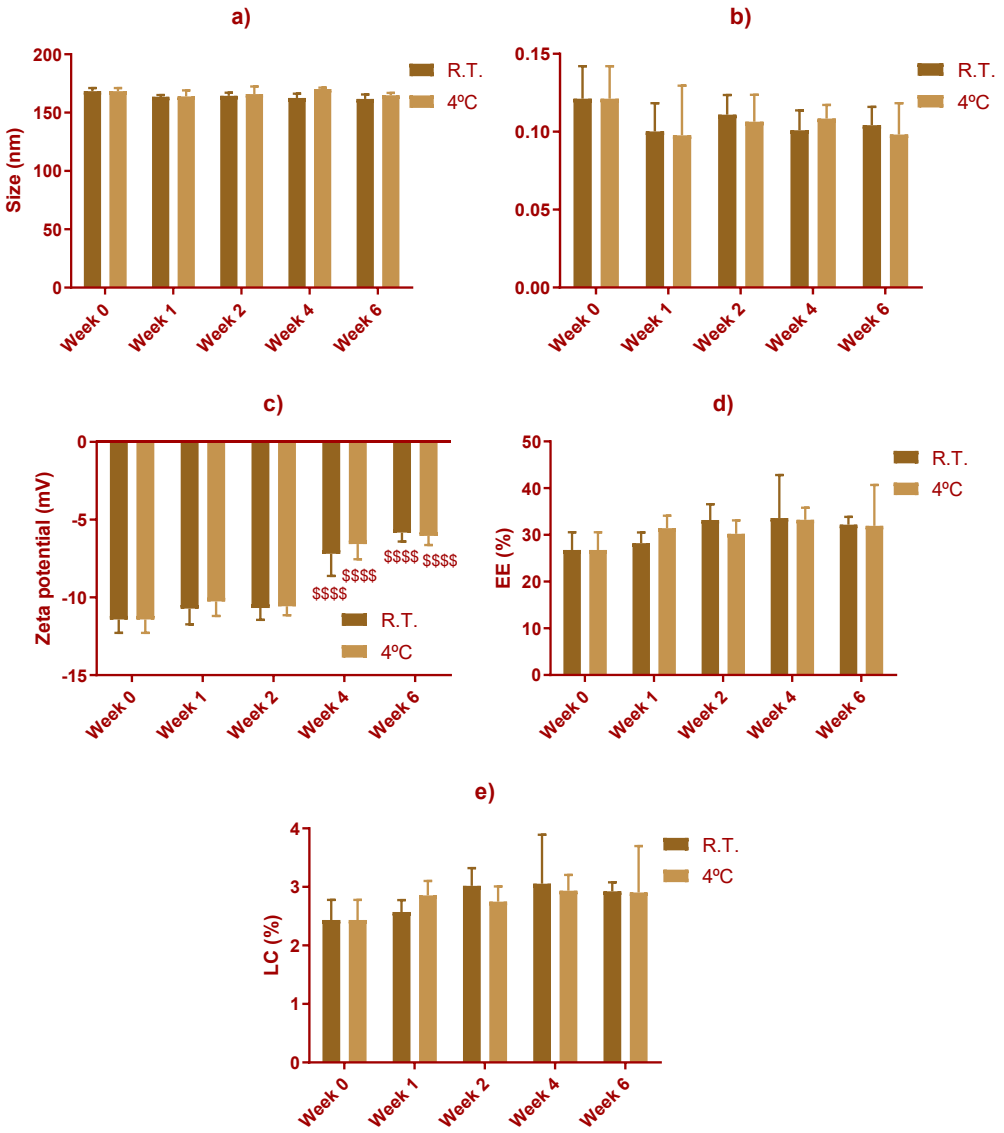

Figure 7A- Size (a), polydispersity index (PDI) (b), zeta potential (c), encapsulation efficiency (EE) (d), and loading capacity (LC) (e) of "medium" FeDM-loaded nanoparticles (NPs) observed over 6 weeks, stored at room temperature (R.T) and 4ºC. Statistical significances are indicated: *p<0.05, **p<0.01, ***p<0.001, ****p<0.0001 (differences between particles kept at 4ºC and room temperature); $$p$<0.05, $$$p$<0.01, $$$$p$<0.001, $$$$$p$<0.0001 (differences from week 0 for the same temperature) by two-way ANOVA with Dunnett's test.

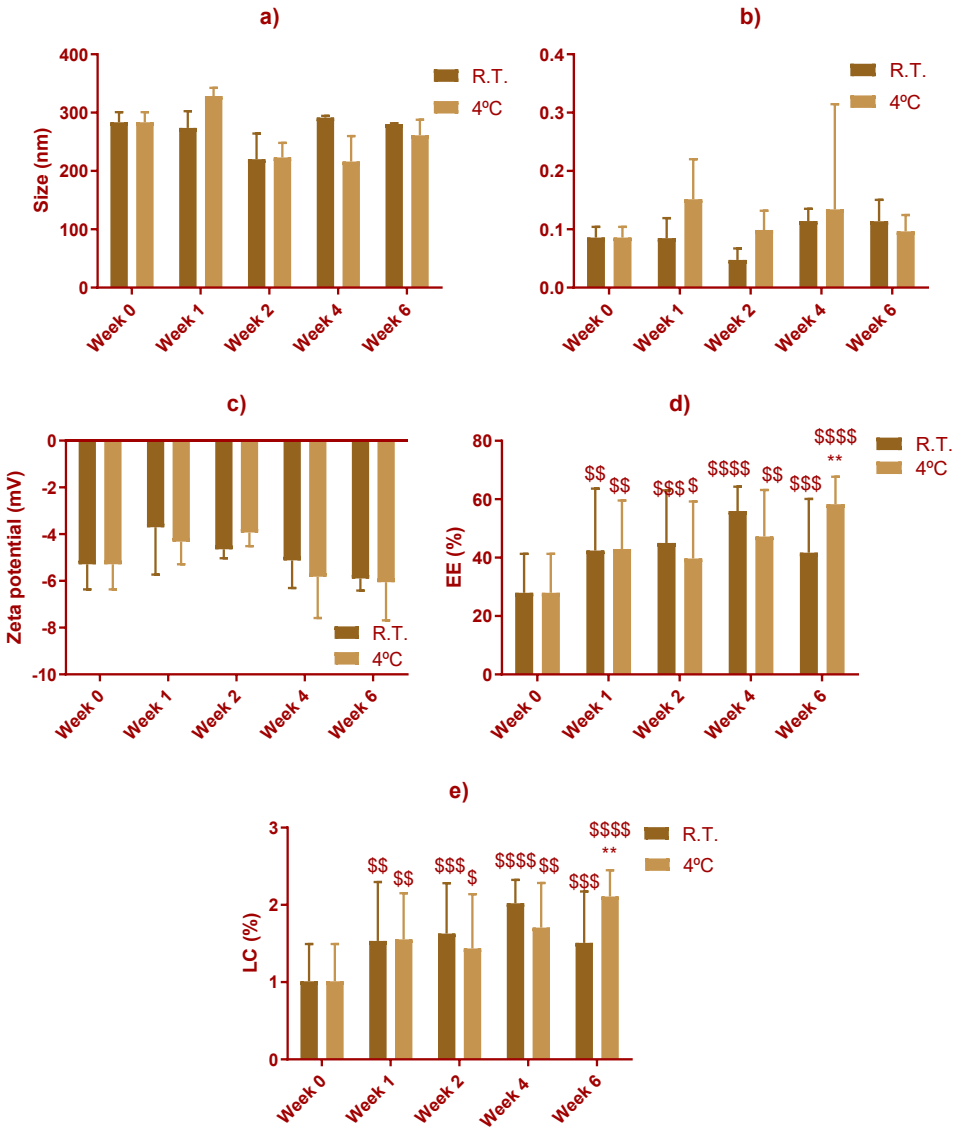

Figure 8A- Size (a), polydispersity index (PDI) (b), zeta potential (c), encapsulation efficiency (EE) (d), and loading capacity (LC) (e) of "large" FeDM-loaded nanoparticles (NPs) observed over 6 weeks, stored at room temperature (R.T) and 4ºC. Statistical significances are indicated: *p<0.05, **p<0.01, ***p<0.001, ****p<0.0001 (differences between particles kept at 4ºC and room temperature); $$p$<0.05, $$$p$<0.01, $$$$p$<0.001, $$$$$p$<0.0001 (differences from week 0 for the same temperature) by two-way ANOVA with Dunnett's test.

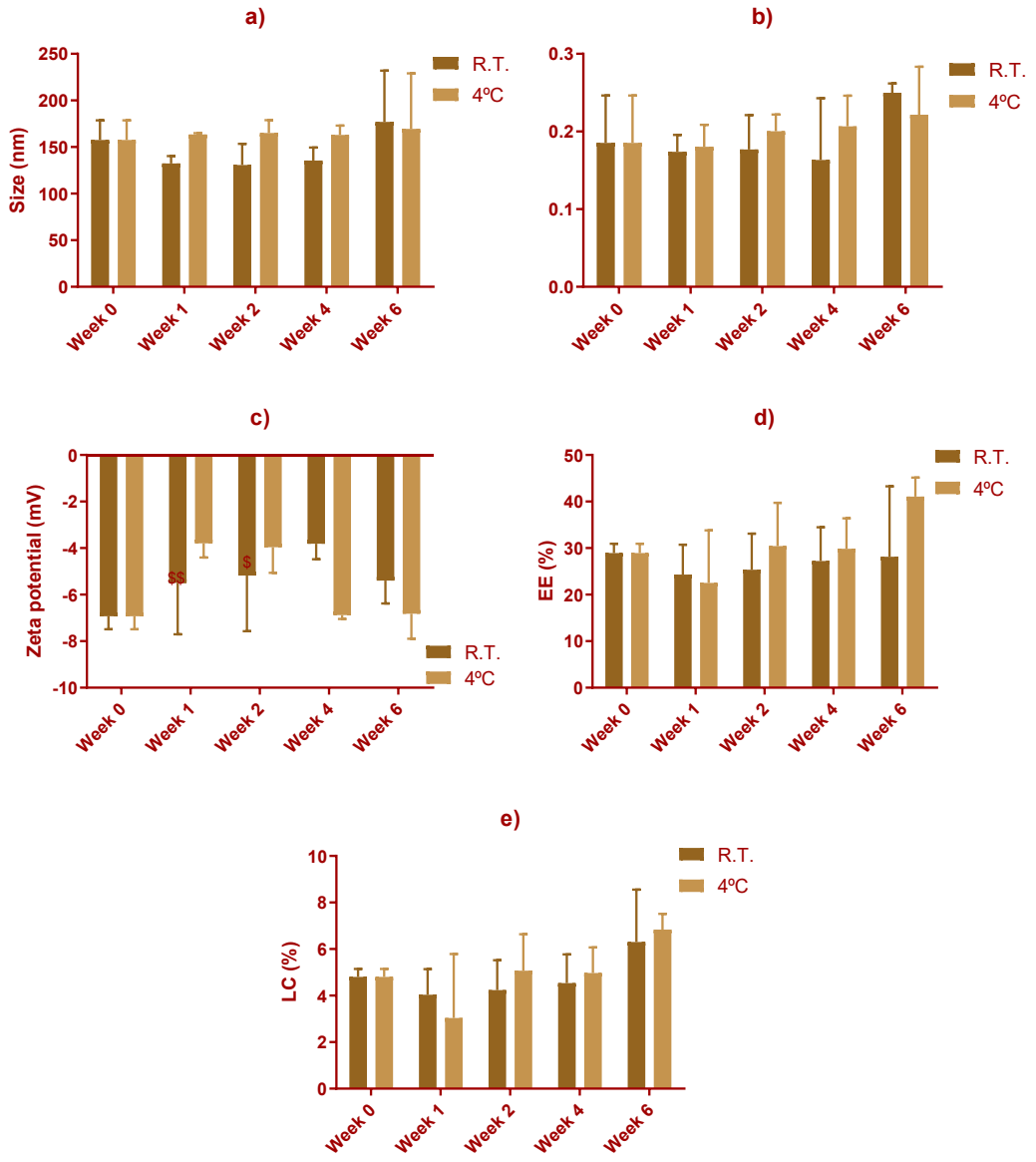

Figure 9A- Size (a), polydispersity index (PDI) (b), zeta potential (c), encapsulation efficiency (EE) (d), and loading capacity (LC) (e) of "small" FeMP-loaded nanoparticles (NPs) observed over 6 weeks, stored at room temperature (R.T) and 4ºC. Statistical significances are indicated: *p<0.05, **p<0.01, ***p<0.001, ****p<0.0001 (differences between particles kept at 4ºC and room temperature); $$p$<0.05, $$$p$<0.01, $$$$p$<0.001, $$$$$p$<0.0001 (differences from week 0 for the same temperature) by two-way ANOVA with Dunnett's test.

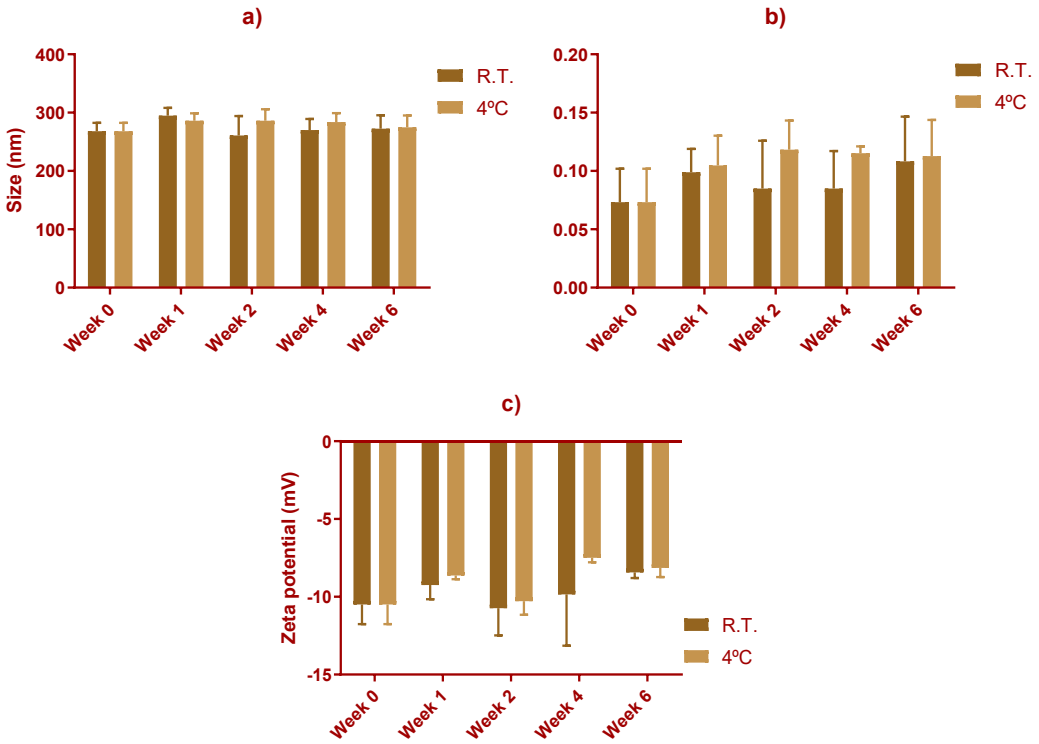

Figure 10A- Size (a), polydispersity index (PDI) (b) and zeta potential (c) of "medium" FeMP-loaded nanoparticles (NPs) observed over 6 weeks, stored at room temperature (R.T) and 4ºC. Statistical significances are indicated: *p<0.05, **p<0.01, ***p<0.001, ****p<0.0001 (differences between particles kept at 4ºC and room temperature); \$$p$<0.05, \$\$$p$<0.01, \$\$\$$p$<0.001, \$\$\$\$$p$<0.0001 (differences from week 0 for the same temperature) by two-way ANOVA with Dunnett's test.

Table 2A - Iron (Fe), zinc (Zn), calcium (Ca), potassium (K), magnesium (Mg), manganese (Mn), sodium (Na), nickel (Ni) and phosphorous (P) concentration (µg/g) in 3rd trifoliates. per treatment. Different letters in each development stage indicate significant differences (p<0.05) by one-way ANOVA with Tukey's multiple comparisons test.

Mineral (µg/g)	Control	10 µM Solution	20 µM Solution	10 µM Nanosuspension	20 µM Nanosuspension
Fe	59±2[a]	53±5[a]	56±5[a]	55±2[a]	56±2[a]
Zn	9±1[a]	10±1[a]	11±1[a]	10±1[a]	11±1[a]
Ca	15274±281[a]	12937±1228[a]	14727±533[a]	14451±449[a]	14045±482[a]
K	25988±1214[a]	24174±2734[a]	26548±1363[a]	23642±1372[a]	23743±1237[a]
Mg	3035±175[a]	2568±317[a]	2847±138[a]	2612±95[a]	2520±101[a]
Mn	14±1[a]	11±2[a]	14±1[a]	13±1[a]	14±1[a]
Na	965±73[a]	1219±154[a]	994±99[a]	936±33[a]	985±27[a]
Ni	0,57±0,07[a]	0,48±0,13[a]	0,66±0,15[a]	0,52±0,08[a]	0,58±0,11[a]
P	4007±255[a]	3105±396[a]	3533±119[a]	3161±182[a]	3384±154[a]

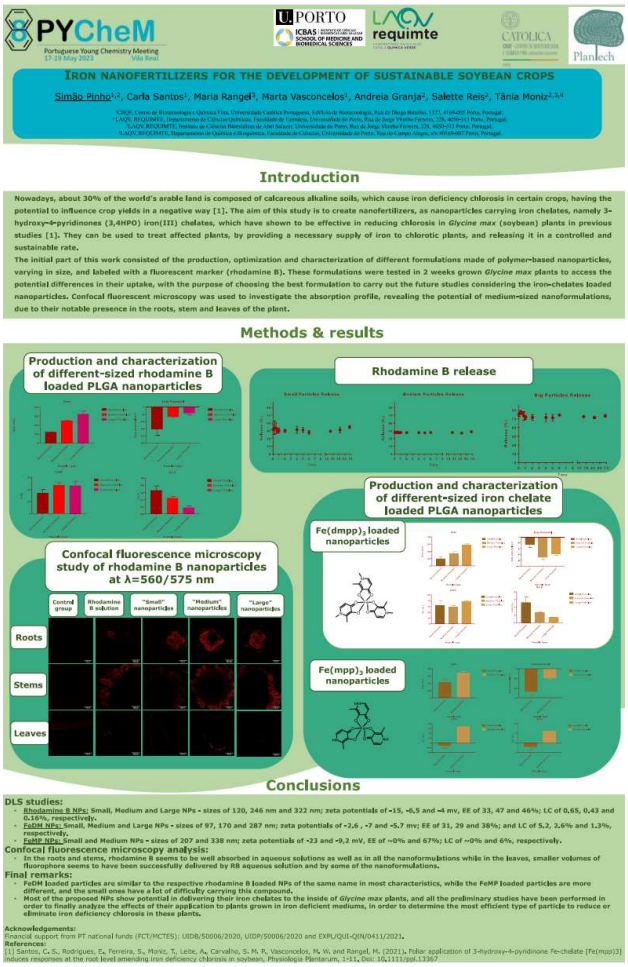

Figure 11A- Poster for the "8th Portuguese Young Chemistry Meeting", 17-19th May 2023.

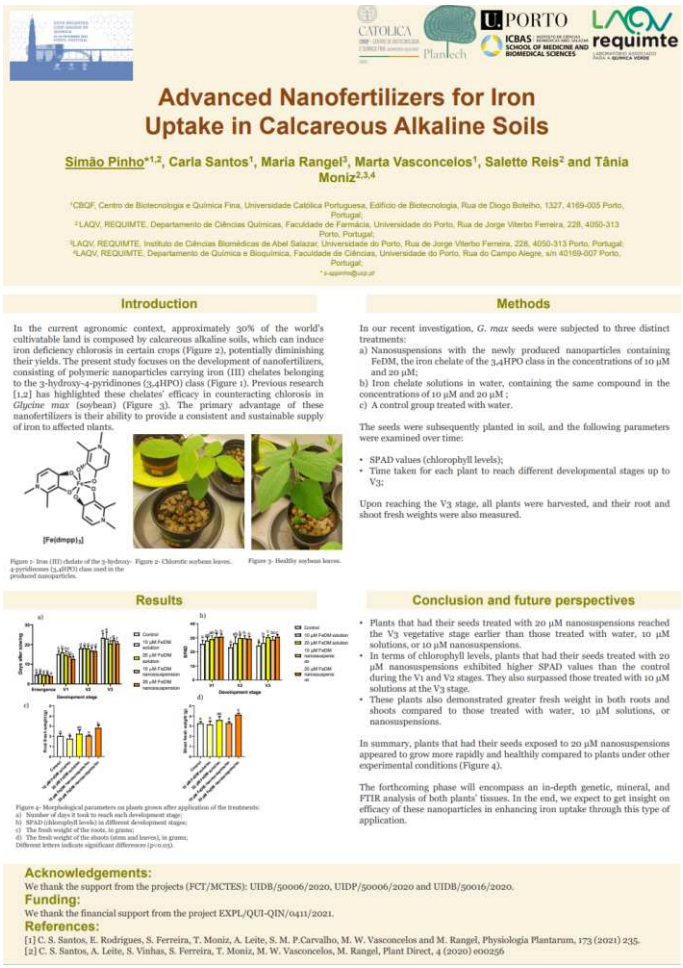

Advanced Nanofertilizers for Iron Uptake in Calcareous Alkaline Soils

Simão Pinho*[1,2], Carla Santos[1], Maria Rangel[3], Marta Vasconcelos[1], Salette Reis[2] and Tânia Moniz[2,3,4]

[1]CBQF, Centro de Biotecnologia e Química Fina, Universidade Católica Portuguesa, Edifício de Biotecnologia, Rua de Diogo Botelho, 1327, 4169-005 Porto, Portugal;
[2]LAQV, REQUIMTE, Departamento de Ciências Químicas, Faculdade de Farmácia, Universidade do Porto, Rua de Jorge Viterbo Ferreira, 228, 4050-313 Porto, Portugal;
[3]LAQV, REQUIMTE, Instituto de Ciências Biomédicas de Abel Salazar, Universidade do Porto, Rua de Jorge Viterbo Ferreira, 228, 4050-313 Porto, Portugal;
[4]LAQV, REQUIMTE, Departamento de Química e Bioquímica, Faculdade de Ciências, Universidade do Porto, Rua do Campo Alegre, s/n 4169-007 Porto, Portugal;
* s-pinho@ucp.pt

Introduction

In the current agronomic context, approximately 30% of the world's cultivatable land is composed by calcareous alkaline soils, which can induce iron deficiency chlorosis in certain crops (Figure 2), potentially diminishing their yields. The present study focuses on the development of nanofertilizers, consisting of polymeric nanoparticles carrying iron (III) chelates belonging to the 3-hydroxy-4-pyridinones (3,4HPO) class (Figure 1). Previous research [1,2] has highlighted these chelates' efficacy in counteracting chlorosis in *Glycine max* (soybean) (Figure 3). The primary advantage of these nanofertilizers is their ability to provide a consistent and sustainable supply of iron to affected plants.

Figure 1- Iron (III) chelate of the 3-hydroxy-4-pyridinones (3,4HPO) class used in the produced nanoparticles.

Figure 2- Chlorotic soybean leaves.

Figure 3- Healthy soybean leaves.

Methods

In our recent investigation, *G. max* seeds were subjected to three distinct treatments:

a) Nanosuspensions with the newly produced nanoparticles containing FeDM, the iron chelate of the 3,4HPO class in the concentrations of 10 µM and 20 µM;
b) Iron chelate solutions in water, containing the same compound in the concentrations of 10 µM and 20 µM ;
c) A control group treated with water.

The seeds were subsequently planted in soil, and the following parameters were examined over time:

- SPAD values (chlorophyll levels);
- Time taken for each plant to reach different developmental stages up to V_3;

Upon reaching the V_3 stage, all plants were harvested, and their root and shoot fresh weights were also measured.

Results

Figure 4- Morphological parameters on plants grown after application of the treatments:
a) Number of days it took to reach each development stage;
b) SPAD (chlorophyll levels) in different development stages;
c) The fresh weight of the roots, in grams;
d) The fresh weight of the shoots (stem and leaves), in grams;
Different letters indicate significant differences ($p<0.05$).

Conclusion and future perspectives

- Plants that had their seeds treated with 20 µM nanosuspensions reached the V_3 vegetative stage earlier than those treated with water, 10 µM solutions, or 10 µM nanosuspensions.
- In terms of chlorophyll levels, plants that had their seeds treated with 20 µM nanosuspensions exhibited higher SPAD values than the control during the V_1 and V_2 stages. They also surpassed those treated with 10 µM solutions at the V_3 stage.
- These plants also demonstrated greater fresh weight in both roots and shoots compared to those treated with water, 10 µM solutions, or nanosuspensions.

In summary, plants that had their seeds exposed to 20 µM nanosuspensions appeared to grow more rapidly and healthily compared to plants under other experimental conditions (Figure 4).

The forthcoming phase will encompass an in-depth genetic, mineral, and FTIR analysis of both plants' tissues. In the end, we expect to get insight on efficacy of these nanoparticles in enhancing iron uptake through this type of application.

Acknowledgements:
We thank the support from the projects (FCT/MCTES): UIDB/50006/2020, UIDP/50006/2020 and UIDB/50016/2020.

Funding:
We thank the financial support from the project EXPL/QUI-QIN/0411/2021.

References:

[1] C. S. Santos, E. Rodrigues, S. Ferreira, T. Moniz, A. Leite, S. M. P.Carvalho, M. W. Vasconcelos and M. Rangel, Physiologia Plantarum, 173 (2021) 235.
[2] C. S. Santos, A. Leite, S. Vinhas, S. Ferreira, T. Moniz, M. W. Vasconcelos, M. Rangel, Plant Direct, 4 (2020) e00256

Figure 12A- Poster for the "XXVII Encontro Luso Galego de Química", 22-24th November 2023.

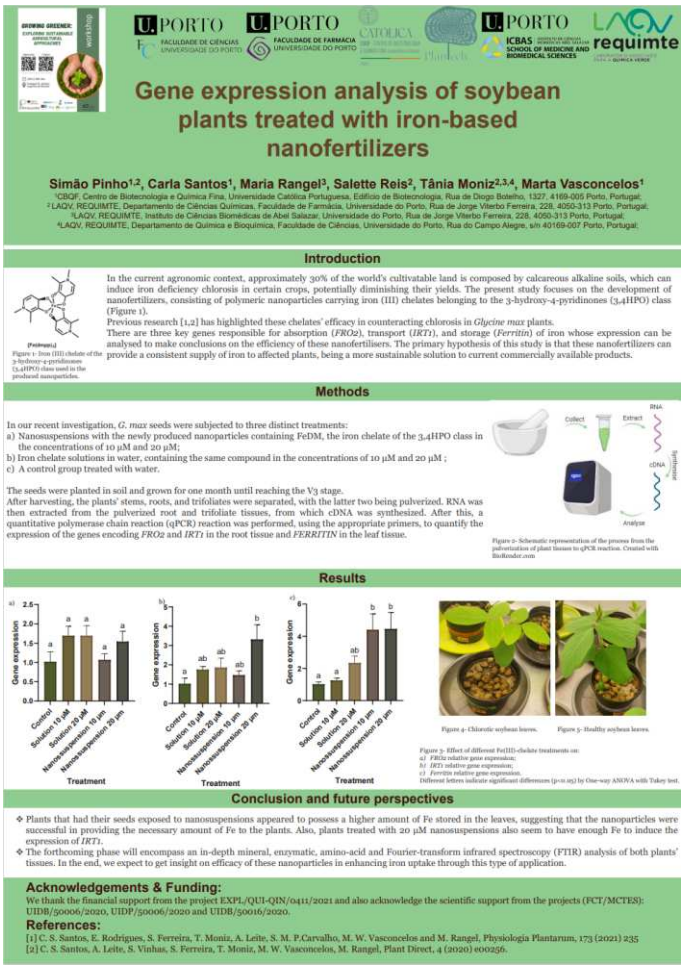

Figure 13A- Poster for the "Growing Greener: Exploring Sustainable Agricultural Approaches" workshop, 29-30th November 2023.

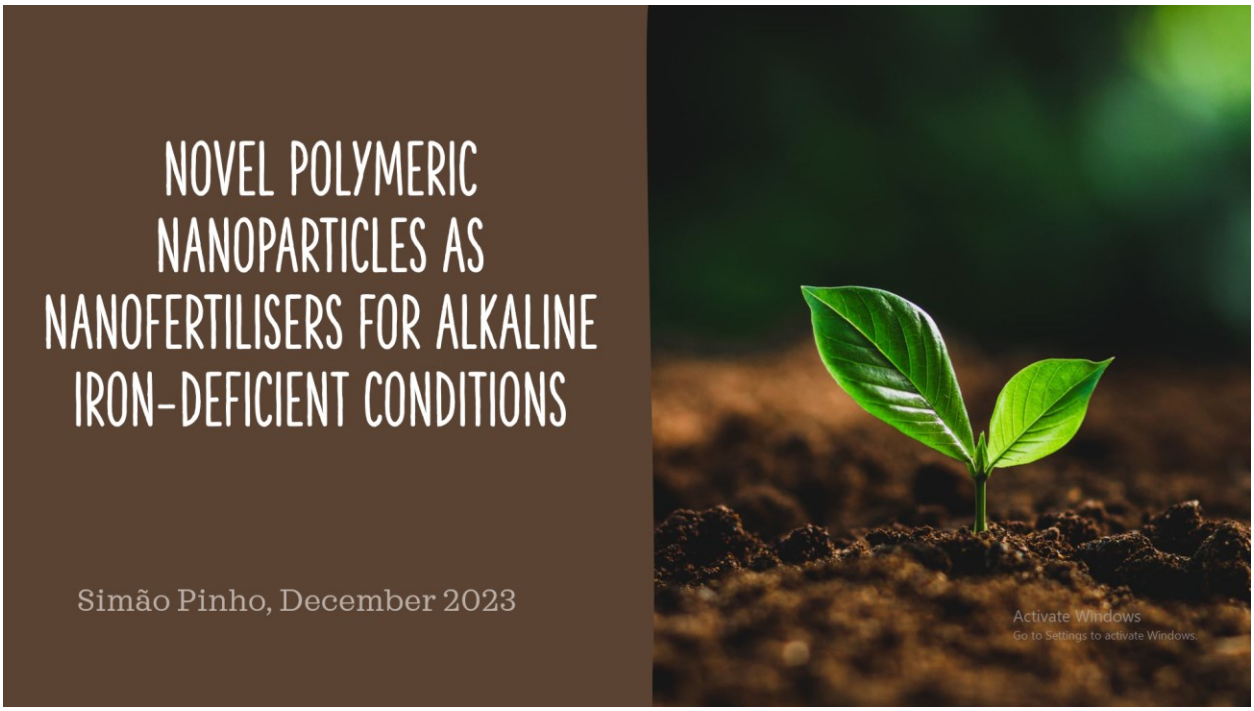

Figure 14A- Cover for oral presentation in the context of the "Advances in Nanotechnology: applications on Agriculture and Health" online workshop, 14th December 2023.

6. References

(CIMMYT), I. M. a. W. I. C. (2023). Twenty Years of Enriching Diets with Biofortification. Retrieved from https://www.cimmyt.org/news/twenty-years-of-enriching-diets-with-biofortification/

Abbaspour, N., Hurrell, R., & Kelishadi, R. (2014). Review on iron and its importance for human health. *Journal of research in medical sciences : the official journal of Isfahan University of Medical Sciences, 19*, 164–174.

Ahmad, N., Ahmad, R., Al Qatifi, S., Alessa, M., Al Hajji, H., & Sarafroz, M. (2020). A bioanalytical UHPLC based method used for the quantification of Thymoquinone-loaded-PLGA-nanoparticles in the treatment of epilepsy. *BMC Chemistry, 14*(1), 10. doi:10.1186/s13065-020-0664-x

Alsaab, H. O., Alharbi, F. D., Alhibs, A. S., Alanazi, N. B., Alshehri, B. Y., Saleh, M. A., . . . Alzhrani, R. M. (2022). PLGA-Based Nanomedicine: History of Advancement and Development in Clinical Applications of Multiple Diseases. *Pharmaceutics, 14*(12). doi:10.3390/pharmaceutics14122728

An, C., Sun, C., Li, N., Huang, B., Jiang, J., Shen, Y., . . . Wang, Y. (2022). Nanomaterials and nanotechnology for the delivery of agrochemicals: strategies towards sustainable agriculture. *Journal of Nanobiotechnology, 20*(1), 11. doi:10.1186/s12951-021-01214-7

Avellan, A., Schwab, F., Masion, A., Chaurand, P., Borschneck, D., Vidal, V., . . . Levard, C. (2017). Nanoparticle Uptake in Plants: Gold Nanomaterial Localized in Roots of Arabidopsis thaliana by X-ray Computed Nanotomography and Hyperspectral Imaging. *Environmental Science & Technology, 51*(15), 8682-8691. doi:10.1021/acs.est.7b01133

Bai, G., Jenkins, S., Yuan, W., Graef, G. L., & Ge, Y. (2018). Field-Based Scoring of Soybean Iron Deficiency Chlorosis Using RGB Imaging and Statistical Learning. *Frontiers in Plant Science, 9*, 1002. doi:10.3389/fpls.2018.01002

Barbosa, A. I., Costa Lima, S. A., & Reis, S. (2019). Development of methotrexate loaded fucoidan/chitosan nanoparticles with anti-inflammatory potential and enhanced skin permeation. *International Journal of Biological Macromolecules, 124*, 1115-1122. doi:10.1016/j.ijbiomac.2018.12.014

Basuchaudhuri, P. (2020). Physiology of Soybean Plant. In (pp. 11): CRC Press. 10.1201/9781003089124

Beard, J. L. (2001). Iron biology in immune function, muscle metabolism and neuronal functioning. *Journal of Nutrition, 131*(2S-2), 568S-579S; discussion 580S. doi:10.1093/jn/131.2.568S

Briat, J. F., Curie, C., & Gaymard, F. (2007). Iron utilization and metabolism in plants. *Current Opinion in Plant Biology, 10*(3), 276-282. doi:10.1016/j.pbi.2007.04.003

Briat, J. F., Duc, C., Ravet, K., & Gaymard, F. (2010). Ferritins and iron storage in plants. *Biochimica et Biophysica Acta, 1800*(8), 806-814. doi:10.1016/j.bbagen.2009.12.003

Briat, J. F., Lobreaux, S., Grignon, N., & Vansuyt, G. (1999). Regulation of plant ferritin synthesis: how and why. *Cellular and Molecular Life Sciences, 56*(1-2), 155-166. doi:10.1007/s000180050014

Brown, J. C., & Jolley, V. D. (2008). Comparative evaluation of iron management in plants, animals, and humans: Possible mechanism for iron use by cancer cells independent of their host. *Journal of Plant Nutrition, 21*(7), 1529-1538. doi:10.1080/01904169809365500

Bukhari, A., Fatima, Z., Atta, M., Nazir, A., Alshawwa, S. Z., Alotaibi, H. F., & Iqbal, M. (2023). Poly Lactic-Co-Glycolic Acid Nano-Carriers for Encapsulation and Controlled Release of Hydrophobic Drug to Enhance the Bioavailability and Antimicrobial Properties. *Dose Response, 21*(1), 15593258231152117. doi:10.1177/15593258231152117

Burgess., J., & Rangel, M. (2008). Hydroxypyranones, Hydroxypyridinones, and their Complexes. In R. v. Eldik (Ed.), *Advances in Inorganic Chemistry* (Vol. 60, pp. 167–243). The Netherlands: Academic Press. doi:10.1016/S0898-8838(08)00005-6

Camaschella, C. (2019). Iron deficiency. *Blood, 133*(1), 30-39. doi:10.1182/blood-2018-05-815944

Carvalho, S. M. P., & Vasconcelos, M. W. (2013). Producing more with less: Strategies and novel technologies for plant-based food biofortification. *Food Research International, 54*(1), 961-971. doi:10.1016/j.foodres.2012.12.021

Chang, J., Jallouli, Y., Kroubi, M., Yuan, X.-b., Feng, W., Kang, C.-s., . . . Betbeder, D. (2009). Characterization of endocytosis of transferrin-coated PLGA nanoparticles by the blood–brain barrier. *International Journal of Pharmaceutics, 379*(2), 285-292. doi:10.1016/j.ijpharm.2009.04.035

Chaves, L. L., Costa Lima, S. A., Vieira, A. C. C., Barreiros, L., Segundo, M. A., Ferreira, D., . . . Reis, S. (2018). Development of PLGA nanoparticles loaded with clofazimine for oral delivery: Assessment of formulation variables and intestinal permeability. *European Journal of Pharmaceutical Sciences, 112*, 28-37. doi:10.1016/j.ejps.2017.11.004

Connorton, J. M., Balk, J., & Rodriguez-Celma, J. (2017). Iron homeostasis in plants - a brief overview. *Metallomics, 9*(7), 813-823. doi:10.1039/c7mt00136c

Cordis. (2022). Europe's plant-based food industry shows record-level growth. Retrieved from https://cordis.europa.eu/article/id/429495-europe-s-plant-based-food-industry-shows-record-level-growth

Darwish, G. A., Ammar, Y. A., Al-Sharbasy, S., & Migahed, M. A. (2022). Synthesis, characterization and evaluation the performance of some novel pyridinone derivatives as corrosion inhibitors in some petroleum applications. doi:10.21203/rs.3.rs-2134906/v1

Debaeke, P., Forslund, A., Guyomard, H., Schmitt, B., & Tibi, A. (2022). Could domestic soybean production avoid Europe's protein imports in 2050? *Oilseeds and fats, Crops and Lipids, 29*. doi:10.1051/ocl/2022031

do Espirito Santo Pereira, A., Caixeta Oliveira, H., Fernandes Fraceto, L., & Santaella, C. (2021). Nanotechnology Potential in Seed Priming for Sustainable Agriculture. *Nanomaterials (Basel), 11*(2). doi:10.3390/nano11020267

Duarte, B. F. (July 2022). Nanopartículas poliméricas fluorescentes como ferramentas de estudo de nanofertilizantes de ferro em culturas de soja. *Projeto Integrador em Engenharia Biológica, Licenciatura em Bioengenharia, ICBAS e FEUP, Universidade do Porto*.

Eide, D., Broderius, M., Fett, J., & Guerinot, M. L. (1996). A novel iron-regulated metal transporter from plants identified by functional expression in yeast. *Proceedings of the National Academy of Sciences of the United States of America, 93*(11), 5624-5628. doi:10.1073/pnas.93.11.5624

El-Hammadi, M. M., & Arias, J. L. (2022). Recent Advances in the Surface Functionalization of PLGA-Based Nanomedicines. *Nanomaterials (Basel), 12*(3). doi:10.3390/nano12030354

FAO, F. a. A. O. o. t. U. N. (2021). Retrieved from https://www.fao.org/faostat/en/#data
Feizi, H., Rezvani Moghaddam, P., Shahtahmassebi, N., & Fotovat, A. (2012). Impact of bulk and nanosized titanium dioxide (TiO2) on wheat seed germination and seedling growth. *Biological Trace Element Research, 146*(1), 101-106. doi:10.1007/s12011-011-9222-7
Fonseca, M., Macedo, A. S., Lima, S. A. C., Reis, S., Soares, R., & Fonte, P. (2021). Evaluation of the Antitumour and Antiproliferative Effect of Xanthohumol-Loaded PLGA Nanoparticles on Melanoma. *Materials (Basel), 14*(21), 6422. doi:10.3390/ma14216421
Fraanje, W. G., T. (2020). Soy: food, feed, and land use change. *Food Climate Research Network, University of Oxford*.
Fukuyama, K. (2004). Structure and function of plant-type ferredoxins. *Photosynthesis Research, 81*(3), 289-301. doi:10.1023/B:PRES.0000036882.19322.0a
Giridhar Reddy, S., & Thakur, A. (2019). Drug Entrapment Efficiency of Silver Nanocomposite Hydrogel. *IOP Conference Series: Materials Science and Engineering, 577*(1). doi:10.1088/1757-899x/577/1/012176
Group, B. (2019). Iron Deficiency Chlorosis. Retrieved from https://www.cropscience.bayer.us/articles/bayer/iron-deficiency-chlorosis
Haque, S., Boyd, B. J., McIntosh, M. P., Pouton, C. W., Kaminskas, L. M., & Whittaker, M. (2018). Suggested Procedures for the Reproducible Synthesis of Poly(d,l-lactide-co-glycolide) Nanoparticles Using the Emulsification Solvent Diffusion Platform. *Current Nanoscience, 14*(5), 448-453. doi:10.2174/1573413714666180313130235
Hell, R., & Stephan, U. W. (2003). Iron uptake, trafficking and homeostasis in plants. *Planta, 216*(4), 541-551. doi:10.1007/s00425-002-0920-4
Hercberg, S., Preziosi, P., & Galan, P. (2001). Iron deficiency in Europe. *Public Health Nutrition, 4*(2B), 537-545. doi:10.1079/phn2001139
Hermila Valdes-Miramontes, E., Rodriguez-Macias, R., & Ruiz-Lopez, M. (2019). Vegetal Sources of Iron. In *Iron Deficiency Anemia*: IntechOpen. doi:10.5772/intechopen.79834
Huang, W., & Zhang, C. (2018). Tuning the Size of Poly(lactic-co-glycolic Acid) (PLGA) Nanoparticles Fabricated by Nanoprecipitation. *Biotechnology Journal, 13*(1), 1-19. doi:10.1002/biot.201700203
Jeyasubramanian, K., Gopalakrishnan Thoppey, U. U., Hikku, G. S., Selvakumar, N., Subramania, A., & Krishnamoorthy, K. (2016). Enhancement in growth rate and productivity of spinach grown in hydroponics with iron oxide nanoparticles. *RSC Advances, 6*(19), 15451-15459. doi:10.1039/c5ra23425e
Jin, B., Zheng, R., Peng, R., & Chu, S. (2016). Synthesis of New Bis(3-hydroxy-4-pyridinone) Ligands as Chelating Agents for Uranyl Complexation. *Molecules, 21*(3), 299. doi:10.3390/molecules21030299
Johnson, D. C., Dean, D. R., Smith, A. D., & Johnson, M. K. (2005). Structure, function, and formation of biological iron-sulfur clusters. *Annual Review of Biochemistry, 74*, 247-281. doi:10.1146/annurev.biochem.74.082803.133518
Joudeh, N., & Linke, D. (2022). Nanoparticle classification, physicochemical properties, characterization, and applications: a comprehensive review for biologists. *Journal of Nanobiotechnology, 20*(1), 262. doi:10.1186/s12951-022-01477-8
Kassebaum, N. J., Jasrasaria, R., Naghavi, M., Wulf, S. K., Johns, N., Lozano, R., . . . Murray, C. J. (2014). A systematic analysis of global anemia burden from 1990 to 2010. *Blood, 123*(5), 615-624. doi:10.1182/blood-2013-06-508325

Kharazmi, A., Faraji, N., Mat Hussin, R., Saion, E., Yunus, W. M., & Behzad, K. (2015). Structural, optical, opto-thermal and thermal properties of ZnS-PVA nanofluids synthesized through a radiolytic approach. *Beilstein Journal of Nanotechnology, 6*, 529-536. doi:10.3762/bjnano.6.55

Kim, S. A., & Guerinot, M. L. (2007). Mining iron: iron uptake and transport in plants. *FEBS Lett, 581*(12), 2273-2280. doi:10.1016/j.febslet.2007.04.043

Kobraee, S. (2016). Effect of zinc, iron and manganese fertilization on concentrations of these metals in the stem and leaves of soybean and on the chlorophyll content in leaves during the reproductive development stages. *Journal of Elementology, 21*(2/2016), 395-412. doi:10.5601/jelem.2015.20.2.966

Liu, K. (1997). Chemistry and Nutritional Value of Soybean Components. In *Soybeans* (pp. 25–113). Boston, MA: Springer. 10.1007/978-1-4615-1763-4_2

Liu, R., & Lal, R. (2015). Potentials of engineered nanoparticles as fertilizers for increasing agronomic productions. *Science of The Total Environment, 514*, 131-139. doi:10.1016/j.scitotenv.2015.01.104

Liu, X., Dong, X., He, C., Zhang, X., Xiang, G., & Ma, X. (2020). New polyazamacrocyclic 3-hydroxy-4-pyridinone based ligands for iron depletion antitumor activity. *Bioorganic Chemistry, 96*, 103574. doi:10.1016/j.bioorg.2020.103574

Livak, K. J., & Schmittgen, T. D. (2001). Analysis of relative gene expression data using real-time quantitative PCR and the 2(-Delta Delta C(T)) Method. *Methods, 25*(4), 402-408. doi:10.1006/meth.2001.1262

Lucena, J. J., & Hernandez-Apaolaza, L. (2017). Iron nutrition in plants: an overview. *Plant and Soil, 418*(1-2), 1-4. doi:10.1007/s11104-017-3316-8

Lv, J., Christie, P., & Zhang, S. (2019). Uptake, translocation, and transformation of metal-based nanoparticles in plants: recent advances and methodological challenges. *Environmental Science: Nano Journal, 6*(1), 41-59. doi:10.1039/c8en00645h

Ma, J. F., & Ling, H.-Q. (2009). Iron for plants and humans. *Plant and Soil, 325*(1-2), 1-3. doi:10.1007/s11104-009-0203-y

Márquez-Quiroz, C., De-la-Cruz-Lázaro, E., Osorio-Osorio, R., & Sánchez-Chávez, E. (2015). Biofortification of cowpea beans with iron: iron´s influence on mineral content and yield *Journal of Soil Science and Plants Nutrition, 15*, 839-847. doi:10.4067/S0718-95162015005000058

Marschner, H., & Römheld, V. (1994). Strategies of plants for acquisition of iron. *Plant and Soil, 165*(2), 261-274. doi:10.1007/bf00008069

Massella, D., Celasco, E., Salaun, F., Ferri, A., & Barresi, A. A. (2018). Overcoming the Limits of Flash Nanoprecipitation: Effective Loading of Hydrophilic Drug into Polymeric Nanoparticles with Controlled Structure. *Polymers (Basel), 10*(10). doi:10.3390/polym10101092

Mastronardi, E. T., Phepafatso & Zhang, Xueru & Monreal, Carlos & Derosa, Maria. (2015). Strategic Role of Nanotechnology in Fertilizers: Potential and Limitations. *Nanotechnologies in Food and Agriculture*, 46. doi:10.1007/978-3-319-14024-7_2

Masuda, T., Goto, F., & Yoshihara, T. (2001). A novel plant ferritin subunit from soybean that is related to a mechanism in iron release. *Journal of Biological Chemistry, 276*(22), 19575-19579. doi:10.1074/jbc.M011399200

Meng, F., Wei, Y., & Yang, X. (2005). Iron content and bioavailability in rice. *Journal of Trace Elements in Medicine and Biology, 18*(4), 333-338. doi:10.1016/j.jtemb.2005.02.008

Merry, R., Dobbels, A. A., Sadok, W., Naeve, S., Stupar, R. M., & Lorenz, A. J. (2022). Iron deficiency in soybean. *Crop Science, 62*(1), 36-52. doi:10.1002/csc2.20661

Mesquita, L. S., Mesquita, R. B. R., Leite, A., Moniz, T., Rangel, M., & Rangel, A. O. S. S. (2020). Integrated Flow-based System Displaying an In-line Mini Soil Column to Monitor Iron Species in Soils Leachates. *Communications in Soil Science and Plant Analysis, 51*(8), 1089-1100. doi:10.1080/00103624.2020.1751186

Mesquita, R. B. R., Moniz, T., Nunes, M. J. M., Mesquita, L. S., Rangel, M., & Rangel, A. (2022). Sequential injection method for bi-parametric determination of iron and manganese in soil leachates. *Analytical Methods, 14*(2), 180-187. doi:10.1039/d1ay01932e

Mittal, D., Kaur, G., Singh, P., Yadav, K., & Ali, S. A. (2020). Nanoparticle-Based Sustainable Agriculture and Food Science: Recent Advances and Future Outlook. *Frontiers in Nanotechnology, 2*, 1-38. doi:10.3389/fnano.2020.579954

Mori, S. (1999). Iron acquisition by plants. *Current Opinion in Plant Biology, 2*(3), 250-253. doi:10.1016/S1369-5266(99)80043-0

Morrissey, J., & Guerinot, M. L. (2009). Iron uptake and transport in plants: the good, the bad, and the ionome. *Chemical Reviews, 109*(10), 4553-4567. doi:10.1021/cr900112r

Naito, M., Yokoyama, T., Hosokawa, K., & Nogi, K. (2018). Basic Properties and Measuring Methods of Nanoparticles. In *Nanoparticle Technology Handbook* (pp. 3-47). 10.1016/b978-0-444-64110-6.00001-9

NDSU, N. D. S. U. (2022). NDSU's soybean iron chlorosis ratings available. *Extension and Agriculture Research News*.

Ning, X., Lin, M., Huang, G., Mao, J., Gao, Z., & Wang, X. (2023). Research progress on iron absorption, transport, and molecular regulation strategy in plants. *Frontiers in Plant Science, 14*, 1190768. doi:10.3389/fpls.2023.1190768

OECD. (1984). Earthworm, Acute Toxicity Tests. *OECD Guidelines for the Testing of Chemicals*. doi:10.1787/9789264070042-en

Prasad, T. N. V. K. V., Sudhakar, P., Sreenivasulu, Y., Latha, P., Munaswamy, V., Reddy, K. R., . . . Pradeep, T. (2012). Effect of Nanoscale Zinc Oxide Particles on the Germination, Growth and Yield of Peanut. *Journal of Plant Nutrition, 35*(6), 905-927. doi:10.1080/01904167.2012.663443

Rapier, C. E., Shea, K. J., & Lee, A. P. (2021). Investigating PLGA microparticle swelling behavior reveals an interplay of expansive intermolecular forces. *Scientific Reports, 11*(1), 14512. doi:10.1038/s41598-021-93785-6

Rehman, A. u., Masood, S., Khan, N. U., Abbasi, M. E., Hussain, Z., Ali, I., & Byers, D. (2020). Molecular basis of Iron Biofortification in crop plants; A step towards sustainability. *Plant Breeding, 140*(1), 12-22. doi:10.1111/pbr.12886

Rodrigues, E. M. d. A. (2018). *Estudo do mecanismo de ação e do método de aplicação de um novo composto [Fe(mpp)3], em plantas de soja (Glycine max L.) crescidas em solo alcalino.* (Mestrado em Engenharia Agronómica), Faculdade de Ciências da Universidade do Porto.,

Roriz, M., Pereira, S. I. A., Castro, P. M. L., Carvalho, S. M. P., & Vasconcelos, M. W. (2021). Iron metabolism in soybean grown in calcareous soil is influenced by plant growth-promoting rhizobacteria – A functional analysis. *Rhizosphere, 17*, 1-7. doi:10.1016/j.rhisph.2020.100274

Roser, H. R. a. M. (2021). Forests and Deforestation. Retrieved from https://ourworldindata.org/soy

Rout, G. R., & Sahoo, S. (2015). Role of Iron in Plant Growth and Metabolism. *Reviews in Agricultural Science, 3*(0), 1-24. doi:10.7831/ras.3.1

Rui, M., Ma, C., Hao, Y., Guo, J., Rui, Y., Tang, X., . . . Zhu, S. (2016). Iron Oxide Nanoparticles as a Potential Iron Fertilizer for Peanut (Arachis hypogaea). *Frontiers in Plant Science, 7*, 815. doi:10.3389/fpls.2016.00815

Safiri, S., Kolahi, A. A., Noori, M., Nejadghaderi, S. A., Karamzad, N., Bragazzi, N. L., . . . Grieger, J. A. (2021). Burden of anemia and its underlying causes in 204 countries and territories, 1990-2019: results from the Global Burden of Disease Study 2019. *Journal of Hematology & Oncology, 14*(1), 185. doi:10.1186/s13045-021-01202-2

Santos, C. S., Carvalho, S. M., Leite, A., Moniz, T., Roriz, M., Rangel, A. O., . . . Vasconcelos, M. W. (2016). Effect of tris(3-hydroxy-4-pyridinonate) iron(III) complexes on iron uptake and storage in soybean (Glycine max L.). *Plant Physiology and Biochemistry, 106*, 91-100. doi:10.1016/j.plaphy.2016.04.050

Santos, C. S., Leite, A., Vinhas, S., Ferreira, S., Moniz, T., Vasconcelos, M. W., & Rangel, M. (2020). A combined physiological and biophysical approach to understand the ligand-dependent efficiency of 3-hydroxy-4-pyridinone Fe-chelates. *Plant Direct, 4*(8), 1–15. doi:10.1002/pld3.256

Santos, C. S., Rodrigues, E., Ferreira, S., Moniz, T., Leite, A., Carvalho, S. M. P., . . . Rangel, M. (2021). Foliar application of 3-hydroxy-4-pyridinone Fe-chelate [Fe(mpp)(3)] induces responses at the root level amending iron deficiency chlorosis in soybean. *Physiologia Plantarum, 173*(1), 235-245. doi:10.1111/ppl.13367

Santos, C. S., Roriz, M., Carvalho, S. M., & Vasconcelos, M. W. (2015). Iron partitioning at an early growth stage impacts iron deficiency responses in soybean plants (Glycine max L.). *Frontiers in Plant Science, 6*, 325. doi:10.3389/fpls.2015.00325

Santos, C. S., Serrão, I., & Vasconcelos, M. W. (2016). Comparative analysis of iron deficiency chlorosis responses in soybean (Glycine max) and barrel medic (Medicago truncatula). *Revista de Ciências Agrárias, 39*(4), 538-549. doi:10.19084/rca16090

Santos, C. S., Sousa, C., Bagheri, M., Pinho, S., & Vasconcelos, M. W. (2023). Predicting iron deficiency and oxidative stress in Glycine max through Fourier transform infrared spectroscopy in a time-course experiment. *Plant and Soil*. doi:10.1007/s11104-023-06143-y

Santos, M. A., Irto, A., Buglyo, P., & Chaves, S. (2022). Hydroxypyridinone-Based Metal Chelators towards Ecotoxicity: Remediation and Biological Mechanisms. *Molecules, 27*(6). doi:10.3390/molecules27061966

Schaefer, B., Meindl, E., Wagner, S., Tilg, H., & Zoller, H. (2020). Intravenous iron supplementation therapy. *Molecular Aspects of Medicine, 75*, 100862. doi:10.1016/j.mam.2020.100862

Senguttuvel, P., G, P., C, J., D, S. R., Cn, N., V, J., . . . Govindaraj, M. (2023). Rice biofortification: breeding and genomic approaches for genetic enhancement of grain zinc and iron contents. *Frontiers in Plant Science, 14*, 1138408. doi:10.3389/fpls.2023.1138408

Shelar, A., Nile, S. H., Singh, A. V., Rothenstein, D., Bill, J., Xiao, J., . . . Patil, R. (2023). Recent Advances in Nano-Enabled Seed Treatment Strategies for Sustainable Agriculture: Challenges, Risk Assessment, and Future Perspectives. *Nano-Micro Letters, 15*(1), 54. doi:10.1007/s40820-023-01025-5

Skrzypczak, D., Jarzembowski, L., Izydorczyk, G., Mikula, K., Hoppe, V., Mielko, K. A., . . . Witek-Krowiak, A. (2021). Hydrogel Alginate Seed Coating as an Innovative Method for

Delivering Nutrients at the Early Stages of Plant Growth. *Polymers (Basel), 13*(23), 4233. doi:10.3390/polym13234233

Slomberg, D. L., & Schoenfisch, M. H. (2012). Silica nanoparticle phytotoxicity to Arabidopsis thaliana. *Environmental Science & Technology, 46*(18), 10247-10254. doi:10.1021/es300949f

Spirescu, V. A., Chircov, C., Grumezescu, A. M., Vasile, B. S., & Andronescu, E. (2021). Inorganic Nanoparticles and Composite Films for Antimicrobial Therapies. *International Journal of Molecular Sciences, 22*(9), 1-25. doi:10.3390/ijms22094595

Su, W.-H., Fennimore, S. A., & Slaughter, D. C. (2020). Development of a systemic crop signalling system for automated real-time plant care in vegetable crops. *Biosystems Engineering, 193*, 62-74. doi:10.1016/j.biosystemseng.2020.02.011

Thomas, D., KurienThomas, K., & Latha, M. S. (2020). Preparation and evaluation of alginate nanoparticles prepared by green method for drug delivery applications. *International Journal of Biological Macromololecules, 154*, 888-895. doi:10.1016/j.ijbiomac.2020.03.167

Tosato, M., & Di Marco, V. (2019). Metal Chelation Therapy and Parkinson's Disease: A Critical Review on the Thermodynamics of Complex Formation between Relevant Metal Ions and Promising or Established Drugs. *Biomolecules, 9*(7). doi:10.3390/biom9070269

Tuso, P. J., Ismail, M. H., Ha, B. P., & Bartolotto, C. (2013). Nutritional update for physicians: plant-based diets. *The Permanente Journal, 17*(2), 61-66. doi:10.7812/TPP/12-085

Varotto, C., Maiwald, D., Pesaresi, P., Jahns, P., Salamini, F., & Leister, D. (2002). The metal ion transporter IRT1 is necessary for iron homeostasis and efficient photosynthesis in Arabidopsis thaliana. *The Plant Journal, 31*(5), 589-599. doi:10.1046/j.1365-313x.2002.01381.x

Vega-Vasquez, P., Mosier, N. S., & Irudayaraj, J. (2020). Nanoscale Drug Delivery Systems: From Medicine to Agriculture. *Frontiers in Bioengineering and Biotechnology, 8*, 79. doi:10.3389/fbioe.2020.00079

Vert, G. A., Briat, J. F., & Curie, C. (2003). Dual regulation of the Arabidopsis high-affinity root iron uptake system by local and long-distance signals. *Plant Physiology, 132*(2), 796-804. doi:10.1104/pp.102.016089

Wang, X., Xie, H., Wang, P., & Yin, H. (2023). Nanoparticles in Plants: Uptake, Transport and Physiological Activity in Leaf and Root. *Materials (Basel), 16*(8), 1-21. doi:10.3390/ma16083097

WHO, W. H. O. (2008). Worldwide prevalence of anaemia 1993-2005. Retrieved from https://www.who.int/

WHO, W. H. O. (2021). Global anaemia estimates in women of reproductive age, by pregnancy status, and in children aged 6-59 months. Retrieved from https://www.who.int/

Yadav, A., Yadav, K., & Abd-Elsalam, K. A. (2023). Exploring the potential of nanofertilizers for a sustainable agriculture. *Plant Nano Biology, 5*, 1-15. doi:10.1016/j.plana.2023.100044

Yetisgin, A. A., Cetinel, S., Zuvin, M., Kosar, A., & Kutlu, O. (2020). Therapeutic Nanoparticles and Their Targeted Delivery Applications. *Molecules, 25*(9). doi:10.3390/molecules25092193

Ylivainio, K. (2010). Effects of iron(III)chelates on the solubility of heavy metals in calcareous soils. *Environmental Pollution, 158*(10), 3194-3200. doi:10.1016/j.envpol.2010.07.004

Zhang, S., & Wang, C. (2023). Effect of stirring speed on particle dispersion in silica synthesis. *Nano-Structures & Nano-Objects, 35*, 1-3. doi:10.1016/j.nanoso.2023.100994